



**Rui Filipe Cantarino Valente de Almeida**

Master of Science

**Development of a Tomographic Atmospheric  
Monitoring System based on Differential Optical  
Absorption Spectroscopy**

Thesis submitted in partial fulfillment  
of the requirements for the degree of

**Doctor of Philosophy in  
Biomedical Engineering**

Adviser: Pedro Vieira, Auxiliar Professor,  
NOVA University of Lisbon

Examination Committee

Chair: Name of the committee chairperson  
Rapporteurs: Name of a rapporteur  
Name of another rapporteur  
Members: Another member of the committee  
Yet another member of the committee



# **Development of a Tomographic Atmospheric Monitoring System based on Differential Optical Absorption Spectroscopy**

Copyright © Rui Filipe Cantarino Valente de Almeida, Faculty of Sciences and Technology, NOVA University Lisbon.

The Faculty of Sciences and Technology and the NOVA University Lisbon have the right, perpetual and without geographical boundaries, to file and publish this dissertation through printed copies reproduced on paper or on digital form, or by any other means known or that may be invented, and to disseminate through scientific repositories and admit its copying and distribution for non-commercial, educational or research purposes, as long as credit is given to the author and editor.



*Lorem ipsum.*



---

```
!TEX root = ./template.tex
```



---

## Acknowledgements



*I know the pieces fit, 'cause I watched them fall away.*

---

## Contents

<b>Acronyms</b>	<b>xxi</b>
<b>1 Introduction</b>	<b>3</b>
1.1 Background, Motivation and Starting Points . . . . .	3
1.1.1 Introduction . . . . .	3
1.1.2 Context . . . . .	4
1.2 Problem Introduction . . . . .	5
1.3 Literature review . . . . .	5
1.3.1 Tomography . . . . .	5
1.3.2 Differential Optical Absorption Spectroscopy (DOAS) . . . . .	7
1.3.3 DOAS Tomography . . . . .	8
1.4 Research Questions . . . . .	9
1.5 Hypothesis . . . . .	10
1.6 Methods and Findings . . . . .	11
1.7 Layout . . . . .	12
<b>2 Literature Review</b>	<b>13</b>
2.1 Air Pollution . . . . .	13
2.1.1 Air Pollution Effects on Human Health . . . . .	14
2.1.2 Air Pollution effects on ecosystems . . . . .	21
2.1.3 Air Pollution Sources . . . . .	23
2.1.4 Detecting and Monitoring Air Pollution . . . . .	30

## CONTENTS

---

2.2 DOAS . . . . .	33
2.3 Tomographic algorithms and reconstruction techniques . . . . .	37
2.3.1 Introduction . . . . .	37
2.3.2 Initial Considerations . . . . .	39
2.3.3 The Fourier Slice Theorem . . . . .	40
2.3.4 The Filtered BackProjection Algorithm . . . . .	41
2.4 DOAS Tomography . . . . .	44
<b>3 Methods</b>	<b>49</b>
3.1 Tomosim . . . . .	49
3.1.1 Discretisation . . . . .	51
3.1.2 Phantoms . . . . .	55
3.1.3 Error Estimation . . . . .	58
3.2 The Experiment . . . . .	59
3.3 Section Objectives . . . . .	60
3.4 Questions the readers should be able to answer once they've read the section . . . . .	61
3.5 How was the question answered? . . . . .	61
3.6 Detailed presentation of projection-based hypothesis . . . . .	62
3.7 Calculation of Projections . . . . .	62
<b>4 Discussion</b>	<b>63</b>
<b>Bibliography</b>	<b>65</b>
<b>Appendix</b>	<b>75</b>
<b>A Systematic Review of DOAS Tomography</b>	<b>75</b>
A.1 Introduction . . . . .	75
A.2 Background . . . . .	76
A.2.1 Differential Optical Absorption Spectroscopy . . . . .	76
A.2.2 Honourable Mentions . . . . .	77
A.2.3 Tomography . . . . .	78
A.2.4 Mapping Study . . . . .	80
A.3 Methods . . . . .	80
A.3.1 Research Questions . . . . .	80
A.3.2 Search Query Definition, Library Selection and Filter Definition	81
A.3.3 Data Extraction Strategy . . . . .	82
A.3.4 Quality Assessment . . . . .	82
A.4 Conduction . . . . .	83
A.4.1 Search Results . . . . .	83
A.4.2 Discussion . . . . .	83

---

## CONTENTS

A.4.3 Validity Threats . . . . .	86
A.5 Conclusions . . . . .	87



---

## List of Figures

1.1 A schematic representation of a projection acquisition. In this image, taken from [11], the clear line that comes down at a diagonal angle is a projection.	6
1.2 Hypothesis schematic. Light captured at point A is used as a light source (or $I_0$ ) for the light captured at point B, just as if using an artificial light source. As long as distances are kept small and the optical thickness is low, scattering will be negligible. This is a huge simplification over the traditional passive DOAS analysis process, as explained in Section ??.	11
2.1 Annotated anatomy of the respiratory system [25]. . . . .	15
2.2 Possible abnormalities caused by Air Pollution (AP) exposure <i>in utero</i> . Notice that time of exposure is of critical importance [25]. . . . .	19
2.3 Developmental stages of the lung throughout life vs the risks of AP exposure in each stage [25]. . . . .	20
2.4 Dramatic photograph depicting the Capelinhos' lighthouse, half a kilometer from the eruption site, surrounded by a cloud of ash Particulate Matter (PM), volcanic gas and water vapor with more than 1km in height[45]. . .	24
2.5 House almost completely buried by the Black Sunday dust storm. Several houses were entirely swallowed during this storm, trapping people inside, as if a big blizzard had hit them. Unlike a blizzard though, there was nothing anyone could do to keep the dirt outside, and all surfaces were covered black [47]. . . . .	25
2.6 Carbon Dioxide ( $\text{CO}_2$ ) atmospheric concentrations since the year 1000. Note the seemingly exponential increase since the 1800s. Plotted and published by the 2 Degrees Institute [50] with data from ice cores [51] and in situ monitors [52]. . . . .	26
2.7 Schematic presentation on the sources of anthropogenic pollution and its categorisation according to the IPCC. Adapted from [20] . . . . .	27

---

**LIST OF FIGURES**

2.8 Chinese energy production, Gross Domestic Product (GDP) and CO <sub>2</sub> emissions. Data collected from the World Bank and International Energy Agency websites [54, 55] . . . . .	28
2.9 General trends for European emissions. Data presented in % emissions of year 2000. Note the downward global trend in pollutant emissions, and its decoupling with the European GDP [56]. . . . .	30
2.10 European emissions divided by activity sector. The global decreasing trend is confirmed, as industries all around are producing less and less AP with the passing years [56]. . . . .	31
2.11 Semiconductor electrochemical sensor basic structure. There are many examples of this type of sensors, but in general they follow this architecture.	32
2.12 There are many spectroscopic techniques for atmospheric trace gas concentration measurement. Although several are depicted here, keep in mind that this is not an exhaustive list and is meant as an example repository.	33
2.13 Active DOAS schematic. . . . .	34
2.14 Passive DOAS schematic. . . . .	34
2.15 A schematic representation of a projection acquisition. In this image, taken from [11], the clear line that comes down at a diagonal angle is a projection.	38
2.16 Schematic representation for coordinate setting. The image depicts a parallel projection setting [62]. . . . .	39
2.17 The Fourier Slice Theorem (FST), a schematic representation [63]. . . . .	41
2.18 Schematic representation of an equiangular fan-beam projection, taken from [7]. . . . .	43
2.19 A schematic representation of an Systematic Mapping Study (SMS) writing process. The whole procedure is comprised of three smaller stages, which in turn are divided into various even smaller parts. The large arrow on the right represents the general evolution direction, although there is no rigid structure, and some back and forth is allowed and even expected. . . . .	45
3.1 Hexacopter in flight. Taken from laksjdlaksjd . . . . .	50
3.2 Illustration of the projection gathering algorithm based on fanbeam assembly of information. On the left the circle which constitutes the general trajectory of the drone. On the right the gymbal points the optical system towards different directions, forming what can be seen as a fan. . . . .	51
3.3 Grid and pixel definition, as they appear in the original article by Robert Siddon [65]. Notice that pixels are formed by line intersections. . . . .	52
3.4 $P_2$ Calculation. The software uses the position of the drone, as defined by the vertical angle, $\beta$ , and the distance between the drone and the centre of the trajectory, $D$ , to determine $P_2$ through the solution of a second degree equation. . . . .	56

3.5 A graphical representation of the new spectral phantom, custom built for the TomoSim application. . . . .	57
3.6 Error estimation graphical representation. Note errors are extremely exaggerated for visualisation purposes. . . . .	59
3.7 Location of observer points for the physical experiment. . . . .	61
A.1 MAX-DOAS schematic representation [14]. . . . .	78
A.2 Conduction stage flowchart. Libraries are searched independently through <i>Publish or Perish</i> , but results must be checked to ensure they are not counted twice, due to the imbalance of power between GS's search engine and the others. . . . .	84



---

## List of Tables

1.1 Main research question. . . . .	9
1.2 Secondary research questions. . . . .	10
2.1 Criteria pollutants as defined by the EPA and the EEA [20]. These are the pollutants whose effect is more significant for society itself, given their level of dangerousness and how common they are. . . . .	14
2.2 Global energy production, divided according to the fuel used to obtain it and the production country. . . . .	29
2.3 Categorization of semiconductor gas sensors. The type of transducer and receptor dictates the type of the sensor. . . . .	33
2.4 PICOC analysis. . . . .	46
2.5 Research question slicing . . . . .	46
2.6 Electronic libraries used in this study. . . . .	46
2.7 Selection filters in use for this study's search. . . . .	46
2.8 Research question slicing . . . . .	47
2.9 Electronic libraries used in this study. . . . .	47
2.10 Selection filters in use for this study's search. . . . .	48
3.1 Table summarising the new phantom's construction details, as a sum of 5 Gaussian profiles and an ellipse designed using TomoPhantom. In this table, C0 is the object's amplitude, X0 and Y0 are its center coordinates, and a and b are the objects half-widths. The table is constructed using TomoPhantom's particular syntax and more information can be obtained at [69]. . . . .	57
A.1 PICOC analysis. . . . .	81
A.2 Research question slicing . . . . .	81
A.3 Electronic libraries used in this study. . . . .	82
A.4 Selection filters in use for this study's search. . . . .	82
A.5 Search results summary. . . . .	83

## LIST OF TABLES

---

## Acronyms

ALRI	Acute Lower Respiratory Infections
ANS	Autonomic Nervous System
AP	Air Pollution
API	Application Programming Interface
ART	Algebraic Reconstruction Technique
BAEP	Brainstem Auditory-Evoked Potentials
BTU	British Thermal Unit
CEM	Continuous Emission Monitoring
CNS	Central Nervous System
CO	Carbon Monoxide
CO <sub>2</sub>	Carbon Dioxide
COPD	Chronic Obstructive Pulmonary Disease
CT	Computed Tomography
CVD	Cardiovascular Disease
CVM	Cardiovascular Mortality
DIAL	Differential Absorption LIDAR
DOAS	Differential Optical Absorption Spectroscopy
EEA	European Environmental Agency
EPA	Environmental Protection Agency (United States)
ESCAPE	European Study of Cohorts for Air Pollution Effects
FBP	Filtered BackProjection

## ACRONYMS

---

FFF	Forest Fire Finder
FP7	European Union's Seventh Framework Programme
FST	Fourier Slice Theorem
FT	Fourier Transform
GDP	Gross Domestic Product
H <sub>2</sub> S	Hydrogen Sulfide
ICE	Internal Combustion Engine
ICE	Internal Combustion Engine
IFT	Inverse Fourier Transform
IOT	Internet Of Things
LPG	Liquefied Petroleum Gas
MAX-DOAS	MultiAxis-DOAS
ML	Machine Learning
MLEM	Maximized Likelihood Expectation Maximization
MSE	Mean Squared Error
NH <sub>3</sub>	Ammonia
NO <sub>2</sub>	Nitrogen Dioxide
NO <sub>X</sub>	Nitrogen Oxides
O <sub>3</sub>	Ozone
PAH	Polycyclic Aromatic Hydrocarbons
PICOC	Population Intervention Context Objective Comparison
PM	Particulate Matter
Project ATMOS	ATmosphere MOnitoring System Project
PT2020	Portugal2020
ROI	Region Of Interest
RQ	Research Question
RTK GPS	Real Time Kinematic Global Positioning System

SART	Simultaneous Algebraic Reconstruction Technique
SGA	Small for Gestation Age
SLR	Systematic Literature Review
SLR	Systematic Literature Review
SMS	Systematic Mapping Study
SMS	Systematic Mapping Study
SO <sub>2</sub>	Sulfur Dioxide
	*
TDL	Tunable Diode Laser
UAV	Unmanned Aerial Vehicle
VOC	Volatile Organic Compound
WHO	World Health Organization



---

## Todo list

citatoins: examples of industrial applications of tomography . . . . .	5
Reference to the chapter in which this technique is explained . . . . .	7
check this! . . . . .	7
This is written in some of the tomographic DOAS papers. . . . .	8
Reference the section in which this paper is more thoroughly discussed . . . . .	8
Check these numbers . . . . .	9
Figure: . . . . .	11
Consider rewriting this section. . . . .	11
citation . . . . .	11
citation . . . . .	11
Criteria Pollutant table . . . . .	14
citations - vallero and lovett + european report . . . . .	21
should I get another source on this problem? . . . . .	22
table with major pollutants? . . . . .	27
citation and examples . . . . .	28
Figure: . . . . .	32
Figure: This is actually a table . . . . .	33
Figure: . . . . .	33
citation Shepp 1979 . . . . .	44
image citation . . . . .	50
Figure: An image of an hexacopter in flight. . . . .	50
Figure: . . . . .	51
Ugly. Rewrite . . . . .	51
Figure: Siddon article grid and pixel definition . . . . .	52
reference the correct subsection after merging with the mac branch . . . . .	59



---

# Introduction

## 1.1 Background, Motivation and Starting Points

### 1.1.1 Introduction

This thesis describes the work that I have done in the past 4 years on the design and development of a miniaturized system for atmospheric monitoring based on optical spectroscopy. The project itself was the major part of the [ATmosphere MOnitoring System Project \(Project ATMOS\)](#), an initiative that was contemplated with European funding through a [Portugal2020 \(PT2020\)](#) initiative and came as a response to the growing weight that [AP](#) has in the whole Western world.

The potential impact of [AP](#) on human health is amply documented. Numerous papers have, for decades, established many links between air quality and several common ailments like respiratory syndromes and cardiovascular diseases. Similar connections have also been found regarding the probability of gestational malformations and several types of cancer. On a different level, and of perhaps less immediate concern, are the effects that have been observed on ecosystems. Many times these effects are difficult to predict (and timely mitigate) and in some cases have been known to interfere with people's livelihood. In time, and if not addressed, these interferences will certainly hinder economies and limit the quality of life of populations globally. The severity of this problem makes it clear that we need to tackle it intelligently, and this approach requires that we can measure, trace and track [AP](#) effectively, which beckons engineers and scientists to create more technology for this specific purpose.

Answering this call, with this work I have tried to create a reply to the question of whether it would be possible to develop a two-dimensional pollutant mapping tool, small enough to be fitted onto a [Unmanned Aerial Vehicle \(UAV\)](#), which came to be a tomographically enabled design. To this end, I have developed a simulation platform that computationally proves the method's feasibility and confirmed through experiments that the hypothesis on which the solution is based, regarding the use of sequentially measured scattered sunlight as analogous to an artificial light source is valid.

### 1.1.2 Context

The idea behind this thesis was born in 2015, at NGNS-IS (a Portuguese tech startup). At the time, the company's flagship product was the [Forest Fire Finder \(FFF\)](#). The [FFF](#) was a forest fire detection system, capable of mostly autonomous and automatic operation. The system was the first application of [DOAS](#) for fire detection, and for that it was patented in 2007 (see [1, 2]). The [FFF](#) is a remote sensing device that scans the horizon for the presence of a smoke column, sequentially performing a chemical analysis of each azimuth, using the Sun as a light source for its spectroscopic operations [3].

The [FFF](#) was deployed in several "habitats", both nationally (Parque Nacional da Peneda-Gerês and Ourém) and internationally (Spain and Brazil). One of the company's clients at the time was interested in a pollution monitoring solution, and asked if the spectroscopic system would be capable of performing such a task. The challenge resonated through the company's structure and the idea that created this thesis was born. The team then started reading about the concept of [AP](#) and how both populations and entities were concerned about it. It became clear that, while there were already several methods to measure [AP](#), there was a clear market drive for the development of a system that could leverage the large area capabilities of a [DOAS](#) device while being able to provide a more spatially resolved "picture" of the atmospheric status. With this in mind, the company managed to have the investigation financed through a [PT2020](#) funding opportunity. This achievement was a clear validation of the project's goals and of the need there was for a system with the proposed capabilities. It was, however, not enough. [FFF](#) was a very good starting point, but there was still a lot of continuous research work needed before any of the goals that had been set were achieved. This led to the publication of this PhD project, in a tripartite consortium between FCT-NOVA, NGNS-IS and the Portuguese Foundation for Science and Technology. Its main goal was to develop an atmospheric monitoring system prototype that would be able to spectroscopically map pollutant concentrations in a two-dimensional way.

In April 2017, NGNS-IS was integrated in the Compta group, one of the oldest IT groups operating in Portugal. Despite its age, this company is one of the main presences in some of the most modern industrial fields, like [Internet Of Things \(IOT\)](#) applications. [Project ATMOS](#)'s pollutant tracing capabilities made it an almost perfect fit in one of [IOT](#)'s most resounding niches, the *Smart Cities* trend. Unfortunately, the transition between one company and the other, regardless of the project's adequacy, was anything but smooth. Almost two years later, in the beginning of 2019, engulfed in a sea of endless bureaucracy and ill intent on behalf of the managing governmental authorities (who seemed always more interested in seeing the project fail than anything else), [Project ATMOS](#) was terminated and financing was cut.

## 1.2 Problem Introduction

Air Pollution poses an important threat to the human way of life. The World Health Organization (WHO) have estimated that 1 out of each 9 deaths in 2012 were AP-related and of these, 3 million were directly attributable to outdoor AP worldwide, most of which in developing countries (87% vs 82% population). Although the European picture is not so dire as this, the topic does cause concern. In 2016, there were an estimated 400.000 deaths due to AP in Europe, 391.000 of which in the EU-28 space [4]. An increased number of premature deaths is sufficiently bad for treating this issue seriously, but the problems brought forth by Air Pollution do not end here. Not only are people dying more, disabilities (namely respiratory) are more frequent, and so are hospital visits. These two factors represent a decrease in productivity and an increase in medical costs, which accrue to the huge burden that AP already represents to any society. In Europe, health impacts of diesel emissions were estimated to be in the region of 60 billion euros [5] for the year of 2016.

These impressive numbers have perspired onto the public opinion, which is (now more than ever) concerned with the whole problem of AP. In fact, the subject is considered by the public the second most important environmental threat (after Climate Change, which is a very related topic), and citizens throughout Europe have been partaking in initiatives which aim to aid and incentivize air quality monitoring, as well as raising awareness to the necessity of paying attention to this issue and for behavioral changes. As tackling Air Pollution and its causes grows ever more popular, so does the political weight associated with the subject, which in turn results in an increased number of measures destined improve air quality. However, effective actions against AP require the approach to be intelligent and knowledgeable, for the more we know, the better we can handle it. It is thus the role of technology and technologists, to develop new ways in which to measure, map, track and trace AP, leveraging the power of human intellect and ingenuity to combat this impending threat that is upon us.

## 1.3 Literature review

### 1.3.1 Tomography

Tomography is the cross-sectional imaging of an object through the use of transmitted or reflected waves, captured by the object exposure to the waves from a set of known angles. It has many different applications in science, industry, and most prominently, medicine. Since the invention of the Computed Tomography (CT) machine in 1972, by Hounsfield [6], tomographic imaging techniques have had a revolutionary impact, allowing doctors to see inside their patients, without having to subject them to more invasive procedures [7].

citations: examples of industrial applications of tomography

Mathematical basis for tomography were set by Johannes Radon in 1917. At the time, he postulated that it is possible to represent a function written in  $\mathbb{R}$  in the space of straight lines,  $\mathbb{L}$  through the function's line integrals. A line integral is an integral in which the function that is being integrated is evaluated along a curved path, a line. In the tomographic case, these line integrals represent a measurement on a ray that traverses the **Region Of Interest (ROI)**. Each set of line integrals, characterized by an incidence angle, is called a projection (see Figure 2.15). To perform a tomographic reconstruction, the machine must take many projections around the object. To the set of projections arranged in matrix form by detector and projection angle, we call sinogram. All reconstruction methods, analytical and iterative, revolve around going from reality to sinogram to image [7, 8, 9, 10, 11, 12].



Figure 1.1: A schematic representation of a projection acquisition. In this image, taken from [11], the clear line that comes down at a diagonal angle is a projection.

There are two broad algorithm families when it comes to tomographic reconstruction, regarding the physics of the problem. It can involve either non-diffracting sources (light travels in straight lines), such as the X-Rays in a conventional **CT** exam; or diffracting sources, such as micro-waves or ultrasound in more research-oriented applications [7]. In this document, I will not address the latter family, since I will not be applying them in my work.

In any tomographic procedure, the first step is to gather information from the target object. The first concept one requires for this is to determine the problem's geometry. There are many different possible geometry, however, there are two that are more important for this thesis: parallel and fan-beam geometries, which are presented in Figure ???. In the parallel case, there are as many light sources as there are detectors. Light travels between the source and the detector in straight lines, and the whole set rotates around the object's location. Fan-beam geometries are characterized by having

only one light source which rotates around the target object. In this geometry, a set of detectors are placed on the other side of the object, and the lines (rays) between the source and the detectors describe a fan, thus the name of the technique [7, 11].

As far as algorithms are concerned, there are two main types: analytical and iterative. The first family includes the most famous algorithm for these applications, the **Filtered BackProjection (FBP)**. Iterative algorithms work by iteratively searching for a solution to the reconstruction equation, which is basically an underdetermined system of equations . There are numerous algorithms that work in this way, but in my work, I have identified three that are extensively used, both in the field of atmospheric tomography and in medicine: **Algebraic Reconstruction Technique (ART)**, **Simultaneous Algebraic Reconstruction Technique (SART)**, and **Maximized Likelihood Expectation Maximization (MLEM)**. The simulator that was developed as part of this project uses the last two and **FBP**.

Reference to the chapter in which this technique is explained

check this!

### 1.3.2 DOAS

Since the beginning of the 20<sup>th</sup> century, scientists have been using spectroscopy to measure reactive trace gases in the atmosphere, especially ozone. The basis for these applications were set by Bouguer, Lambert and Beer, which have separately presented the law (Lambert-Beer's) that determines the relationship between light extinction and the concentration of an absorber, when it must traverse a medium in which this absorber is present. **DOAS** is one of the methods that is applied for this purpose. It was developed in 1976, by Perner and his colleagues [13], to detect and quantify the hydroxyl radical in the atmosphere. The book by Jochen Stütz and Ulrich Platt [14] is considered by most researchers one of the most important references in the field and is present in most bibliographies of the literature in this subject (it is also one of the main references in this thesis). Platt, in particular, has been working with the technique since its beginning, as one of the elements of Perner's team that published the article about the hydroxyl radical mentioned some lines above [13].

Besides **DOAS**, Lambert-Beer's law is the basis of many quantitative spectroscopy applications. However, most of these techniques are used in a laboratory context, in which conditions are controlled and very well known. Atmospheric studies do not have this luxury. In the open atmosphere, there are a number of factors, like Mie and Rayleigh scattering, atmospheric turbulence or thermal fluctuations in the optical path that make outdoor spectral measurements more complicated. **DOAS** is able to circumvent these difficulties by measuring differential absorptions, which is to say the difference in absorption between two different wavelengths [14, 15].

There are two modalities for **DOAS** experiments, Active and Passive, which differ mainly on the use of artificial or natural light sources, respectively. Both methods have their advantages and disadvantages. Active systems are more similar to a bench spectroscopy experiment. Conditions are more controlled (starting with the light source)

and therefore, results are usually more reliable and precise, not to mention simpler to reach, since there is no need to account for complex physical phenomena, like radiative transfer [14]. However, these systems do require additional material, and many times entire infrastructures have to be built around them [16]. Passive systems, on the other hand, can be comprised of just a computer, a spectrometer and a telescope, making them instrumentally much simpler than their active counterparts. This flexibility also comes with the possibility to develop new interesting sub-techniques, like **MultiAxis-DOAS (MAX-DOAS)**, which allows (for instance) the determination of the stratospheric contribution of a certain trace gas (in opposition to its tropospheric contribution). The mathematical processing of the acquired spectra, nonetheless, is much more complex.

### 1.3.3 DOAS Tomography

DOAS tomography is a relatively new subject within the realm of **DOAS**. It consists in the application of tomographic methods to reconstruct a two-dimensional or three-dimensional *map* of the concentrations of trace gases in study. The seminal paper that originated this and other remote sensing tomographic techniques was published by Shepp in xxxx. It is not by any means a very populated literary space. In a systematic review that was performed as part of a course I took during the development of this PhD thesis, I managed to identify a total of 13 papers that were clearly about DOAS tomography. In doing this review, I have also found that the largest DOAS tomography study was performed in Germany, during the first years of the 21<sup>st</sup> century. This research campaign, called BAB-II [17], aimed to measure and map traffic-related concentrations for **Nitrogen Dioxide (NO<sub>2</sub>)** in the motorway that goes between Heidelberg and Mannheim. A more recent effort that is mention worthy is the paper by the Stutz [18], in which the group created a tomographic system that was able to perform as a fence line monitor for a refinery in Houston, Texas. In between the two studies, and right after BAB-II, Erna Frins published her paper [19], in which she described the use of a **MAX-DOAS** system alternately pointed towards sun-illuminated and dark targets in a tomographic manner.

Besides the birds eye view of the literary panorama of the DOAS tomography field, this systematic review allowed me to understand two important gaps in the technology being employed for this research. The first is that all of the studies that were featured in my review used a very low number of tomographic projections (some dozens of line integrals). This is a problem because it is the single most important factor for the resolution of any tomographic procedure, and although resolution is not an absolutely critical factor in atmospheric analysis (because the sizes of the target objects - gas plumes - are very large and diffuse), it is an important system feature that should be improved. Moreover, the second important pattern that was clear from my research was that all but one of the described systems were fixed, and the one that was mobile

This is written in  
one of the tomographic DOAS pa-  
pers.

reference the sec-  
on in which this  
paper is more thor-  
oughly discussed

was composed of a minimum of two spectral acquisition devices and had one of the lowest numbers of projections in all papers. This is a very important gap. DOAS tomography has the ability not only to measure but also to map pollutant concentrations and can be an invaluable technique in the fight to understand and track the movement of pollutant plumes, but the fact that the available systems require dedicated infrastructure to operate and have no mobility at all may be the most important factor leading to the almost non-existing investment DOAS tomography systems.

More than half of the world's population is expected to be living in cities by the year 2050, and in the next 10 years we will see an increase in the number of so-called megacities of more than 30% [20]. This puts a lot of pressure on governmental agencies and municipalities (specially in the West) to "smarten up" their urban infrastructures, so that cities can harbor their inhabitants with reasonable quality of life for everyone. In fact, a recent report by xxx concluded that in the next yyy years, states and cities will spend more than 150 billion Euros on this kind of infrastructure. The flexibility and mobility that the system I am developing brings to the table are two very heavy points in its favor as a pollution mapping tool which is unobtainable with the traditional methods, whether *in-situ* or remote.

Check these numbers

## 1.4 Research Questions

In Section 1.1.2, I have introduced the reasons which led NGNS-IS to pursue the development of an atmospheric monitoring system, and that what set it apart from other systems was the ability to spectroscopically map pollutants concentrations using tomographic methods, thus defining a primary objective for this thesis.

Two secondary objectives were born from the necessary initial research, which had a very heavy influence over the adopted methods:

- To use a tomographic approach for the mapping procedure;
- To ensure the designed system would be small and highly mobile;
- To use a single light collection point, minimizing material costs.

Taking all the above into account, we arrive at the main Research Question (Research Question (RQ)), presented in Table 1.1.

Table 1.1: Main research question.

---

<b>RQ1</b>	<i>How to design a miniaturized tomographic atmosphere monitoring system based on DOAS?</i>
------------	---

---

This is the main research question. It gave rise to four other more detailed research questions. These secondary questions allow a better delimitation of the work at hand and are important complements to RQ1. These questions are presented in Table 1.2.

Table 1.2: Secondary research questions.

<b>RQ1.1</b>	<i>What would be the best strategy for the system to cover a small geographic region?</i>
<b>RQ1.2</b>	<i>What would be the necessary components for such a system?</i>
<b>RQ1.3</b>	<i>How will the system acquire the data?</i>
<b>RQ1.4</b>	<i>What should the tomographic reconstruction look like and how to perform it?</i>

## 1.5 Hypothesis

As stated in Section 1.4, the main goal of my work was to provide an answer to the question of how to design a miniaturized tomographic atmosphere monitoring system, based on DOAS. This sentence is the most important point of the project. Every development from this point forward stems from it and is motivated by it. It also requires some deconstruction in order to understand the true scope of the matter. First, it is a miniaturized device. This means that besides all the habitual requirements (performance, function, adequacy, compatibility with the other components, safety and security) in defining components in an engineering project, one must also keep in mind the footprint of each component, and how much it weighs. Second, it is a tomographic system, which means that not only the device must be able to take line integrals from some kind of medium, it must also be able to describe a predefined trajectory, with admissible levels of geometric error, which complies to a certain projection geometry. Otherwise, one would not be able to apply a tomographic reconstruction routine to obtain the map of the target species concentrations. Finally the system is supposed to monitor the atmosphere in some way. Now, as implied in the same sentence, DOAS is the technique that I am trying to apply in this system. But as I point out in Section 1.3.2 and with more depth in Section ?? , there are two families of DOAS, and within them, many sub-techniques. This system which I am developing is based on the hypothesis that we can use an almost hybrid approach to DOAS: passive DOAS instrumental simplicity and active DOAS retrieval simplicity. As illustrated in Figure 1.2, one could use a scattered sunlight measurement as a light source for a DOAS analysis, provided distances between the two points are kept small, optical densities are low (clear atmosphere), and both spectral measurements are taken in the same angle. With this process, we would only effectively be using as projections the spectral measurements of the ROI. This hypothesis, while not being mentioned in the library directly, has already been hinted at in several papers, namely references [19, 21, 22].



Figure 1.2: Hypothesis schematic. Light captured at point A is used as a light source (or  $I_0$ ) for the light captured at point B, just as if using an artificial light source. As long as distances are kept small and the optical thickness is low, scattering will be negligible. This is a huge simplification over the traditional passive DOAS analysis process, as explained in Section ??.

## 1.6 Methods and Findings

Consider rewriting this section.

The system proposed in this thesis is a conjunction of sub-components that work together towards the final goal. The first division is between what is a physical, tangible component and what is just software related. On the first level, developing this project involved selecting the components for a custom made UAV to which the spectroscopic system will be attached to. In addition to this, I also had to select the on-board electronics module, which is comprised of the flight controller, which takes care of the device's movement; and the on-board computer, which handles the acquisition of data via the optical module, an assembly of spectrometers and telescopes connected through a custom-built coupling part. All this assembly will perform according to what is programmed using ArduCopter's SITL programming suite .

citation

On a software level, developing this project implied the creation of a tomographic simulation tool, written in Python (and more particularly, NumPy) [23, 24]. This tool was coded considering the hypothesis described in Section 1.5, and includes the description of the trajectory that the system must conduct in order to reconstruct the target species concentration maps. Regarding the reconstruction itself, this tool includes custom-built routines for the FBP algorithm and the MLEM algorithm, and applies a SciPy library method to perform SART reconstruction. Moreover, the simulation platform also takes into consideration geometric and reconstruction errors, proper to this kind of system.

citation

The rest of this thesis describes my best efforts in developing a spectral system that would provide an affirmative reply to the research question, taking into account the literary gaps that we have found in our literature review. In doing this, I have successfully built a software simulation tool that computationally proves that our tomographic assumptions are reasonable and allow the concentration mapping of any trace species that can be targeted by the DOAS technique. On an experimental level,

I have also managed to validate the hypothesis described in Section 1.5.

## 1.7 Layout

After this introduction, in Chapter 2, we can find a more thorough literature review than the one presented in Section 1.3. After that, I have included the chapter in which I present and discuss the methods employed in this project's development (Chapter 3). Finally, in Chapter ??, I present what could be concluded as a result of this project.

# CHAPTER 2

---

## Literature Review

### 2.1 Air Pollution

Daniel Vallero, in his book "Fundamentals of Air Pollution" [25] makes a very important observation: Air Pollution has no universal definition. Its meaning is intertwined with the context with which it is measured and observed, with the ecosystem in which it is perceived and even with the pollutant concentration (not every toxic compound is toxic at every concentration). The [Environmental Protection Agency \(United States\) \(EPA\)](#) defines Air Pollution as the following:

*Air Pollution is the presence of contaminants or pollutant substances in the air that interfere with human health or welfare, or produce other harmful environmental effects.*

He then analyzes this definition through two possible lenses, the one that comes with the interference produced by air contaminants; and the one that comes from the harm they may cause. He notes that both points of view come with a heavy burden of ambiguity, incompatible with a scientific definition. We can thus observe that preferable to address the issue through its measurable effects and consequences. These are well-established and well known, and scientists all around the world have been publishing extensively about them for some decades now. The correlation between Air Pollution and an increased mortality in heavily industrialized areas was first established in Europe, in the 19<sup>th</sup> century, but the first time it was taken seriously was during the 1952 killer-smog incidents, in London [14]. At the time, a combination of very cold weather, an anticyclone and fireplace emissions caused a thick smog to fall over London, directly causing thousands of deaths and indirectly many more [26, 27]. The disastrous consequences of this incident had a huge impact in the civil society, resulting in a series of policies and laws, among which the Clean Air Acts of 1956 and 1968, which are broadly considered to be some of the first actions to decrease pollution in human societies. Much work has been done, and it has resulted in remarkable progress since the definition of those two policies. We are in fact in a much better place

than we were some years or decades ago, but pollution is still a part of everyday reality for the whole of civilization. In the current day and age, both European and American regulatory and surveillance bodies (the [European Environmental Agency \(EEA\)](#) and the [EPA](#), respectively) have identified a group of six *criteria pollutants* that need to be monitored effectively. These gases, whose effects this section particularly focuses, are presented in Table 2.1. In this section, I will present the most significant aspects of [AP](#) that are described in the literature, including health effects, environmental effects and [Air Pollution](#) monitoring.

Table 2.1: Criteria pollutants as defined by the EPA and the EEA [20]. These are the pollutants whose effect is more significant for society itself, given their level of dangerousness and how common they are.

Criteria Pollutant table

### 2.1.1 Air Pollution Effects on Human Health

Arguably, there is no medium in which it is more important to consider [AP](#) by its effects than in the human body. However, even this has its caveats. The body's response to any given substance changes with the dose that is administered to it, something which has been known to us for centuries:

*What is it that is not poison? All things are poison and nothing is without poison. It is the dose alone that makes a thing not poison.*

– Paracelsus

This quote, originally in the writings of one of the fathers of modern medicine, the Swiss Paracelsus, was taken from Patricia Frank's book called *The Dose Makes The Poison* [28] and is one of the core tenets of toxicology even today. There are, however, some substances which do not need anything close to a high dose to cause harm to human health, and in general, atmospheric pollutants fall in that category. According to the [EEA](#), heart disease and stroke are the most common causes of premature death due to [Air Pollution](#). The same organization states that the most prominent atmospheric pollutants in terms of the effects they have on human health are [PM](#), [NO<sub>2</sub>](#) and [Ozone \(O<sub>3</sub>\)](#) [29, 30]. In this thesis, I will focus mostly on them, not only because of their health importance, but also because of their spectral nature, which allows us to detect them using [DOAS](#) [14]. Of course, a complete description of how [AP](#) affects the human body is a colossal task which is well beyond the scope of this thesis. Therefore, I will focus my attention on the more prominent symptoms that are results of these chemicals: respiratory syndromes, cardiovascular diseases, problems during gestation and finally, neurologic consequences of [AP](#).

### 2.1.1.1 Respiratory effects of Air Pollution

The respiratory system's main functions are the delivery of oxygen into the blood stream and the removal of carbon dioxide from the body. Air enters the body from the upper airways and flows to the alveolar region, where oxygen diffuses across the lung wall into the blood stream, from which it is transported to the tissues where it diffuses yet again and is made available to the mitochondria in the cells, that use it for cellular respiration [31]. The whole system is in permanent interaction with the atmosphere, and is therefore exposed to all kinds of air pollutants and trace gases, and therefore it is only natural that respiratory effects are among the most direct health complications originating in AP [25].

The region in which a given pollutant is, within the respiratory system (see Figure 2.1), is of great importance. After the air is inhaled through the nose, the air is heated or cooled to body temperature, as well as humidified, in the upper airways. The trachea leads the air into the bronchi, where flow is divided several times before reaching the alveoli, where oxygen is supposed to enter circulation. Since air flows within the different regions of the pulmonary system are completely different, AP is also handled differently among them. Moreover, it is also important to consider that pollutants also vary according to their own physical properties, and pollutant absorption is also a function of this. Particles' absorption depends on their aerodynamic characteristics, as well as soluble fraction and density. Gaseous pollutants are dependent exclusively on their vapor pressure, solubility and density [25, 31].

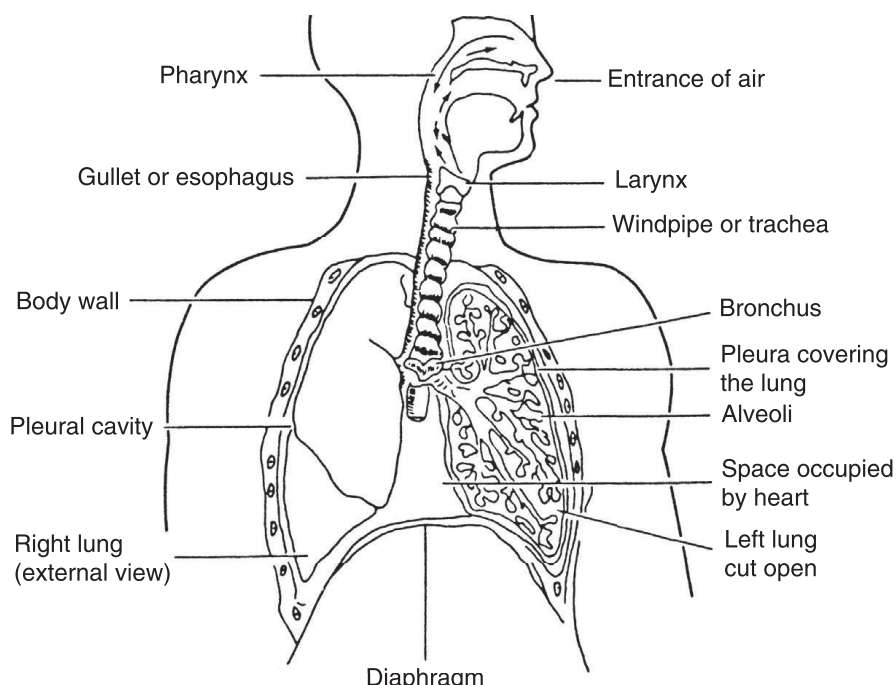


Figure 2.1: Annotated anatomy of the respiratory system [25].

The respiratory system has several (imperfect) mechanisms in place to prevent particles from reaching the blood stream. Larger particles are deposited in the nose, by impaction on the hairs and bends of the nose. Smaller particles are immune to this first barrier, and manage to get to the trachea and bronchi, where they are filtered also by impaction, this time on the walls of the innumerable bifurcations of the bronchial tree. The smallest particles are removed through Brownian motion, which ends up pushing them against the alveolar membrane. Deposited substances are then removed through the action of cilia in the pulmonary system's walls or by coughing, sneezing or blowing one's nose [25].

While the body is quite efficient at filtering out particles from the respiration process, the same cannot be said about gaseous pollutants. Removal of these compounds can only be achieved through absorption, which depends almost exclusively in the gases' solubility. High solubility compounds are absorbed directly in the upper airways ( $\text{SO}_2$ , for instance), while less soluble gases (such as  $\text{O}_3$  and  $\text{NO}_2$ ) are absorbed in the lungs themselves. Irritant gases trigger a variety of responses, in which one can include sneezing, coughing or bronchoconstriction. These gaseous compounds are then diffused through to the bloodstream or the lungs themselves try to convert them into other substances via biochemical processes. In some cases, this attempt to detoxify a pollutant can lead to much more problematic circumstances. For instance, the lung is known to activate procarcinogens, substances that are only carcinogenic after being metabolized in a certain way [25].

Acute symptoms of AP exposure are very varied, and range from mild irritation to complete respiratory failure, depending mostly on level of exposure and individual sensitivity to the chemical compound. One of the most important acute manifestations of AP exposure are encompassed within the Acute Lower Respiratory Infections (ALRI) group. There are several studies in which the relationship between this issue and AP is deducted and explained, mostly in developing countries, and it remains as one of the major causes for infantile death [20, 32]. Children are one of the most affected demographics by AP [29], and one of the chief reasons for this is that the human respiratory system is still developing in this stage of life.

In a 2016 review [33], the authors searched the literature for childhood adverse effects of AP, with a particular focus on respiratory problems. They have found evidence for a number of respiratory complications and diseases that were previously reported in the literature caused or exacerbated by AP. Effects are many, and vary immensely in nature, severity and affected populations. Short term effects, like coughing and wheezing were found for the three types of major pollutant and several others; several papers mention an association between the occurrence of respiratory infections and exposure to AP, namely concerning PM and  $\text{NO}_2$ . The same review found reports of decreased lung function in children and asthma exacerbation in children due to Air Pollution. Moreover, a person exposed to high levels of AP during childhood are also more likely to develop syndromes like Chronic Obstructive Pulmonary Disease

(COPD), and to have exacerbated symptoms of this disease. Finally, and perhaps more concerning, the carcinogenic nature of several of the constituents of AP leads to findings relating the appearance of respiratory cancers to exposure levels during childhood. Many of the conclusions of this review come from a large-scale European effort called European Study of Cohorts for Air Pollution Effects (ESCAPE), that intended to investigate long-term health effects of AP in Europe. ESCAPE was an European Union's Seventh Framework Programme (FP7) initiative that ended in 2014.

### 2.1.1.2 Air Pollution and cardiovascular issues

After being absorbed by the respiratory system, oxygen is distributed to all cells of the body through the cardiovascular system. Air pollutants, like particles and trace gases, are also capable of penetrating the lung barrier and therefore share the same fate. There are several pathways with which AP and negatively affect the cardiovascular system. The most immediate of which is probably an imbalance in the Autonomic Nervous System (ANS) caused by direct inflammation and oxidative stress in the respiratory system. The second most immediate pathway is systemic inflammation caused by Air Pollution. Finally, soluble AP compounds in the bloodstream also contribute to Cardiovascular Disease (CVD) by increasing inflammation and oxidative stress in the cardiovascular system [25, 34].

The link between Air Pollution and cardiovascular effects started being made during the twentieth century, given a series of incidents (like London's 1952 killer-smog) that happened in the urban areas of industrialized countries. Nowadays, Cardiovascular Mortality (CVM) has been shown to be intricately connected to AP. In fact, in a 2013 review indicated that an annual increase of  $10\mu\text{g}/\text{m}^3$  in fine PM and  $\text{NO}_2$  led to an increase of 11% and 13% respectively in terms of CVM and premature atherosclerosis, in spite of absolute AP concentrations were maintained below the European policy-recommended thresholds. Road traffic exposure studies have reported similar findings, with subjects having increased coronary calcium scores [35].

Arrhythmia is one of the other cardiovascular issues that might be caused by AP. There is still some debate regarding whether or not there is a causal relationship between the two, but there have been several studies in which increased levels of Air Pollution were correlated with arrhythmia-related hospital admissions. Moreover, there seems to be a correlation between low heart rate variability and AP, which is considered a marker for ANS imbalance and an important risk factor for CVM[35].

The risk of stroke is also clearly exacerbated by the presence of increased levels of AP. In fact, it is currently thought that AP is responsible for about 29% of the burden of stroke, globally. Studies have shown that an increase of  $5\mu\text{g}/\text{m}^3$  in the annual  $\text{PM}_{2.5}$  concentration leads to a remarkable 19% increase in the risk of stroke, which was found to be more significant in non-smokers. A positive correlation was also found between gaseous pollutants ( $\text{no}_2$ , CO and  $\text{SO}_2$ ) concentration and the risk of stroke or

stroke mortality.

Short term effects of AP on the cardiovascular system seem to be predominantly the triggering acute coronary incidents. For instance, a positive correlation was found between short term increases in AP and non-fatal myocardial infarctions.

### 2.1.1.3 Gestational and developmental complications

Mammals are in their life's most vulnerable stage while they are still developing inside their mother's womb. This is the time when there is a greater rate of tissue expansion and creation, creating an enormous need for nutrients. These are supplied by the mother's blood, crossing the placenta and reaching the fetus through its umbilical cord. High rates of tissue formation and proliferation render the forming being unstable and therefore more susceptible to the appearance of some kind of morphological abnormality. At this time, there is no separation between the mother's blood and the fetus, meaning that whatever chemical reaches the progenitor's bloodstream also reaches the growing fetus. If the mother is exposed, so is the fetus [25].

There are numerous chemicals that can affect the female reproductive system, of which some are habitual components of AP. They have been associated to several highly adverse affects, and interfere with such things as the processes by which the body is able to produce eggs, or other processes that enable the formation of a single cell by the union of the sperm and the egg (the zygote). After conception, AP has been known to reduce uterine nurturing capabilities, and hinder the new being's development. Some of them are even teratogens, meaning that they induce birth defects. Figure 2.2 illustrates the kind of defects that come with exposure, according to the time at which the mother was exposed.

There are already several studies that correlate higher AP exposure levels to birth defects or the probability of negative outcomes. For instance, in [36], researchers have studied the association between AP exposure levels (for the mother) and the appearance of premature Small for Gestation Age (SGA) by collecting more than 40000 births in Changzhou Maternity (China) and studying the mother's typical environment. This study has found a positive association between SGA and exposure to PM<sub>2.5</sub> in two or three pollutants models of AP (with NO<sub>2</sub> and Sulfur Dioxide (SO<sub>2</sub>)), during the third trimester of gestation. Another, perhaps more comprehensive study, was performed using Swedish data from 1997 to 2007, and found that there was a positive association between O<sub>3</sub> exposure and the appearance of pre-eclampsia (a potentially deadly complication of pregnancy), estimating that about 1 in 20 pre-eclampsia cases were caused by AP [37].

Besides uterine development compromises, birth defects and reproductive difficulties, Air Pollution has also been associated with hindrances to the child's neurodevelopment. In a New York study was able to associate lower levels of mental development

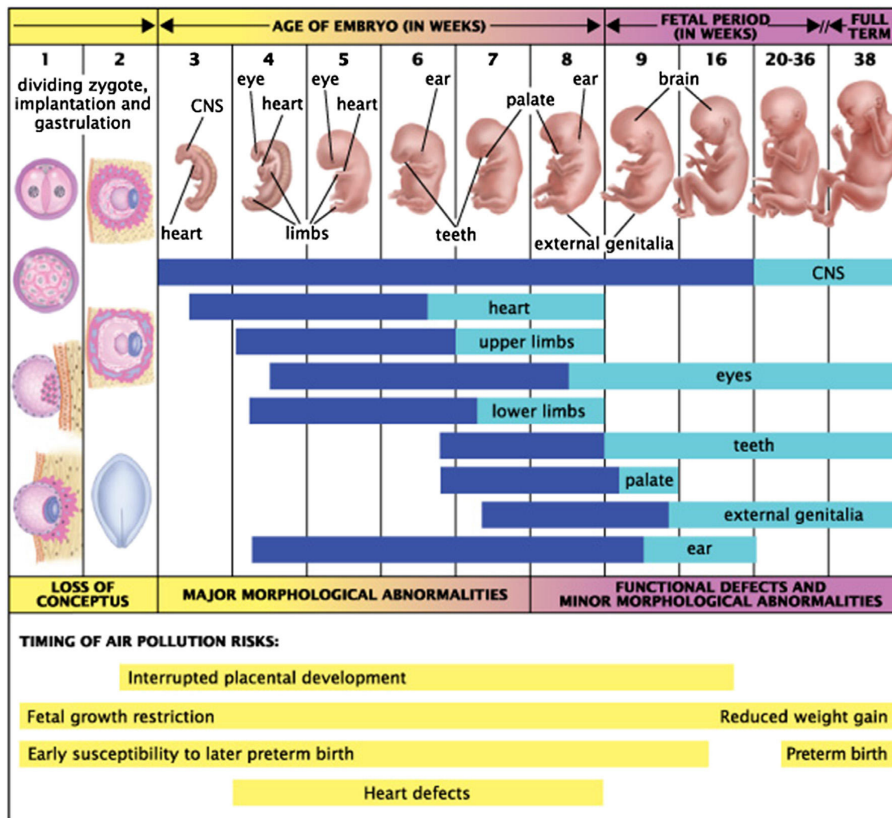
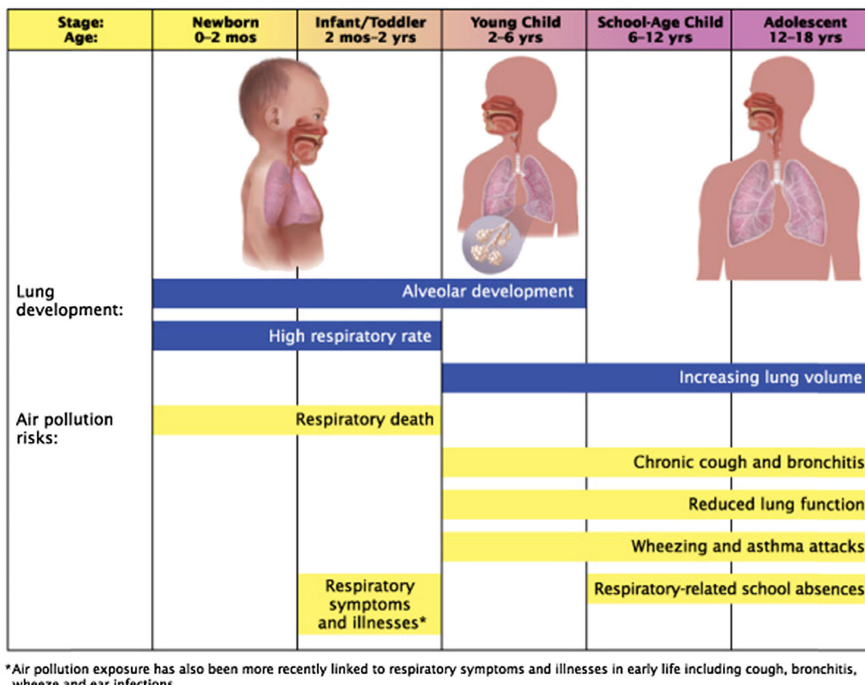


Figure 2.2: Possible abnormalities caused by AP exposure *in utero*. Notice that time of exposure is of critical importance [25].

at age 3, in African-American children with valid prenatal Polycyclic Aromatic Hydrocarbons (PAH) exposure data. In another study from the neighboring Boston, AP was associated with generally lower cognitive test scores, even when correcting for several influencing factors. On a different level, AP was shown to produce significant delays in the central conduction times of Brainstem Auditory-Evoked Potentials (BAEP) tests in children, indicating that there might be important repercussions of AP to vestibular and auditory development.

Although most other systems are affected by AP, it does have a particularly heavy toll on the respiratory development. This is because the lungs are not completely developed at birth, and are only finished in the late teens. The level to which AP affects the respiratory system development varies greatly with the stage of life in which the effect is produced, and severity is also very varied. Acute negative effects range from respiratory death to chronic cough [25]. Moreover, childhood (and prenatal) exposure to AP has been associated with the emergence of conditions such as COPD and asthma.



\*Air pollution exposure has also been more recently linked to respiratory symptoms and illnesses in early life including cough, bronchitis, wheeze and ear infections

Figure 2.3: Developmental stages of the lung throughout life vs the risks of AP exposure in each stage [25].

#### 2.1.1.4 Neurological disorders

The brain and the **Central Nervous System (CNS)** were one of the last to be included in the range of organs that are affected by **AP**. While the effects of **AP** on the respiratory and cardiovascular systems are quite broad and include some "surprises", the fact that these systems were affected by **Air Pollution** was evident and expectable, given the type of exposure these systems endure. The **CNS**, on the other hand, has a more difficult to express relationship with **AP**, and has required more sophisticated methods to detect [25, 38]. It was in the beginning of this century that the first connections between **AP** and the emergence of neurological disorders started to be made, and from then on, we have progressed into thinking that not only are they related, but also that **AP** might be one of the key driving forces in the onset of certain neurological diseases, including the most dreaded of them all, Alzheimer's and Parkinson's [38, 39, 40].

The reason why **AP** is able to reach and damage the **CNS** is a continuation (or even an extension) of the ways in which it affects the cardiovascular system. By crossing the alveolar barrier into the bloodstream, **AP** acts as an oxidative stress source. As it can also do in lung tissue, **Air Pollution** creates some local proinflammatory effects in the cardiovascular system, affecting the vascular endothelium cells. This can lead to a systemic inflammatory status, which is accompanied by the production of proinflammatory cytokines (a type of message-protein that is used by organisms to trigger certain types of response, like inflammation [41]). Now, since blood vessels in the

brain are extremely responsive to this kind of message, their presence can activate cerebral endothelial cells and disrupt the blood-brain barrier [38].

In 2018, a consortium of several Spanish universities and researchers wrote a review detailing the until-then-published articles dealing with the neurological implications of AP [39]. This review identifies several articles that connect the long-term exposure to Air Pollution with adverse impacts on the brain and brain structures. *In vitro* and *in vivo* studies, focusing on traffic related emissions and their effect on gray matter cells, have found that these display significant alterations. On other studies identified by the review, it was shown that white matter, the myelinated part of the brain, is particularly sensitive to AP and its volume is significantly decreased both in the elderly and children, as consequence of prolonged exposure to it.

There are also several articles that show that there is an association between exposure to air pollutants and impairments on brain function. In Section 2.1.1.3, I have already mentioned a study that was conducted in New York, and that found that the children that they were using as subjects were found to have measurable cognitive deficits in comparison with children of the same age living in less polluted areas which are compatible with the affected areas of the brain that were detected through neuroimaging studies [39].

## 2.1.2 Air Pollution effects on ecosystems

citations - vallero and lovett + european report

The Earth is home to an almost unbelievable number of different ecosystems. The ubiquitousness of AP means that all of them are in some way or another affected by this problem. In general terms, the threat posed by AP to any given habitat is a function of its biodiversity, defined as the number of different living beings that inhabit a certain environment (in all biological kingdoms) [42]. Living beings within an ecosystem are like nodes in a graph, with many connections to any particular node. More biodiversity corresponds to a greater number of nodes and an even larger number of links, which means that there is a greater probability that some of those links become disrupted by Air Pollution in some way.

Water based environments are greatly affected by AP. Material deposition on the surface of the water can have serious consequences in terms of habitat conditions for holding life. In this regard, the most important air pollutants are NO<sub>2</sub> and SO<sub>2</sub>, which significantly decreases the water's pH. On its own, this represents a major problem. The acidifying effects of nitrogen and sulfur deposition became very pronounced in Scandinavia (among other places). Thousands of this territory's lakes, once teeming with wildlife, became effectively lifeless. Those that did not reach this point, have seen the number of fish living on their waters dwindle to numbers from which there may be no return [43]. Sulfur and nitrogen depositions also enrich surface waters, altering the solubility and other physical aspects on the surface of the water, which in turn

## CHAPTER 2. LITERATURE REVIEW

---

inevitably leads to disruptions in species abundance and diversity. Moreover, indirect effects may also take their tolls. For instance,  $O_3$  does not play any significant role in the chemical behavior of a water body, but it can influence the number of predators around this habitat, which will compromise the predator-prey balance of the aquatic environment [25, 44].

In terrestrial ecosystems, AP effects are not smaller in importance or complexity, and they are different for each type of being. To the Flora, AP can have a subtle to deadly effect, depending on variables like pollutant chemical species, exposure time, or plant life stage in which exposure happens. For instance,  $O_3$  is especially poisonous to plants. Even small concentrations of this gas will cause plant growth to decrease significantly. It enters the plant through the stomata and reduces photosynthesis through increased oxidative stress. Many times, although concentrations are not enough to outright kill the plant, they are enough to make them more susceptible to other attacks like pathogens, insects or environmental conditions. Ozone is commonly responsible for huge financial losses that come from the diminished agricultural yields. And while it is true that due to several policies, AP is in a clear downward trend since the 1980s in urban regions, it is also true that in many rural areas, these changes have been smaller or non-existent, making these losses even more relevant.

Forests are among the most susceptible environments to AP. They suffer from the previously described mechanisms of AP damage, like acidic deposition, but also suffer from other, less direct pollution risks. Emission of greenhouse gases can induce changes in humidity, temperature, and general climate profile of a forest. The combination of direct and indirect risks result in an exacerbation of both, leading to more and more forest losses due to Air Pollution. The damage done to forests all around the world is especially problematic given the biodiversity that these ecosystems contain within themselves. Rainforests in particular are thought to contain more than half of the world's terrestrial species. These species have many times adapted to a particular kind of microhabitat which only exists in the specific rainforest in which it lives. Changes in these specific conditions, whether caused by Air Pollution or any other cause, are leading to alarming extinction rates in forests and rainforests globally.

Of course it is not only the flora that suffers with Air Pollution. Direct implications of AP on animals approximate those that fall upon humans. We are an animal species, after all. Our main difference is the adaptation capabilities that our superior intellect grants us, which allows us to escape more or less unscathed for a longer period of time, and to combat what we cannot escape from in ways which are simply unaccessible to other animal species. So, although AP has direct effects on all animals that are exposed to it, ecosystem damage and eventual destruction remains the most perilous factor for this biological realm.

Could I get another source on this problem?

### 2.1.3 Air Pollution Sources

There are almost as many AP sources as there are pollutants. The first major division between these sources is whether they are natural or anthropogenic. However, this separation is not always clear, as one source can lead to another and boundaries become fuzzy within their own context. The most prominent example of such is the case of accidental fires. While they are most of the times classified as a natural source of AP, their origin lies most of the times in human activities. In this section, I will present a selection of the most important naturally occurring air pollutants and examples of how they have affected human lives throughout the times. The selection itself does not intend to be complete description of pollution sources, but rather paint a general picture of the subject.

#### 2.1.3.1 Natural Sources of Air Pollution

Although people, governments and institutions tend to speak far more seldomly of them than of their man-made counterparts, natural sources of air pollutant are not only abundant, but also important. One of the main natural sources of AP are volcanic eruptions. These phenomena are responsible for the emission of immense quantities of PM and gases such as SO<sub>2</sub>, Hydrogen Sulfide (H<sub>2</sub>S) and methane. Depending on the type of volcanic eruption, the emitted cloud of gas and PM can remain airborne for long periods of time, even disrupting modern life at times, namely in what concerns air travel. The last eruption to happen in Portuguese soil took place in the remote Azorian island of Faial. In September 1957, the Earth shook almost continuously for around two weeks. Finally, on the 27<sup>th</sup>, 100 m Northeast the Capelinhos islands, the sea was seen to boil and project vapor and volcanic material hundreds of meters into the air. In the following hours, the underwater volcano finally exploded, emitting large quantities of volcanic ash and gases into the atmosphere. The phenomenon lasted for more than a year, and the final ejection of lava took place in October 1958 (see Figure 2.4). The eruption had a significant social impact, in addition to its ecologic importance. In the end, 40% of Faial's population left the island as a result [25, 45].

Oceans are also a significant source of AP. Aerosol particles of salt are continuously emitted from these large masses of salt water, which damage many human created structures, namely metallic constructions. In certain parts of the world, another important source of Particulate Matter (especially because of its consequences in the inhabitants' daily life) are dust storms. The most famous of these events, and one of the most deadly storms in the recorded history of the US territory was the infamous *Black Sunday* dust storm. Starting on Palm Sunday, 14 April, this sky-blackening dust storm punished the peoples from the panhandles of Texas and Oklahoma, burying entire houses (see Figure 2.5) under the dust and destroying the livelihoods of thousands of Americans. Dust storms were an important part of the US history during the 1930s and led to the creation of the Soil Conservation Service, a branch of the US Department



Figure 2.4: Dramatic photograph depicting the Capelinhos' lighthouse, half a kilometer from the eruption site, surrounded by a cloud of ash PM, volcanic gas and water vapor with more than 1km in height[45].

of Agriculture [25, 46, 47].



Figure 2.5: House almost completely buried by the Black Sunday dust storm. Several houses were entirely swallowed during this storm, trapping people inside, as if a big blizzard had hit them. Unlike a blizzard though, there was nothing anyone could do to keep the dirt outside, and all surfaces were covered black [47].

Fires are also one of the largest sources of natural air pollution in the world. The uncontrolled burning of organic matter that is a large forest fire creates a large quantity of air pollutants that range from smoke to unburned (or partially burned) hydrocarbons, nitrogen and carbon oxides, and ash particles. Besides the obvious dangers of this kind of burnings for human life and activities, forest fires can also cause indirect damages, such as disruptions in supplies and travel due to reduced visibility [25].

Trees and forests in themselves are also responsible for a certain quantity of air pollution. Although they have the main part in the carbon dioxide conversion into oxygen, through photosynthesis, plants and trees are still the largest emitters of hydrocarbons in the planet, as attested by the blue haze that is visible on top heavily forested areas, resulting from chemical reactions between **Volatile Organic Compound (VOC)**s produced by the trees. This counter-intuitive fact was in the origin of the infamous Ronald Reagan speech in which he "blamed" trees for much of **AP**, in a time when anthropogenic **AP** was at its apogee in the US and Europe. Plants are also the emitters of another kind of **PM**, which is of particular importance both to themselves and humans, which are the pollens. This is a bio-aerosol - a type of aerosol that is or was part of a living being - associated with a number of diseases [25].

Finally, I will discuss Radon gas. This is a natural occurring radioactive gas that is part of the radiative decay of Uranium present in all rocks. Although chemically inert,

Radon is radioactive and, as all radioactive substances, emits particles when it decays. Although present virtually everywhere, outdoor concentrations of Radon are typically too small to cause any problems. The problem with this gas comes essentially from indoor concentrations, namely at home. Being a gas, Radon is able to enter people's houses, exposing the inhabitants. Prolonged exposure to Radon gas is the second biggest cause of lung cancer and authorities estimate that between 3 and 14% of lung cancer cases are caused by this gas. In Portugal, Radon concentrations were found to be below the European prescribed limit in two thirds of the houses in a 2001 study, but in 17% of the cases, concentrations were not only above this limit, but also over the highest tolerable limit [25, 48, 49].

### 2.1.3.2 Anthropogenic Sources of Air Pollution

Air Pollution that originates from human activities is called anthropogenic. Since the first industrial revolution, mankind has been using more and more resources to fuel our progress and continuously improving way of life. Of course, the consumption of natural resources has some unpleasant and sometimes dangerous consequences. The most important of which, looking from the lens of this thesis, is the incredible increase in the levels of AP. If one had any doubts whatsoever, all it would take would be a look into the atmospheric CO<sub>2</sub> concentration chart (Figure 2.6) from a few centuries back to the current day to completely dissipate them.

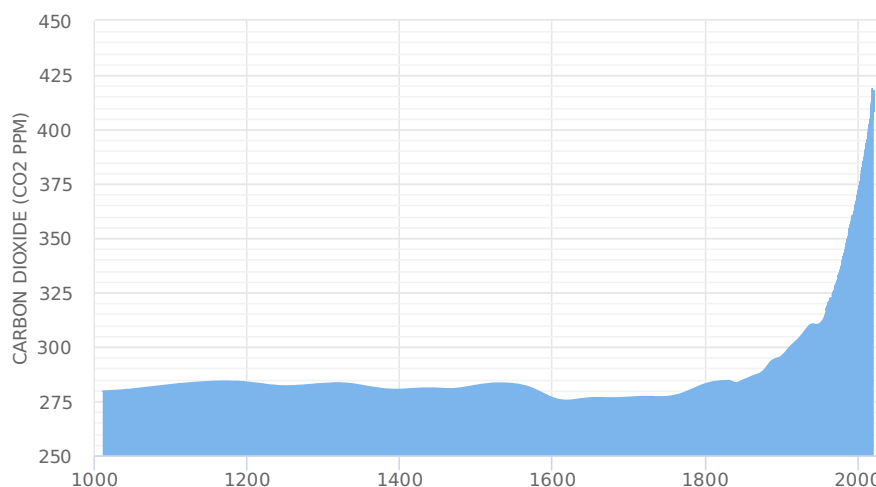


Figure 2.6: CO<sub>2</sub> atmospheric concentrations since the year 1000. Note the seemingly exponential increase since the 1800s. Plotted and published by the 2 Degrees Institute [50] with data from ice cores [51] and in situ monitors [52].

There are literally hundreds of sources of AP, but it is possible to categorize them into 4 main *families*: industrial processes, energy (includes transportation), agriculture and forestry, and waste. Of these 4 broad categories, as displayed in Figure 2.7. The most prominent is without a doubt the energy sector, although we also have to

bear in mind that any and all combustion used in the other sectors is counted as energy production [20, 53].

table with major pollutants?

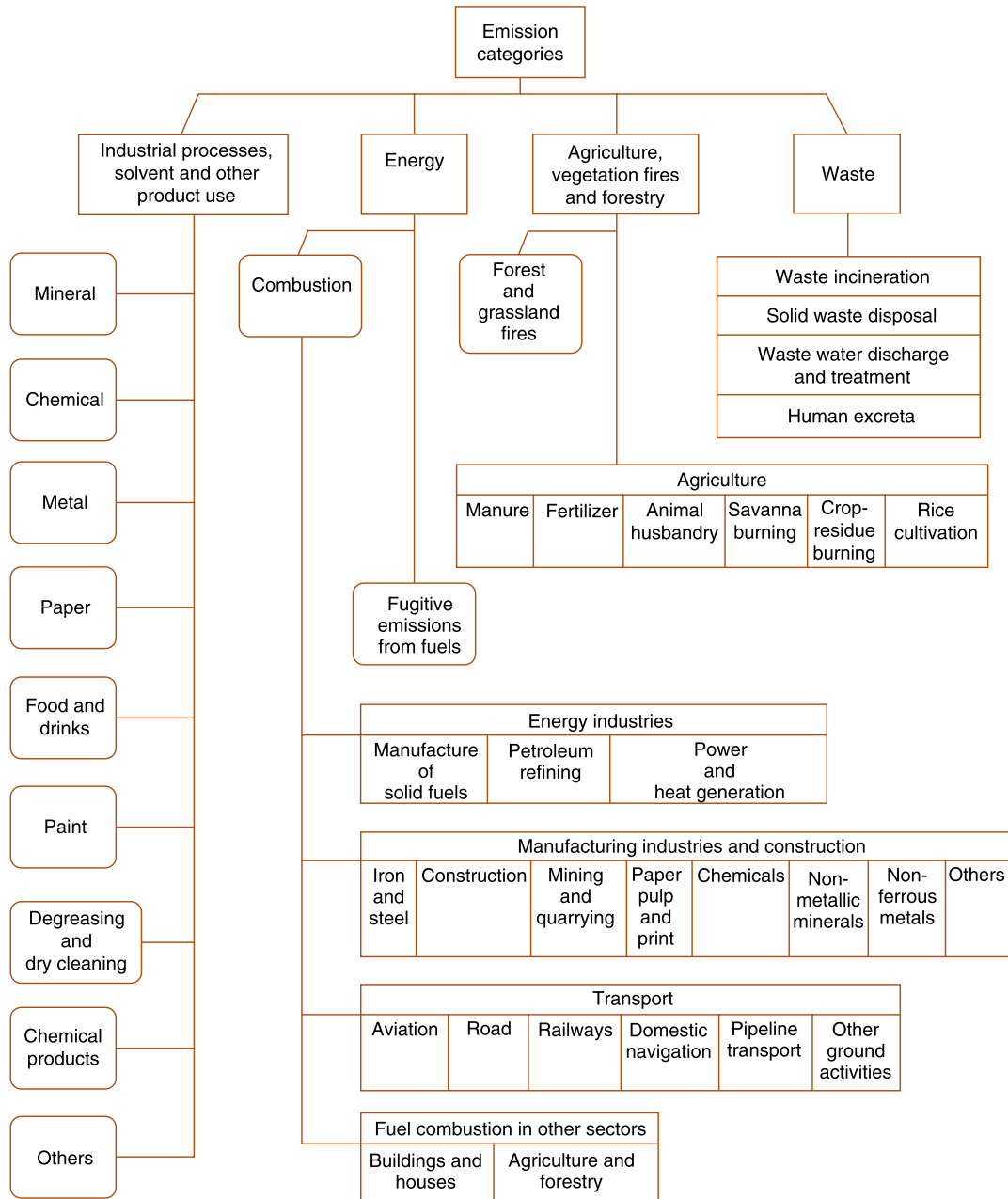


Figure 2.7: Schematic presentation on the sources of anthropogenic pollution and its categorisation according to the IPCC. Adapted from [20]

From 2002 to 2011, fossil fuel combustion has been responsible for an average of 8.3 petagrams of carbon per year. This truly gigantic carbon footprint is in its majority explained by the world's energy needs, which are ever increasing up to now. In 1990, total energy demand was situated at 356 quadrillion British Thermal Unit (BTU),

## CHAPTER 2. LITERATURE REVIEW

---

having grown to 410 quadrillion BTU in 2010. In 2020, energy demand estimates are located at 600 quadrillion BTU, of which almost a quarter was expended by China [20].

It is important that we focus a little bit more on the Chinese case. It is now somewhat near commonsense to regard China as the factory of the world, and this of course is tied to Chinese energy consumption and production. On the same line of reasoning, this must mean that in some way, the country's energy expenditure is connected to the amount of financial resources that it produces, the GDP. Looking at the plots in Figure 2.8, one can see that all these numbers are highly correlated. When we ponder on the case of Chinese AP, and wonder why has this problem not been addressed previously, given its imposing dimensions and growing importance, one must take into account that, given the indirect importance of AP on Chinese people's gains, it is highly likely that the country's governments will be reluctant to decrease it in any expedient form [20, 54, 55].

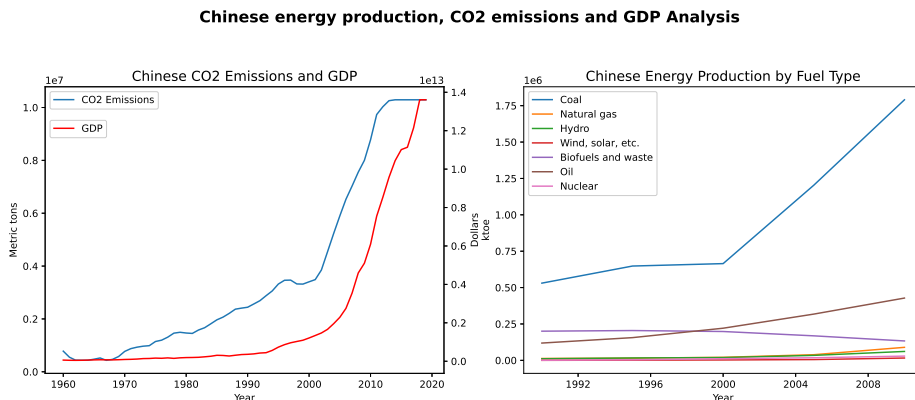


Figure 2.8: Chinese energy production, GDP and CO<sub>2</sub> emissions. Data collected from the World Bank and International Energy Agency websites [54, 55]

Another important conclusion that we can take from the plot in Figure 2.8 is that China has a large and historical dependence on the use of coal as fuel for energy production. This adds to the problem described in the above paragraphs, as coal is the single most damaging fossil fuel available. Not only does China get most of its energy from coal burning, but is also responsible for more than half of the worlds production and consumption of this substance (see Table 2.2).

**Internal Combustion Engine (ICE)** are the single most important means for powering human transportation. Almost every vehicle in the world uses a kind of ICE. These motors operation is an application of the Otto cycle, in which the chemical energy in the fuel is converted to mechanical energy. These engines are as ubiquitous as the fossil fuels that have powered them since the beginning of the automobile revolution, in the early 20<sup>th</sup> century. Fossil fuels have several features that make them ideal to power our vehicles. Their energy density is generally high, they are incredibly safe to manipulate and use, and fossil fuel infrastructure can be found in almost every far

Table 2.2: Global energy production, divided according to the fuel used to obtain it and the production country.

<b>Country</b>	<b>Liq. Fuel</b> (M barrels / day)	<b>Coal</b> (BTU)	<b>Nat. Gas</b> (T cu. ft)	<b>Renew.</b> (BTU)	<b>Nuc.</b> (b kWh)
<b>China</b>	10,6	80,6	5,1	10,6	93
<b>USA</b>	18,5	17,3	25,5	7,8	769
<b>Europe</b>	14,4	12,5	17,9	11,7	837
<b>Middle East</b>	16	0,1	14,8	0,2	1
<b>India</b>	3,6	12,6	2,1	3,5	30
<b>Russia</b>	3,4	4,5	15,7	1,7	166
<b>Africa</b>	3,5	4,3	2,7	4,7	12
<b>Brazil</b>	3,3	0,5	1,1	6,8	15
<b>World</b>	91,4	153,9	120,8	63,7	2345

corner of the Earth. However, using them releases a number of gaseous and particle-condensed side products into the atmosphere, and this makes traffic one of the most important sources of AP. For instance, traffic pollution is the main responsible for human exposure to Nitrogen Oxides (NO<sub>X</sub>) gases. Without countermeasures, gasoline ICE equipping passenger vehicles emit around 1.8 g/km of these gases, while diesel emits 2.8 g/km and Liquefied Petroleum Gas (LPG) around 2.1 g/km. On heavy duty engines, like on trucks and tractors, these figures skyrocket to 14.7 g/km for diesel engines and around 5.1 g/km for LPG [20].

Energy production (including transportation) is clearly the single largest contributor to global AP. This does not mean that other human activities do not pollute or produce air pollutants. Pollutant contributions from the industry, the agricultural activities and waste disposal are also non-negligible. In fact, industries around the world are responsible for the production and emission of all the criteria pollutants. It is important to single out one particular activity, which is the burning of forest for land-use changes. Carbon Monoxide (CO) emissions for this purpose are very high due to the nature of the burning material, which emits more than 50 times more CO than fuel or coal [20].

### 2.1.3.3 The European Case

Europe has for long been on the forefront of the fight against AP emissions. The European Union has put in place a number of policies aiming at cutting (or even eliminating) emissions of human health compromising pollutant components. Few places in the world have been so demanding regarding their environmental practices, and numbers are a clear reflection of these adaptation efforts. In their 2019 report, the EEA state that European emissions have globally declined, and have been declining since at least the year 2000. Moreover, and in contrast with China's case, the GDP does not seem to be connected to AP emissions. As can be seen in Figure 2.9, emissions are decoupled from economic growth, as there are now less emissions per GDP unit

than before [56].

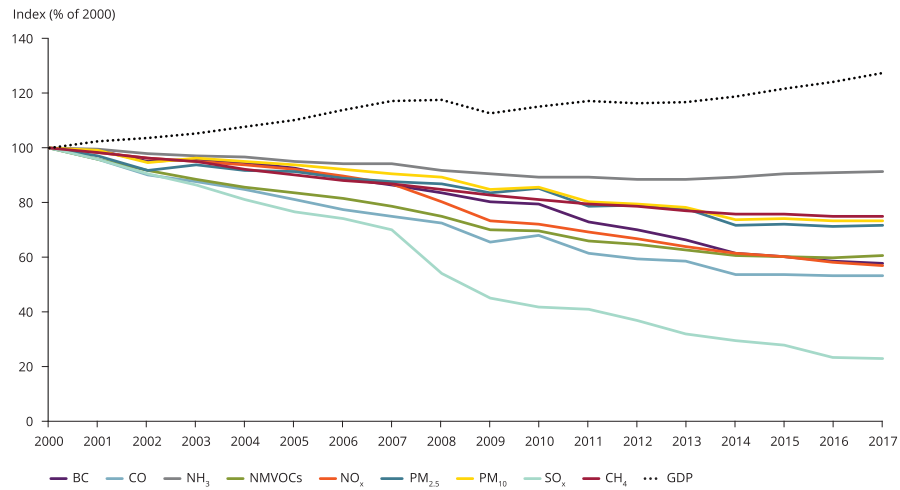


Figure 2.9: General trends for European emissions. Data presented in % emissions of year 2000. Note the downward global trend in pollutant emissions, and its decoupling with the European GDP [56].

If one extends this analysis further, and separates emissions by using their origin, the trends are approximately the same: except for Ammonia (NH<sub>3</sub>) (a side product of agricultural activities) a clear reduction is present in all sectors. These results can be seen in Figure 2.10 and were presented in [56].

### 2.1.4 Detecting and Monitoring Air Pollution

There is no doubt that AP is a global threat that affects everyone, both in personal terms (through the degradation of their health) and in societal terms, through the investments and limitations that we as a whole have to commit to in order to prevent larger, unmanageable problems. Reducing AP is a priority and a requirement for today's modern societies. This demands immediate and effective actions, which in turn imply that we have a solid and profound understanding of how pollutants are created, transported and transformed in the atmosphere. The scale on which these interventions must be conducted requires them to be made on a concerted and collaborative manner, and always leveraged by technological development [56]. Many of the air pollutants cannot be detected solely by our senses, or even if they can is at already dangerous concentrations. Technology is therefore a prerequisite to our fighting the problem of Air Pollution [25].

Pollution monitoring is itself based on the ability of a given measurement method to determine concentrations for trace gases, aerosols or radiation quantities. As with many other test techniques, in various fields, pollution monitoring techniques have three very important aspects to verify. The first of which is sensitivity, and also the most demanding. Important trace gases in atmospheric chemistry have sometimes

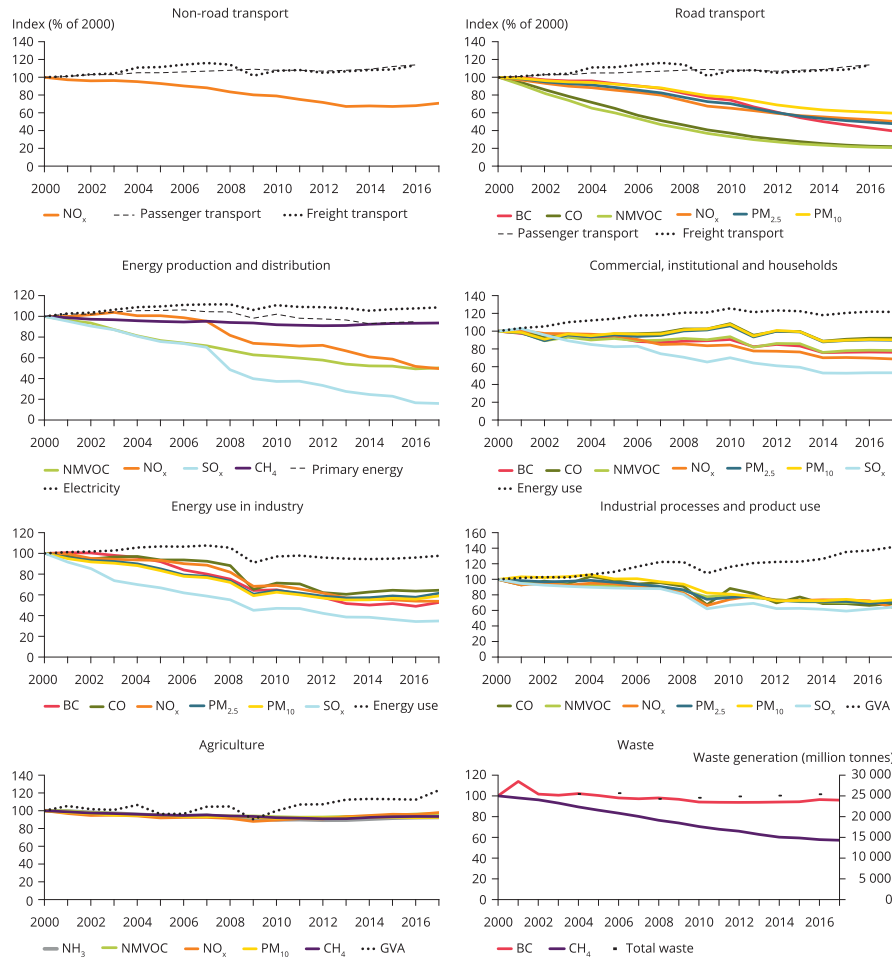


Figure 2.10: European emissions divided by activity sector. The global decreasing trend is confirmed, as industries all around are producing less and less AP with the passing years [56].

vestigial concentrations, and the ability to correctly detect them is many times a technical challenge. The second most important is specificity, which is the ability of an atmospheric measurement to measure each compound independently, without a component influencing another component's measurement either positively or negatively. Finally, any usable monitoring technique must be sufficiently precise as to provide valid measurements.

Air Pollution monitoring techniques and devices are too many to address them all in this document. Besides, the physical principles involved are completely different from one to another, making it very difficult to make a broad generalization, other than the fact that they can be divided into local and remote sensing devices. The gold standard for air quality measurements remains those techniques in which a sample is collected in the field and then taken to the laboratory to be analyzed by very powerful analytical methods such as chromatography or mass spectroscopy. While undoubtedly providing the most accurate representation of the air composition at the time and

place the sample was collected, it is also true that this method's results are too slow to use regularly in the field.

Another very important air quality monitoring method is the use of electrochemical sensors. The first variants (wet cells) of this kind of sensor became very popular in the field of industrial hygiene, where they were applied in many portable flue gas analyzers. They were very attractive to companies worldwide given their potential for very low costs in comparison to optical or other more complex techniques. Apart from the oxygen wet cell sensor, that has a slightly different configuration, these electrochemical devices are comprised of three electrodes - a sensing electrode, a counter electrode and a reference electrode - separated by a thin layer of electrolyte. The gas that is diffused to the surface of the electrode is either oxidized or reduced, thus changing the systems electrical properties, in a way that is then captured by an amplification circuit.

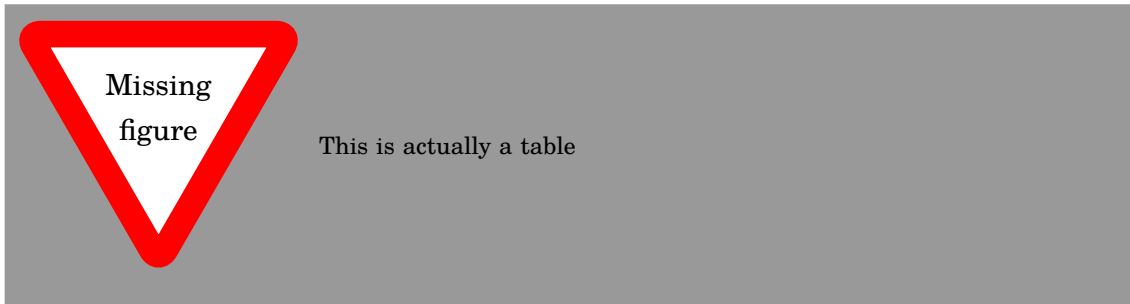
Wet cell electrochemical sensors were the precursors of the now more common solid state sensors. These sensors are the ones that we see in every subterranean parking lot, measuring several traffic related gases such as  $\text{CO}$ ,  $\text{CO}_2$  or  $\text{NO}_2$ . In general semiconductor gas detectors are comprised of two modules: a receptor and a transducer (see Figure 2.11). The receptor has in its composition a material (or set of materials) that, in contact with the target gas, induces a change in the systems inherent properties (work function, dielectric constant, resistance, etc.) or emits heat or light. The transducer is a device or circuit that converts the receptor's changes into an electrical signal. There are 5 types of semiconductor sensors, according to the material from which the transducer is made. These types are enumerated in Table 2.3.



Figure 2.11: Semiconductor electrochemical sensor basic structure. There are many examples of this type of sensors, but in general they follow this architecture.

Optical (spectroscopic) systems are fundamentally different from the other techniques that have already been presented. They can be used to perform remote sensing measurements (as far as being used for measurements aboard satellites). In the last few decades, these techniques have gained a lot of ground in atmospheric research, due to their high sensitivity and specificity and the universality of their applicability. Spectroscopic methods are based on Lambert-Beer's law (see Section 2.2 for a more thorough explanation), and make use of the fact that the way in which gases interact

Table 2.3: Categorization of semiconductor gas sensors. The type of transducer and receptor dictates the type of the sensor.



with light is well known and follows an exponential expression. There are many spectroscopic techniques for measuring AP. Selecting one requires careful consideration of a number of factors like the target gases, optical path arrangement, type of light source, etc. Figure 2.12 provides several examples of optical measurement methods, and how they can be divided.



Figure 2.12: There are many spectroscopic techniques for atmospheric trace gas concentration measurement. Although several are depicted here, keep in mind that this is not an exhaustive list and is meant as an example repository.

One of the most important atmospheric analysis methods, and especially in what concerns this document, is **DOAS**. While it is based on the same mathematical formulation as the other spectroscopic methods, it is also based on other factors, which shall be discussed in Section 2.2.

## 2.2 DOAS

Differential Optical Absorption Spectroscopy is a well established absorption technique that is widely used in the field of atmospheric studies [14]. In this section, I present a short introduction to the field, extracted from [3], an article we have published in 2017, marking the conclusion of the initial studies for this PhD thesis.

There are two main families of **DOAS** assemblies, with different goals and capabilities:

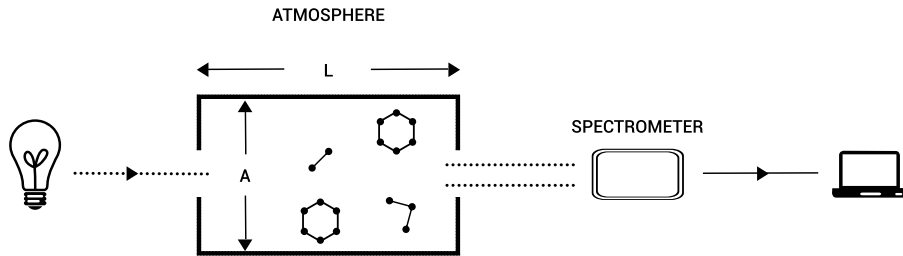


Figure 2.13: Active DOAS schematic.

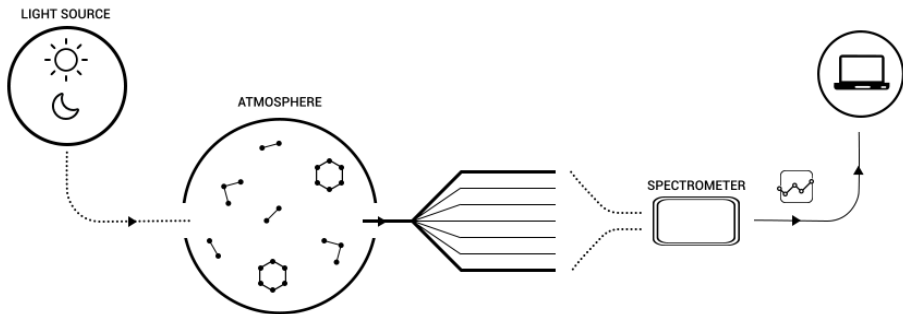


Figure 2.14: Passive DOAS schematic.

- Active systems, of which a simple illustration is presented in Fig. 2.13, are characterized by relying on an artificial light source for their measurements. A spectrometer at the end of the light path performs spectroscopic detection. Active DOAS techniques are very similar to traditional in-lab absorption spectroscopy techniques [14];
- Passive DOAS techniques, illustrated in Fig. 2.14, use natural light sources, such as the Sun and the moon, in their measurement process. An optical system is pointed in certain elevation and azimuth angles and sends the captured light into a spectrometer, connected to a computer. The system returns the total value of the light absorption in its path [14, 15].

DOAS itself is based on Lambert–Beer’s law, which can be written as [14]

$$I(\lambda) = I_0(\lambda) \cdot \exp(-\sigma(\lambda) \cdot c \cdot L), \quad (2.1)$$

Where  $\lambda$  is the wavelength of the emitted light;  $I(\lambda)$  is the light intensity as measured by the system;  $I_0(\lambda)$  is the intensity of the light as emitted by the source; and  $\sigma(\lambda)$  is the absorption cross section of absorber, which is wavelength dependent;  $c$  is the concentration of the absorber we want to measure.

This law allows the definition of optical thickness ( $\tau$ ) [14]:

$$\tau(\lambda) = \ln \left( \frac{I_0(\lambda)}{I(\lambda)} \right) = \sigma(\lambda) \cdot c \cdot L. \quad (2.2)$$

In a laboratory setting, Eq. (2.1) or (2.2) can be used to directly calculate an absorber's concentration, provided there is knowledge of its cross section. In the open atmosphere, however, absorption spectroscopy techniques are far more complex. On one hand,  $I_0(\lambda)$  is not accessible since we measure from inside the medium we want to measure. On the other hand, there are several environmental and instrumental effects that influence measurement results. These effects include the following [14].

- Rayleigh scattering is due to small molecules present in the atmosphere and is heavily influenced by wavelength (hence the blue colour of the sky).
- Mie scattering is caused by particles and larger molecules suspended in the atmosphere and is not very dependent on the wavelength (hence the white colour of clouds).
- Instrumental and turbulence effects are the instrument's transmissivity and atmospheric turbulence in the optical path also limit light intensity.

In addition, we also have to take into account that, in the atmosphere, there are a number of trace gases that interfere with passing light.

Another aspect worth mentioning is that our device is never pointed directly at the light source (the Sun) but always processes light that has been scattered at some unknown point in the optical path. This means that the light that reaches our detector is only the scattered fraction of the sunlight, depending on the system's position and geometry, as well as wavelength.

The expansion of Lambert–Beer's equation to include all these effects results in Eq. (2.3).

$$\begin{aligned} \epsilon_{TG}(\lambda, s) &= \sum_i \sigma_i(\lambda, s) \cdot c_i(s) \\ I(\lambda) &= I_0(\lambda) \cdot A(\lambda, \dots) \cdot S(\lambda) \cdot \\ &\quad \cdot \exp \left[ - \int [\epsilon_{TG}(\lambda, s) + \epsilon_M(\lambda, s) + \epsilon_R(\lambda, s)] \right] \end{aligned} \tag{2.3}$$

Where  $A(\lambda, \dots)$  is the fraction of scattered light that reaches the device,  $S(\lambda)$  represents instrumental and turbulence effects,  $\sigma_i(\lambda, s)$  is the absorption cross section of absorber  $i$ ,  $c_i$  is the concentration of absorber  $i$ .  $\epsilon_{TG}(\lambda, s)$  is the absorption by the  $i$  trace gases,  $\epsilon_R(\lambda, s)$  represents Rayleigh's extinction coefficient and  $\epsilon_M(\lambda, s)$  represents Mie's extinction coefficient.

The interest of this equation lies within the retrieval of  $c_i$ , a given absorber's concentration. Since the integral is taken along the total atmospheric path of the measured

photons, and considering that their cross sections do not vary significantly in atmospheric conditions, it is possible to define the concept of slant column, which is of great importance [15].

$$\text{SC}_i = \int c_i(s)ds \quad (2.4)$$

This quantity, as Eq. (2.4) shows, equals the integral of an individual absorber's concentration along the atmospheric optical path of relevance.

Now, without knowledge of  $I_0(\lambda)$ , these equations cannot give us absolute concentration values. We can, however, use another scattered light spectrum as reference in Eq. (2.2). Instead of absolute densities, this will yield relative changes in the atmosphere. We thus arrive at Eq. (2.5).

$$\begin{aligned} \ln\left(\frac{I_{\text{ref}}}{I}(\lambda)\right) &= \ln\left(\frac{A_{\text{ref}}}{A}(\lambda, \dots)\right) + \ln\left(\frac{S_{\text{ref}}}{S}(\lambda)\right) \\ &\quad + \sum_i (\sigma_i(\lambda) \cdot \Delta \text{SC}_i(\lambda)) + \Delta \tau_M(\lambda) \end{aligned}$$

Where  $\Delta \text{SC}_i$  is the relative slant column of absorber  $i$ ;  $\Delta \tau_M$  is the relative Mie scattering term, integrated to its optical thickness; and  $\Delta \tau_R$  is the relative Rayleigh scattering term, integrated to its optical thickness.

This is where the principle of DOAS is applied. Instrument features, scattering and other atmospheric effects have broad absorption spectral profiles, which vary slowly with wavelength. Several trace absorbers have narrow and rapidly varying spectral signatures in at least a small section of the spectrum. By using Eq. (2.5), we can separate these contributions [57].

$$\sigma(\lambda) = \sigma'(\lambda) + \sigma_0(\lambda) \quad (2.5)$$

Here, the broad part of the optical thickness ( $\sigma_0(\lambda)$ ) can be separated from the narrow part ( $\sigma'(\lambda)$  – differential) by approximating it by a low-order polynomial, resulting in Eq. (2.6).

$$\ln\left(\frac{I_{\text{ref}}}{I}(\lambda)\right) = \sum_{i=1}^n \sigma'_i(\lambda) \cdot \Delta \text{SC}_i + \sum_{j=0}^m a_j \cdot \lambda^j \quad (2.6)$$

Where  $\sum_{i=1}^n \sigma'_i(\lambda) \cdot \Delta \text{SC}_i$  is the differential part (narrowband, rapidly varying with wavelength) and  $\sum_{j=0}^m a_j \cdot \lambda^j$  is a low-order polynomial, used to remove the broadband spectral features resulting from atmospheric and instrumental phenomena.

In practice, the mathematical solving of Eq. (2.6) is not enough since it does not account for the Ring effect or the non-linearities that result from stray light and wavelength shift in measured and cross-section spectra.

The Ring effect is a consequence of rotational Raman scattering: molecules in the atmosphere do not absorb photons in a purely elastic (Rayleigh scattering) fashion. A

small portion of the light–matter interaction is in fact inelastic [15, 58]. This changes the light source frequencies as seen from the detector. This phenomenon was first noticed by Grainger and Ring in 1962. At the time, they noticed that the well-known Fraunhofer lines would slightly change when one observed them by using moonlight instead of scattered daylight [59].

From the occurrence of these phenomena, it results that the mathematical procedure for DOAS measurements consists in solving a linear and a non-linear problem. The linear problem is solved by writing Eq. (2.6) in its matrix form:

$$\tau = \mathbf{A} \cdot X. \quad (2.7)$$

$\mathbf{A}$  is an  $m \times n$  matrix, with its columns being the differential cross sections  $\sigma_i'(\lambda)$  and the wavelength powers taking the polynomial  $P(\lambda) = \sum_{j=0}^m a_j \cdot \lambda^j$  into account. Since the number of lines in  $A$  is much larger than the number of columns, the system is overdetermined and, in this case, we must use methods to numerically approximate a solution. It is common to use the least-squares approach, in which the best solution is the one that minimises  $\chi^2 = [\tau - A \cdot X] \cdot [\tau - A \cdot X]^T$ .

While the Ring effect is treated as a pseudo-absorber, a synthetically produced [60] cross section that is fitted just like any other absorber, non-linearities are addressed by applying Levenberg–Marquardt’s approach to non-linear fitting problems to Eq. (2.8) [15, 61]:

$$\ln \left( \frac{I_{\text{ref}}(\lambda)}{I(\lambda + \text{shift}) + \text{offset}} \right) = \sum_{i=1}^n \sigma_i'(\lambda) \cdot \Delta \text{SC}_i + \sum_{j=0}^m a_j \cdot \lambda^j \quad (2.8)$$

Where shift and offset, which represent spectral wavelength shifts and stray light offsets, respectively, are responsible for the non-linear character of the problem.

## 2.3 Tomographic algorithms and reconstruction techniques

### 2.3.1 Introduction

Tomography is the cross-sectional imaging of an object through the use of transmitted or reflected waves, captured by the object exposure to the waves from a set of known angles. It has many different applications in science, industry, and most prominently, medicine. Since the invention of the Computed Tomography (CT) machine in 1972, by Hounsfield [6], tomographic imaging techniques have had a revolutionary impact, allowing doctors to see inside their patients, without having to subject them to more invasive procedures [7].

Mathematical basis for tomography were set by Johannes Radon in 1917. At the time, he postulated that it is possible to represent a function written in  $\mathbb{R}$  in the space

of straight lines,  $\mathbb{L}$  through the function's line integrals. A line integral is an integral in which the function that is being integrated is evaluated along a curved path, a line. In the tomographic case, these line integrals represent a measurement on a ray that traverses the Region Of Interest (**ROI**). Each set of line integrals, characterized by an incidence angle, is called a projection (see Figure 2.15). To perform a tomographic reconstruction, the machine must take many projections around the object. To the set of projections arranged in matrix form by detector and projection angle, we call sinogram. All reconstruction methods, analytical and iterative, revolve around going from reality to sinogram to image [7, 8, 9, 10, 11, 12].



Figure 2.15: A schematic representation of a projection acquisition. In this image, taken from [11], the clear line that comes down at a diagonal angle is a projection.

There are two broad algorithm families when it comes to tomographic reconstruction, regarding the physics of the problem. The problem can involve either non-diffracting sources (light travels in straight lines), such as the X-Rays in a conventional **CT** exam; or diffracting sources, such as micro-waves or ultrasound in more research-oriented applications [7]. In this document, I will not address the latter family, since I will not be applying them in my work. In the next few paragraphs, I will discuss the first family of algorithms, and describe how an image can be reconstructed from an object's projections when the radiation source is non-diffracting.

Let's consider the case in which we deal with a single ray of solar light entering the atmosphere at a given point. Since the atmosphere contains numerous absorbents and comparable atmospheric effects, the ray changes from the point where it enters the atmosphere to the point at which it is measured by a detector. Total absorption will depend on the pollutant species, their cross-section and their concentration, since it obeys Lambert-Beer's law. Looking from another angle, this absorption is also the line integral that we will use to reconstruct our image. With **DOAS**, it is possible to

### 2.3. TOMOGRAPHIC ALGORITHMS AND RECONSTRUCTION TECHNIQUES

---

measure several pollutants at the same time, but for simplicity (and since it is one of the most studied compounds in the field), let's consider that the single pollutant in our atmospheric mixture is NO<sub>2</sub>.

#### 2.3.2 Initial Considerations

The problem of tomographic reconstruction can be approached in a number of ways, depending mostly on the authors. In my literary search, I have found that Kak and Slaney [7] have certainly explained this problem in one of the clearer ways available. Therefore, I shall base the rest of my presentation in their writings, and complement with other authors' notes wherever necessary.

Considering the coordinate system displayed in Figure 2.16. In this schematic, the object is represented by the function  $f(x, y)$ . The  $(\theta, t)$  parameters can be used to define any line in this schematic. Line AB in particular can be written:

$$x \cdot \cos(\theta) + y \cdot \sin(\theta) = t \quad (2.9)$$

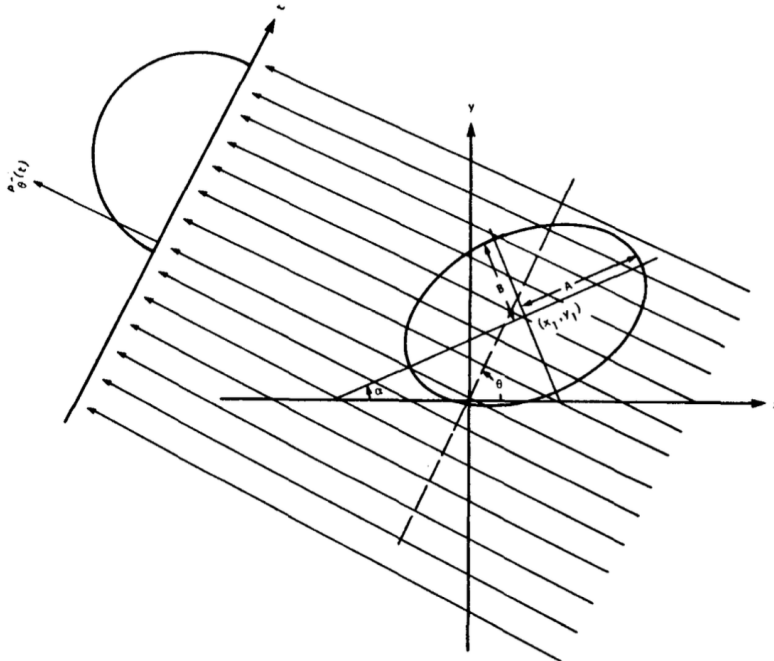


Figure 2.16: Schematic representation for coordinate setting. The image depicts a parallel projection setting [62].

And if we were to write a line integral along this line, it would look like Equation 2.10, the Radon transform of function  $f(x, y)$ :

$$P_\theta(t) = \int_{-\infty}^{\infty} f(x, y) \cdot \delta(x \cdot \cos(\theta) + y \cdot \sin(\theta) - t) dx dy \quad (2.10)$$

Where  $\delta$ , the delta function, is defined in Equation 2.11.

$$\delta(\phi) = \begin{cases} 1, & \phi = 0 \\ 0, & \text{otherwise} \end{cases} \quad (2.11)$$

As I have mentioned previously, a projection is a set of line integrals such as  $P_\theta(t)$ . Geometry plays a very important role in how the integrals are written and solved for reconstruction. The simplest case is the one where the set is acquired in a row, describing what is called a parallel geometry. Another more complex case is when a single point source is used as origin for all rays, forming a fan. This is called a fan-beam array. There are other possible geometries, but they fall out of the scope of this work and will therefore not be addressed any further.

### 2.3.3 The Fourier Slice Theorem

The Fourier Slice Theorem (**FST**) is the most important component of the most important algorithm in tomographic inversion, the Filtered BackProjection algorithm (**FBP**). **FST** is based on the equality relation between the two-dimensional Fourier Transform (**Fourier Transform (FT)**) of the object function and the one-dimensional **FT** of the object's projection at an angle  $\theta$ . Let's start by writing the 2D **FT** for the object function, Equation 2.12, and the 1D **FT** of projection  $P_\theta$ , in Equation 2.13.

$$F(u, v) = \int_{-\infty}^{\infty} \int_{-\infty}^{\infty} f(x, y) \cdot \exp[-j2\pi(ux + vy)] dx dy \quad (2.12)$$

$$S_\theta(\omega) = \int_{-\infty}^{\infty} P_\theta \cdot \exp[-j2\pi\omega t] dt \quad (2.13)$$

For simplicity, let's consider the 2D **FT** at the line defined by  $v = 0$  in the frequency domain. We rewrite the 2D **FT** integral as:

$$F(u, 0) = \int_{-\infty}^{\infty} \int_{-\infty}^{\infty} f(x, y) \cdot \exp[-j2\pi\omega ux] dx dy \quad (2.14)$$

Notice that  $y$  is not present in the phase factor of the **FT** expression anymore, and this means we can rearrange the integral as:

$$F(u, 0) = \int_{-\infty}^{\infty} \left[ \int_{-\infty}^{\infty} f(x, y) dy \right] \cdot \exp[-j2\pi\omega ux] dx \quad (2.15)$$

Now, the **bold** part of Equation 2.15 is similar to Equation 2.10. It is precisely that equation, considering  $\theta = 0$  and a constant value of  $x$ , as in Equation 2.16.

$$P_{\theta=0}(x) = \int_{-\infty}^{\infty} f(x, y) dy \quad (2.16)$$

This in turn can be substituted in Equation 2.15, finally arriving at:

$$F(u, 0) = \int_{-\infty}^{\infty} P_{\theta=0}(x) \cdot \exp[-j2\pi\omega ux] dx \quad (2.17)$$

And this is the one-dimensional **FT** for the projection at angle  $\theta = 0$ . Finally, the enunciation of the Fourier Slice Theorem:

***The Fourier Transform of a parallel projection of an image  $f(x, y)$  taken at angle  $\theta$  gives a slice of the two-dimensional Fourier Transform,  $F(u, v)$ , subtending an angle  $\theta$  with the  $u$ -axis (see Figure 2.17)***

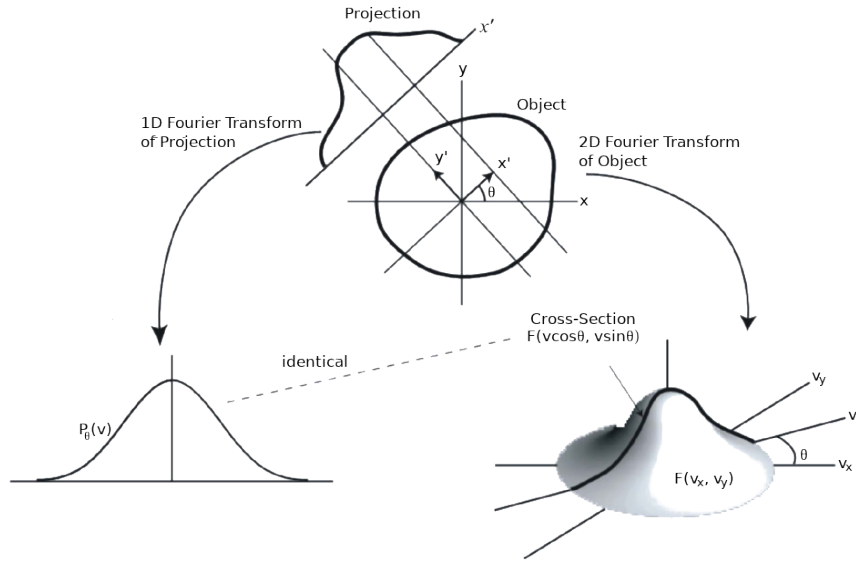


Figure 2.17: The **FST**, a schematic representation [63].

### 2.3.4 The Filtered BackProjection Algorithm

#### 2.3.4.1 The rationale for FBP

If one takes the **FST** into account, the idea behind the **FBP** seems to appear almost naturally. Say one has a single projection and its Fourier transform. From the **FST**, this projection is the same as the object's two-dimensional **FT** in a single line. A crude reconstruction of the original object would result if someone were to place this projection in its right place in the Fourier domain and then perform a two-dimensional **Inverse Fourier Transform (IFT)**, while assuming every other projection to be 0. The result, in the image space, would be as if someone had smeared the object in the projections direction.

What is really needed for a correct reconstruction is to do this many times, with many projections. This brings a problem with the method: smearing the object in all directions will clearly produce a wrong *accumulation* in the center of the image, since every projection passes through the middle (remember we are still talking about parallel geometry projections) and are summed on top of each other, but on the outer edges, this does not occur. If one does not address this, the image intensity levels

in the reconstructed image will be severely overestimated in the center and underestimated in the edges (due to normalization). The solution is conceptually easy: we multiply the Fourier transform by a weighting filter proportional to its frequency ( $\omega$ ) and that encompasses its relevance in the global scheme of projections. If there are  $K$  projections, then it is adequate for this value to be  $\frac{2\pi|\omega|}{K}$ . As an algorithm, **FBP** can be written as in Algorithm 1.

---

**Algorithm 1:** The Filtered BackProjection Algorithm

---

**Result:** A reconstructed image of the projected object.

```

for  $\theta \leftarrow 0$  to  $180$  by  $\frac{180}{K}$  do
    measure projection  $P_{\text{theta}}(t)$ ;
    FT( $P_{\theta}(t)$ ), rendering  $S_{\theta}(\omega)$ ;
    Multiply by  $\frac{2\pi|\omega|}{K}$ ;
    Sum the IFT of the result in the image space;
end
```

---

### 2.3.4.2 Fan Projections Reconstruction

Parallel projections, in which the object is scanned linearly from multiple directions, have the advantage of having a relatively simple reconstruction scheme. However, they usually result in acquisition times which are in the order of minutes. A faster way of collecting the data is one where all radiation emanates from a single point-source, which rotates around the target object (as well as the detectors). There are two types of fan-beam projections: equiangular and equally spaced. In this project, I have only worked with equiangular processes, so I will not include an explanation for equally spaced fan-beam projections. The reader may find this well described (much better than I would be able to) in [7] and [9].

Consider Figure 2.18. If our projection data were acquired through a parallel ray geometry, we would be able to say that ray SA belonged to a projection  $P_{\theta}(t)$ , in which  $\theta$  and  $t$  would be written:

$$\theta = \beta + \gamma \quad \text{and} \quad t = D \cdot \sin \gamma \quad (2.18)$$

In Equation 2.18,  $D$  is the distance between the source  $S$  and the origin  $O$ ;  $\gamma$  is the angle of a ray within a fan and  $\beta$  is the angle that the source  $S$  makes with a reference axis. Through these relationships one can *translate* the parallel projection's FBP algorithm to the fan-beam case, which involves several complex geometric transformations, although the overall rationale is exactly the same.

Another particularity of fan-beam projection data is the fact that they can be sorted into a parallel projection. For that, one starts with the premise that if one were to substitute the fan geometry for parallel beams, most of the fan-beam rays would also appear in some projection of the parallel setup. This re-sorting algorithm starts with

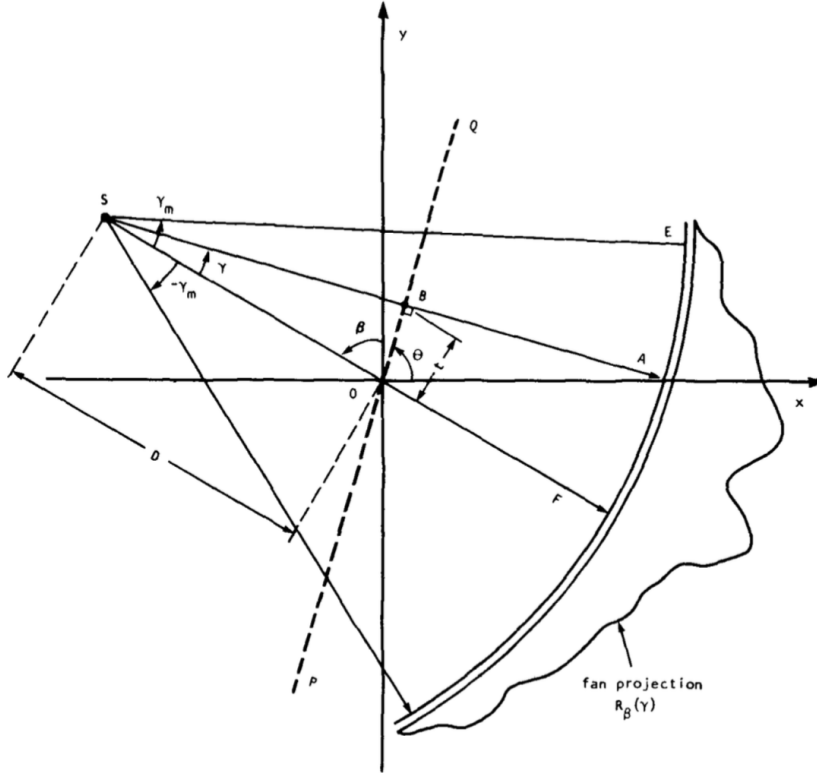


Figure 2.18: Schematic representation of an equiangular fan-beam projection, taken from [7].

**Equation 2.18.** Now, if we call a fan-beam projection taken at angle  $\beta$   $R_\beta(\gamma)$ , and a parallel projection taken at angle  $\theta$   $P_\theta(t)$ , one could thus write Equation 2.19, which can already be used to re-sort any fan-beam projection into parallel beam geometry.

$$R_\beta(\gamma) = P_{\beta+\gamma}(D \cdot \sin \gamma) \quad (2.19)$$

Let's call the angular interval between fan-beam projections can be written  $\delta\beta$ , and the angular interval of rays within each fan is written  $\delta\gamma$ . In the case that they are the same ( $\beta = \gamma = \alpha$ ), then it is the case that they can both be replaced by multiples of that interval in Equation 2.19, which becomes Equation 2.20.

$$R_{m \cdot \alpha}(n \cdot \alpha) = P_{m \cdot \alpha + n \cdot \alpha}(D \cdot \sin n \cdot \alpha) \quad (2.20)$$

Or, in non-mathematical notation, the  $n^{\text{th}}$  ray of the  $m^{\text{th}}$  radial projection ( $R$ ) is the same as the  $n^{\text{th}}$  ray in the  $(m+n)^{\text{th}}$  parallel projection. Although being much simpler than directly applying the **FBP** algorithm to the fan-beam projection data, this method has a limitation, which is the non-uniformity of the generated parallel projections. This can usually be corrected through interpolation [62].

## 2.4 DOAS Tomography

Measurement results from DOAS experiments are line integrals. They describe the number of molecules that is traversed by light in a given direction (the direction towards which the instrument is pointing). Thus, we can consider an experiment in which many of these instruments are covering a given geographic region of the atmosphere in either 2 or 3 dimensions. This is a tomographic inversion problem, with the projections being the DOAS measurements.

Atmospheric spectroscopy as the data generating part of a tomographic problem was first addressed in . In this paper, the authors propose a computerised method employing a tunable laser and a set of mirrors for the retrieval of concentration values in a two-dimensional circular region. Although not specifically concerning DOAS, the article established the basis for the technique. The most significant work corpus regarding DOAS Tomography came about only in the 21<sup>st</sup> century, when a group in the University of Heidelberg dedicated themselves to determining two-dimensional trace-gas concentration variations over a busy motorway in Germany - the BABII campaign.

During the course of this PhD, and as a credit requirement, I attended several courses, namely in the Computer Science Department. One of them, entitled "*Advanced Software Development*" had as final requirement the writing of a SMS on a topic of my choosing. This course happened around the time I was starting to develop a DOAS tomography system, and one of the requirements of that work was to study the state of the art to get a clear notion of how these systems were being applied and developed globally. Therefore, this was the topic that I chose for my SMS. The article (currently awaiting acceptance for publication) is transcribed in full in Appendix A, but I include a selection of the most important parts in this section.

An SMS is a systematic first approach to a subject, and are normally designed to retrieve a broad view of a given research area and quantify the amount of evidence that there is in that specific field. They share some similarities with Systematic Literature Review (SLR) but work with much broader data extraction and analysis procedures. Many times, they are used as guides for primary research [64]. In our case, the goal was to understand the literary landscape of DOAS tomographic applications.

Figure 2.19 denotes the whole process of conducting an SMS. In general, Systematic Mapping Study are comprised of 3 stages: planning, conduction and reporting. The first stage is where the study itself is parametrized. This stage does not directly represent any kind of practical application, but it conditions and defines how the other two stages will take place, and is probably the most important stage.

There are two main components to the planning stage: the context and the review. Broadly, these could be understood to define (respectively) how the topics are to be searched and what it is that the authors are looking for.

The context definition of the planning stage is when the authors define the research

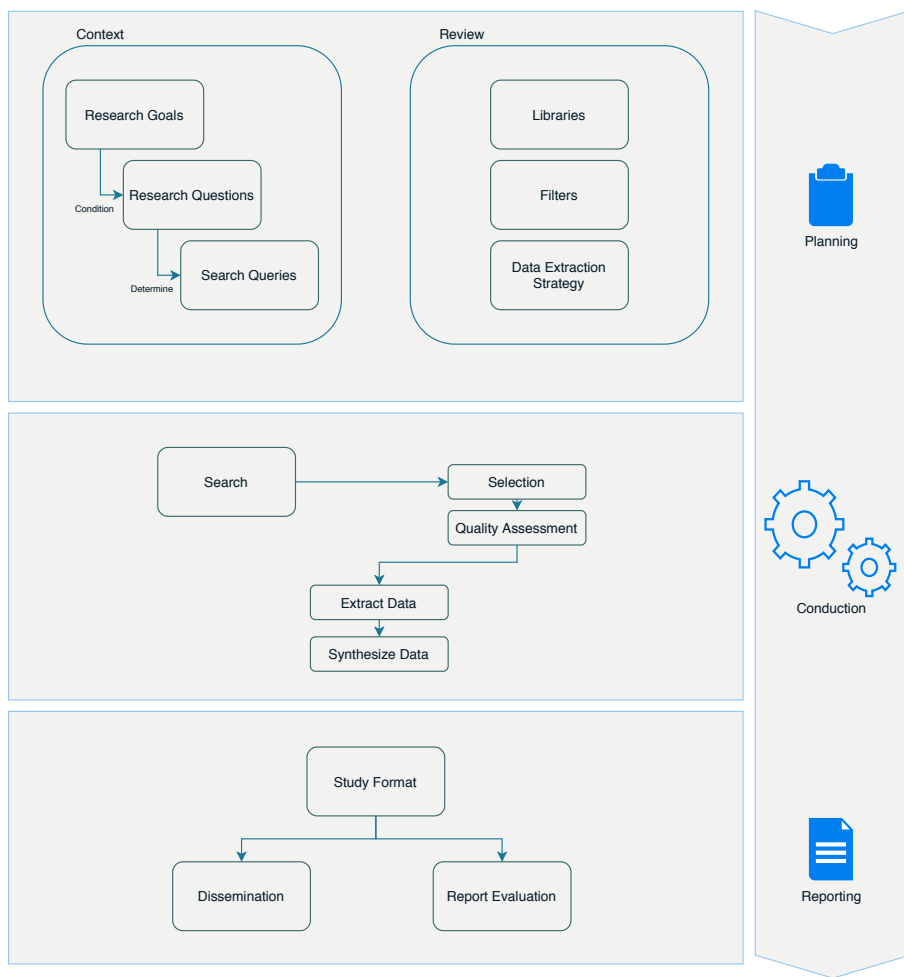


Figure 2.19: A schematic representation of an **SMS** writing process. The whole procedure is comprised of three smaller stages, which in turn are divided into various even smaller parts. The large arrow on the right represents the general evolution direction, although there is no rigid structure, and some back and forth is allowed and even expected.

questions and decide on the search protocol. The research questions are defined according to the research goal, which in this case was to assess the current status of the technology used in tomographic **DOAS**. A very common method for structuring the study's efforts is the **Population Intervention Context Objective Comparison (PICOC)** method. In our own case, this method is reflected in Table 2.4. The **PICOC** process rendered the original research question, but it was not sufficiently specific in order to conduct the search on. Therefore, we have sectioned the question into three smaller and more manageable questions. The several questions are detailed in Table 1.2.

The review step of the planning stage starts by the definition of the search queries and the electronic libraries in which they would be searched. Preliminary searches indicated that, although the topic was well-established as a measuring technique, literature on the subject was not widely available. Therefore, the search query was

Table 2.4: PICOC analysis.

<b>Population</b>	DOAS research in general.
<b>Intervention</b>	The papers must address tomographic DOAS.
<b>Outcome</b>	Status <b>assessment</b> for <b>DOAS tomography</b> .
<b>Context</b>	Research papers.

Table 2.5: Research question slicing

<b>Original</b>	What is the current status of the technology used in tomographic DOAS?
<b>RQ1</b>	Is there a typical hardware setup used in tomographic DOAS studies?
<b>RQ2</b>	Is there a standard software used to perform these analysis?
<b>RQ3</b>	What are the algorithms more commonly used?

intentionally vague: **DOAS atmospher\*** **tomography**, with the asterisk working as a wild card. As to the electronic libraries, and from the same preliminary searches, we understood that the search would have to involve the broadest repositories available. After experimenting a little further, we decided to base our study in the libraries presented in Table ??.

Table 2.6: Electronic libraries used in this study.

Library	URL
Google Scholar (GS)	<a href="https://scholar.google.com/">https://scholar.google.com/</a>
Web of Knowledge (WoK)	<a href="https://webofknowledge.com">https://webofknowledge.com</a>
Scopus (SD)	<a href="https://www.scopus.com">https://www.scopus.com</a>

Exclusion and inclusion filters are what determines what papers are kept from those that are originally found by the search process and are therefore important parameters of an **SMS** study. Table A.4 provides a list of the filters that were used in our study. To a certain degree, the application of these filters are the first step of the data extraction process. Their definition is thus part of the data extraction strategy, which determines the guidelines with which the authors are to retrieve the target information from the resulting literary corpus.

Table 2.7: Selection filters in use for this study's search.

	Criterion	Definition
<b>Exc. Criteria</b>	EC1	Satellite data papers are not accepted
	IC1	Results must be journal papers
<b>Inc. Criteria</b>	IC2	Results must be about Tomographic DOAS
	IC3	Results must be written in English

One of the most important parts of the data extraction strategy is how to evaluate each paper with respect to its quality. For this study, and although this is anything but an objectively defined topic, evaluation was performed according to the formula

in Equation 2.21, where  $Q_i$  is the paper's quartile and  $C_i$  is the number of citations that each particular study has gathered throughout the years, which are represented by  $Age_i$ . In this equation,  $S$  represents the final quality score.

$$S = Q_i \cdot \frac{C_i}{Age_i} \quad (2.21)$$

While being a good indication on how the study will be conducted, the presented method is not sufficiently specific for direct application. Before proceeding, the research question is sliced according to the **PICOC** analysis, resulting in what is presented through Table ??.

Table 2.8: Research question slicing

---

<b>Original</b>	What is the current status of the technology used in tomographic DOAS?
<b>RQ1</b>	Is there a typical hardware setup used in tomographic DOAS studies?
<b>RQ2</b>	Is there a standard software used to perform these analysis?
<b>RQ3</b>	What are the algorithms more commonly used?

---

The next step in this planning stage was to define the search queries and the electronic libraries in which they would be searched. Preliminary searches indicated that, although the topic was well-established as a measuring technique, literature on the subject was not widely available. Therefore, the search query was intentionally vague: **DOAS atmospher\*** **tomography**, with the asterisk working as a wild card. As to the electronic libraries, and from the same preliminary searches, we understood that the search would have to involve the broadest repositories available. After experimenting a little further, we decided to base our study in the libraries presented in Table ??.

Table 2.9: Electronic libraries used in this study.

---

Library	URL
Google Scholar (GS)	<a href="https://scholar.google.com/">https://scholar.google.com/</a>
Web of Knowledge (WoK)	<a href="https://webofknowledge.com">https://webofknowledge.com</a>
Scopus (SD)	<a href="https://www.scopus.com">https://www.scopus.com</a>

---

In the planning stage of the **SMS** it is also necessary to determine the study's exclusion and inclusion criteria for found papers. Ours was not an exception and these filters are presented in Table ??.

Table 2.10: Selection filters in use for this study's search.

	<b>Criterion</b>	<b>Definition</b>
<b>Exc. Criteria</b>	EC1	Satellite data papers are not accepted
<b>Inc. Criteria</b>	IC1	Results must be journal papers
	IC2	Results must be about Tomographic DOAS
	IC3	Results must be written in English

# CHAPTER 3

---

## Methods

Macroscopically, the approach to the RQ was conducted by working with two hypothesis:

**First Hypothesis:** The definition of a particular set of algorithmically defined projections in such a manner that they might be used for tomographic reconstruction of column densities of trace gases in the atmosphere, in a given ROI;

**Second Hypothesis:** We can retrieve the column density for a given trace gas (or set of trace gases) between two points by performing a spectral measurement in both of these points in the same direction and subtracting them one from the other.

To test the first hypothesis, I have used a number of computational methods to define and create projection and backprojection matrix operators, resulting in a dedicated simulation software tool that proves without a doubt that the devised projection gathering strategy is able to produce projection information in sufficient quantity as to perform tomographic reconstruction. This procedure is detailed in Section 3.1.

The second hypothesis was experimentally tested, by the conduction of a number of field experiments designed to determine the validity of measurement hypothesis with the equipments to which I have current access. The experiment and the protocol that was followed is detailed in Section 3.2. This chapter is heavily based on one of the two articles generated by the work of this thesis.

### 3.1 Tomosim

Tomosim was the (somewhat unoriginal) name given to the tomographic simulation software tool that was designed and built as part of this project. It was created to tackle the trajectory-related hypothesis, briefly described in this chapter's introduction.

The final system must be able to gather projection information by reading spectral information, in this case the DOAS-retrieved column density for an atmospheric trace

gas (or several) from a set of predetermined directions. In "normal" tomographic DOAS application, these directions are fixed and depend on the experiment infrastructure's geometry (see Section 2.4). One of the main novelties that I am trying to create with this project is a very high degree of geometric freedom. A mobile system has no custom infrastructure, and therefore has no fixed positions to which it is tied. Instead its ability measure and monitor its atmospheric surroundings relies on its movement.

A ground-based mobile DOAS-tomography system would have too strong a dependency on open spaces and the topography of its ROI to be useful in any *real world* scenario. A much more interesting and feasible approach would be to use some kind of flying machine that could carry spectroscopic equipment, and that could be programmed to fly in a precise manner. Fortunately, current day technology provides a very strong immediate candidate: a UAV of the n-copter type, such as the one in

Figure 3.1.

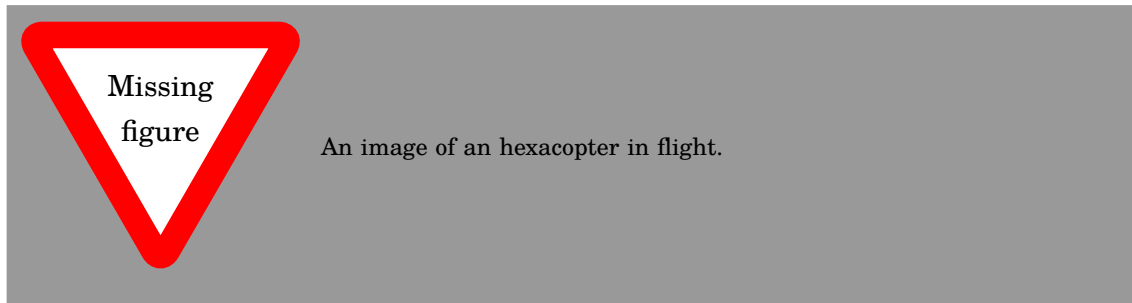


Figure 3.1: Hexacopter in flight. Taken from laksjdlaksjd

A natural choice as it may seem as means for the measurements I am describing in this document, its programming is almost as important as the hardware itself (if not more). The vehicle must be programmed to describe a very precise (taking into account the type of operation we are proposing) trajectory. In flight, the drone should be able to carry and point an optical system towards any direction and in a short time. Said optical system should be attached to a computer-controlled spectrometer. This would allow the whole system to determine target trace gas concentration on demand and programmatically.

The programmed trajectory should make use of these capabilities and gather enough information for tomographic reconstruction. This also means that the trajectory must be comprised of a sufficient number of spectral projection acquisition opportunities.

Of the several geometries that are described in the literature for tomographic reconstructions, the one that seemed to be more promising in terms of the balance between reconstruction complexity and the information / flight time ratio was the fanbeam assembly (described in Section 2.3). It was the feasibility of this trajectory for the proposed purposes that this simulation aimed to prove.

In essence, the drone's trajectory (illustrated in Figure ??) is a horizontal circle

which is parametrised to be at a certain height and to have a certain diameter. Both of these dimensions are set at experiment / measurement time. The drone stops on this circle at regular angular intervals, say  $\alpha$  degrees. Each one of these stops ( $360 / \alpha$  stops) will generate a fanbeam projection, by pointing the optical system inwards (with respect to the circular macro-trajectory) and performing a series of spectroscopic measurements in different directions and also at regular intervals, say  $\gamma$  degrees. The particular case in which  $\alpha = \gamma$  is very interesting, because it then opens the possibility for resorting the fanbeams into parallel virtual-projections that are much easier to reconstruct tomographically, as introduced in Section 2.3.



Figure 3.2: Illustration of the projection gathering algorithm based on fanbeam assembly of information. On the left the circle which constitutes the general trajectory of the drone. On the right the gymbal points the optical system towards different directions, forming what can be seen as a fan.

### 3.1.1 Discretisation

Discretisation is the process by which the **ROI** is digitised into a computational platform. There are several algorithms designed for this effect that are available in the literature. One of the easiest to implement that is also adequate to this application (unsurprisingly) comes from the medical imaging field. It was published in 1985 by Robert Siddon [65].

The Siddon algorithm is one of the foremost path calculation algorithms in the medical field of radiology. It is not only used for the discretisation of tomographic fields, but also in the dose calculation process of radiation therapy patients. The idea behind the algorithm is that the total dose of a radiation ray, i.e., its path, is given by the sum of the length within each pixel that this ray traverses multiplied by the density of said pixel. In mathematical notation, one can write this as in Equation 3.1.

Ugly. Rewrite

$$d = \sum_i \sum_j \sum_k kl(i, j, k) \cdot \rho(i, j, k) \quad (3.1)$$

In Equation 3.1,  $d$  is the radiological path (the projection value),  $i, j, k$  are the coordinate vectors,  $l$  is the length within a pixel and  $\rho$  is the pixel density. In our case, this last value is the trace gas column density for that pixel.

The main reason for Siddon's algorithm being easy to implement is its treatment of pixels (or voxels if in 3D). Instead of considering pixels as *atomic*<sup>1</sup> units, it defines them as the intersections of orthogonal sets of equally spaced lines (planes in 3D). Pixel lengths are determined by looking at the intersections between the orthogonal lines and the radiation ray.

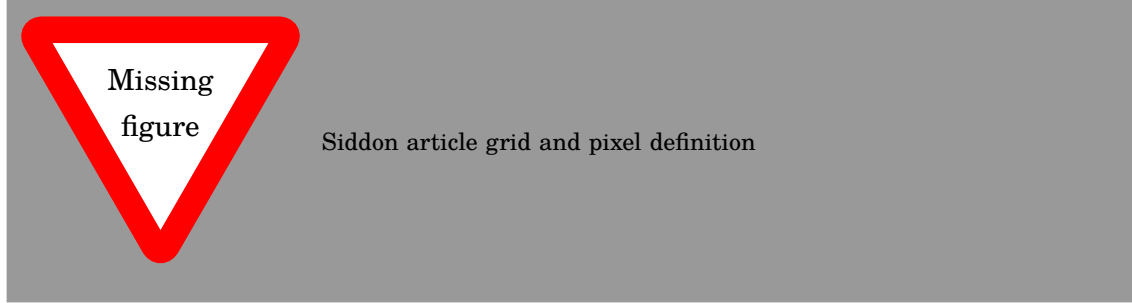


Figure 3.3: Grid and pixel definition, as they appear in the original article by Robert Siddon [65]. Notice that pixels are formed by line intersections.

Since lines are orthogonal and equally spaced, all intersections can be calculated recursively after knowing where the first intersection is located. The calculation of the radiologic path is achieved by determining the subset of the intersections between the orthogonal lines and the ray that identifies individual pixels.

If  $P_1 \rightarrow (X_1, Y_1)$  and  $P_2 \rightarrow (X_2, Y_2)$  are the start and end of the radiologic path within the ROI, the line between them can be parametrically written as in Equation 3.2.

$$\begin{aligned} X(\alpha) &= X_1 + \alpha \cdot (X_2 - X_1) \\ Y(\alpha) &= Y_1 + \alpha \cdot (Y_2 - Y_1) \end{aligned} \tag{3.2}$$

In Equation 3.2,  $\alpha$  is 0 at  $P_1$  and 1 at point  $P_2$ . Values of  $\alpha$  within the ROI vary according to the positions of  $P_1$  and  $P_2$  with respect to the ROI. By determining  $\alpha$  values of each intersection (in both directions), one can determine the length of the ray within the pixel by the difference of adjacent intersections. The whole algorithm

---

<sup>1</sup>In their undivisible sense.

can be written as in Algorithm 2.

---

**Algorithm 2:** Siddon's algorithm's procedural steps. After running this algorithm, one is able to represent any continuous ray through the analysis field as a sum of discrete lengths

---

**Result:** Discretised ROI space.

- calculate range of parametric values;
  - calculate range of pixel indices;
  - calculate parametric sets;
  - merge sets;
  - calculate pixel(or voxel) lengths;
  - calculate pixel indices;
- 

Detailing the two-dimensional case<sup>2</sup> should start by the definition of the discretisation grid itself, as in Equation 3.3. The equation reflects the recursive nature of the grid definition. In it,  $d_x$  and  $d_y$  are the distances between the  $x$  and  $y$  planes, which correspond to the lengths of the pixels in those coordinates.  $N_x$  and  $N_y$  are the number of pixels in  $x$  and  $y$  that are contained in the grid.

$$\begin{aligned} X_{\text{plane}}(1) &= X_{\text{plane}}(1) + (i - 1) \cdot d_x \\ Y_{\text{plane}}(1) &= Y_{\text{plane}}(1) + (j - 1) \cdot d_y \end{aligned} \quad (3.3)$$

The parametric values  $\alpha_{\min}$  and  $\alpha_{\max}$  are given by the intersections of the ray with the sides of the grid ( $i = 1$  and  $i = N_x$ ) and can be written as in Equation 3.4.

$$\begin{aligned} \alpha_{\min} &= \max \{0, \min [\alpha_x(1), \alpha_x(N_x)], \min [\alpha_y(1), \alpha_y(N_y)]\} \\ \alpha_{\max} &= \min \{1, \max [\alpha_x(1), \alpha_x(N_x)], \max [\alpha_y(1), \alpha_y(N_y)]\} \end{aligned} \quad (3.4)$$

Not all line intersections have a corresponding parametric value. The ones that do are comprised within index ranges that are defined by Equation 3.5. This equation presents the case for the first coordinate ( $x$ ), with the second coordinate having an identical expression.

$$\begin{aligned} i_{\min} &= N_x - \frac{X_{\text{plane}}(N_x) - \alpha_{\min}(X_2 - X_1) - X_1}{d_x} \\ i_{\max} &= 1 + \frac{X_1 + \alpha_{\max}(X_2 - X_1) - X_{\text{plane}}(1)}{d_x} \end{aligned} \quad (3.5)$$

Equation 3.5 defines a range of possible indices for the pixels, in parametric fashion. We can use this range to construct the set of used parametric indices, given in Equation 3.6 for the  $x$  coordinate.

$$\{\alpha_x\} = \{\alpha_x(i_{\min}), \dots, \alpha_x(i_{\max})\} \quad (3.6)$$

Although Equation 3.6 only presents the expression for the first coordinate, there are similar expressions for the other coordinates at play. After determining the set of

---

<sup>2</sup>A three-dimensional case would be just the same but with an additional coordinate.

possible indices for  $x$  and  $y$ , these sets must be arranged in ascending order, creating an index superset. To this the minimum and maximum values, calculated in Equation 3.4, are appended. The resulting and final set of parametric values is presented in Equation 3.7.

$$\begin{aligned}\alpha^* &= \text{merge}(\alpha_x, \alpha_y) \\ \{\alpha\} &= \{\alpha_{min}, \alpha^*, \alpha_{max}\} \\ &= \alpha(0), \dots, \alpha(n)\end{aligned}\tag{3.7}$$

Where the last term,  $n$ , is given by the sum of all index range numbers, as in Equation 3.8, again for the two-dimensional case.

$$n = (i_{max} - i_{min} + 1) + (j_{max} - j_{min} + 1)\tag{3.8}$$

Each element of the array defined in Equation 3.7 is an intersection between the ray and a given pixel. Since they are ordered, it is possible to calculate the array of pixel lengths for each ray, using the expression in Equation 3.9.

$$l_m = d_{12}[\alpha(m) - \alpha(m - 1)] \quad (m = 1 \dots n)\tag{3.9}$$

With  $d_{12}$  being the distance between  $P_1$  and  $P_2$ , calculated through the Euclidean formula for distance between two points. In Tomosim, this distance is always equal to the trajectory's diameter.

Pixel  $[i(m), j(m)]$  is located in the midpoint between the  $m^{\text{th}}$  and the  $(m-1)^{\text{th}}$  intersections. It is given by the expression in Equation 3.10.

$$\begin{aligned}\alpha_{mid} &= \frac{\alpha(m) + \alpha(m - 1)}{2} \\ i(m) &= 1 + \frac{X_1 + \alpha_{mid} \cdot (X_2 - X_1) - X_{plane}(1)}{d_x} \\ j(m) &= 1 + \frac{Y_1 + \alpha_{mid} \cdot (Y_2 - Y_1) - Y_{plane}(1)}{d_y}\end{aligned}\tag{3.10}$$

Knowing the pixels and the ray lengths for each of them makes the application of the radiological path equation (Equation 3.1) trivial. From another perspective, Siddon's algorithm produces an even more important piece of information. One gets total geometric knowledge of the tomographic assembly. If matrix form, this is called the system matrix, and it is an essential part of the application of any iterative algorithm.

Figure ?? aims to graphically explain the formation of this matrix. Each line in the matrix can be thought of as a flattened matrix of the same size as the tomographic image to reconstruct. There are as many of these lines as there are rays in the tomographic assembly. Each element of the matrix contains the length of the ray corresponding to each line, as it is calculated (through the application of Siddon's algorithm) for the corresponding pixel of the aforementioned flattened matrix.

### 3.1.1.1 Exit Point Calculation

Figure 3.4 is a schematic snapshot of a point in which the drone is taking a spectrum in one of its stops. Here, the drone's position ( $P_1$ ) is given by the distance  $D$  and the angle  $\beta$ . The gimbal is pointing at a direction at an angular distance of  $\gamma$  from line  $0P_1$ . Point  $P_2$ , which is not known, is at the intersection between the trajectory's circumference and line  $P_1P_2$ . Now, any point on this line can be expressed parametrically, with the sum of a point and a vector; while to say a point is on a circumference is the same as saying the distance between that point and the centre of this circumference is equal to its radius. The situation can be described by the expressions in Equation 3.11.

$$\begin{aligned} X &= P_1 + t \cdot (P_2 - P_1) \\ |P_2| &= D^2 \end{aligned} \tag{3.11}$$

Unravelling these expressions, and making use of the algebraic property that says that  $|A|^2 = A \cdot A$ , the expression becomes a second degree equation, as stated in Equation 3.12, writing  $P_2 - P_1$  as  $V$ .

$$t^2 V^2 + 2 \cdot V \cdot P_1 \cdot t + P_1^2 - D^2 = 0 \tag{3.12}$$

If line  $P_1P_2$  non-tangentially intersects the circumference, solving Equation 3.12 renders two values for  $t$  (which correspond to  $P_1$  and  $P_2$ ). Selection is made by determining the returned value of  $t$  which maximises the euclidean distance between the produced point and  $P_1$ .

### 3.1.2 Phantoms

A phantom is a device that represents the human body or some of its parts. They have been used in medical physics since the beginning of the field. In medical imaging, for instance, phantoms started being used in the late nineteenth century and early twentieth century. At the time, it was very difficult to find volunteers for any kind of experiment that involved radiation, due to the common effects that were rapidly reported by the first people subject to this kind of intervention [66]. In spite of this difficulty, scientists and researchers still had to determine the dosimetry properties and physical limitations of their radiative devices, so medical physicists had to develop their own test models, or phantoms, for this effect. More recently, phantoms have been designed to develop computed tomography applications and algorithms. These phantoms mimic the body's attenuation properties in the X-Ray section of the electromagnetic spectrum, for instance.

Although the system that I propose does not aim at measuring or using the human body (or any other animal's), the concept still stands. To evaluate our reconstruction methods and the validity of our data gathering strategies, I needed an atmospheric phantom.

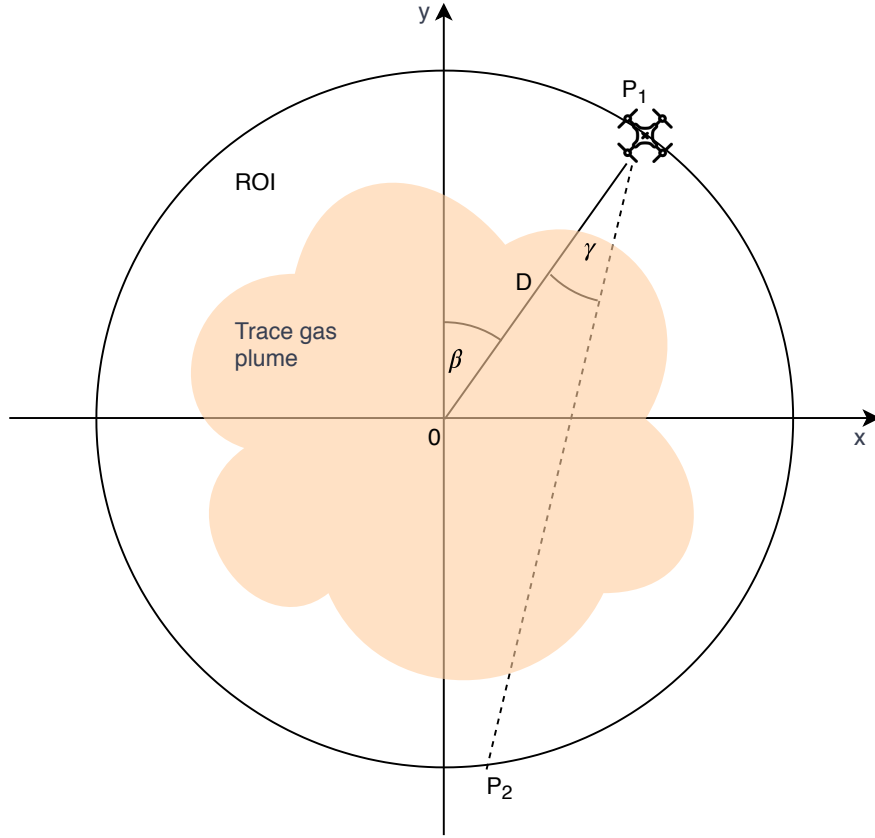


Figure 3.4:  $P_2$  Calculation. The software uses the position of the drone, as defined by the vertical angle,  $\beta$ , and the distance between the drone and the centre of the trajectory,  $D$ , to determine  $P_2$  through the solution of a second degree equation.

The distribution of gases in the atmosphere is completely different from biological tissue. Therefore, medical imaging phantoms were not adequate. The design that I have created is based on the premise that a two-dimensional Gaussian peak is more appropriate to describe the smoother nature of gaseous distribution [67]. This in contrast with the crisply defined edges of a medical tomography phantom such as Shepp-Logan's head phantom [68].

To design the phantom itself, I used a library called TomoPhantom [69], a tomographic phantom generator that provides a Python Application Programming Interface (API), making it trivial to include in the Tomosim simulator. The new phantom is comprised of 5 Gaussian profiles, depicting a static gas mixture. An ellipse is also in the phantom, near one of the corners. This serves mainly as a reference point for reconstruction, given its more solid and crisp nature. The new phantom can be seen in Figure 3.5 and its features are stated in Table 3.1.

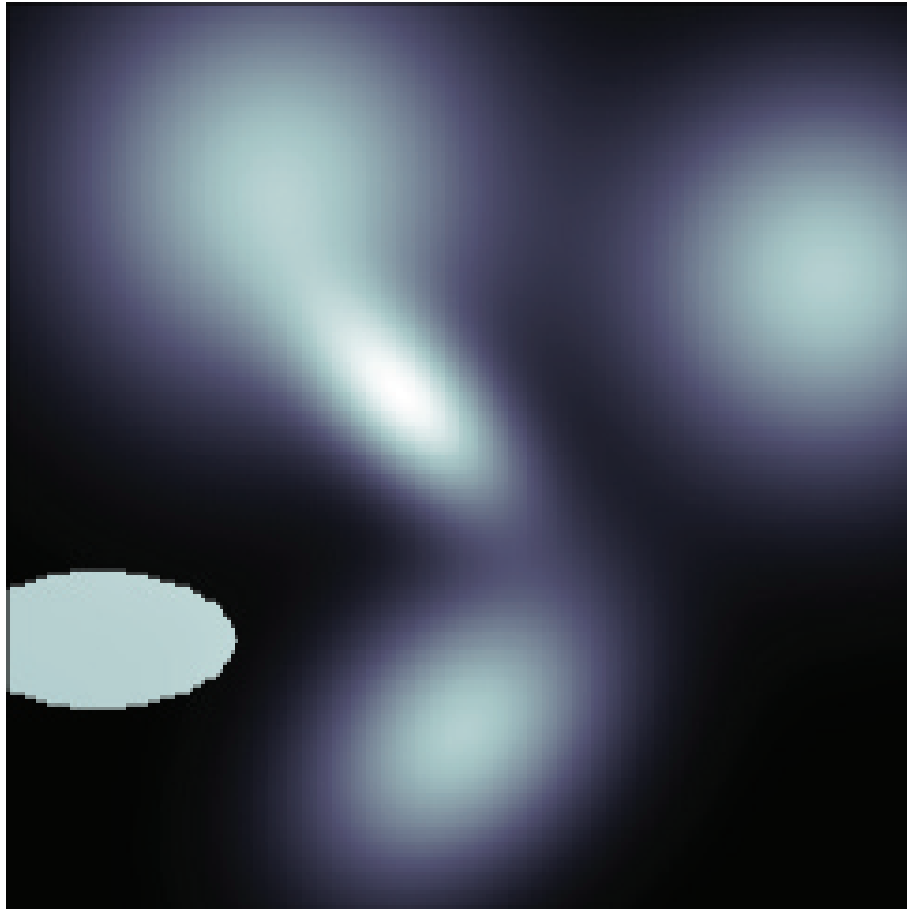


Figure 3.5: A graphical representation of the new spectral phantom, custom built for the TomoSim application.

Table 3.1: Table summarising the new phantom's construction details, as a sum of 5 Gaussian profiles and an ellipse designed using TomoPhantom. In this table, C0 is the object's amplitude, X0 and Y0 are its center coordinates, and a and b are the objects half-widths. The table is constructed using TomoPhantom's particular syntax and more information can be obtained at [69].

Type	C0	X0	Y0	a	b	Angle
Gaussian	1	-0,1	-0,1	0,25	0,5	-45
Gaussian	1	0,6	0	0,65	0,45	-45
Gaussian	1	-0,6	-0,4	0,8	0,8	0
Gaussian	1	-0,4	0,8	0,7	0,7	0
Ellipse	1	0,4	-0,8	0,3	0,15	0

### 3.1.3 Error Estimation

Error sources for the Tomosim simulator come in four different natures: time errors, geometric errors, spectroscopic errors and reconstruction errors.

Time errors come from the fact that there are two moments of measurement. In a dynamic system, the time that passes between the two is enough for concentrations to change significantly. Tomosim does not address these errors, because they can be eliminated by the introduction of a second drone carrying the same type of equipment, which would eliminate said time difference.

Geometric errors exist due to the drone not being able to situate itself perfectly. There is always a positioning error, no matter how sophisticated the onboard equipment is. This type of error is addressed in the simulation through a Monte Carlo like approach.

Positioning and pointing errors are assumed to have normal distributions. Each time a point is calculated by the drone, a normally distributed random number, with a mean of 0 and a standard deviation equal to the nominal error of the positioning system. This number is then added to the theoretical point. Figure 3.6 is a graphical representation of the reasoning behind the calculation of the geometric error. The image deals with two types of error. One comes from the [Real Time Kinematic Global Positioning System \(RTK GPS\)](#) positioning system (the positioning error,  $\epsilon_p$ ); and the other that comes from the gimbal (the pointing error,  $\epsilon_\gamma$ ). The two  $\epsilon$  values are the nominal error for the positioning and the pointing devices. The error is introduced in the simulation through the values of  $\beta$  and  $D$  (see Figure 3.4) while calculating  $P_2$ . Given the very low nominal error for the gimbal, the small angle approximation is valid ( $\sin \theta = \theta$ ). This is used to determine the theoretical value of  $P_2$ , located on the device's circular trajectory. Finally, the software adds the positioning error, using the same process as in  $P_1$ 's case. The error depiction in Figure 3.6 is extremely exaggerated for visibility.

The third type of error are the spectroscopic errors. These come from the spectroscopic equipment that is used to gather projections. To take this noise into account, the simulator adds a Gaussian noise spectrum to each measurement, which is configurable through its standard deviation, as was previously done in [70]. This is a valid approach, insofar as the captured spectra are perfectly calibrated regarding spectral shift and squeeze. Since this is a simulation software, this is an acceptable assumption.

The final type of error that the system needs to contend with is the reconstruction error. In tomographic inversion problems, it is common to use techniques such as the [Mean Squared Error \(MSE\)](#) as a metric for an algorithm's performance. Tomosim was also evaluated in this light and in two separate ways. The first was to calculate the [MSE](#) for each pixel of the whole image. This information can still be viewed as an image (it is a two-dimensional grid of values) and paints an immediate picture of the general behaviour of the reconstruction algorithm. Moreover, it can tell the viewer if

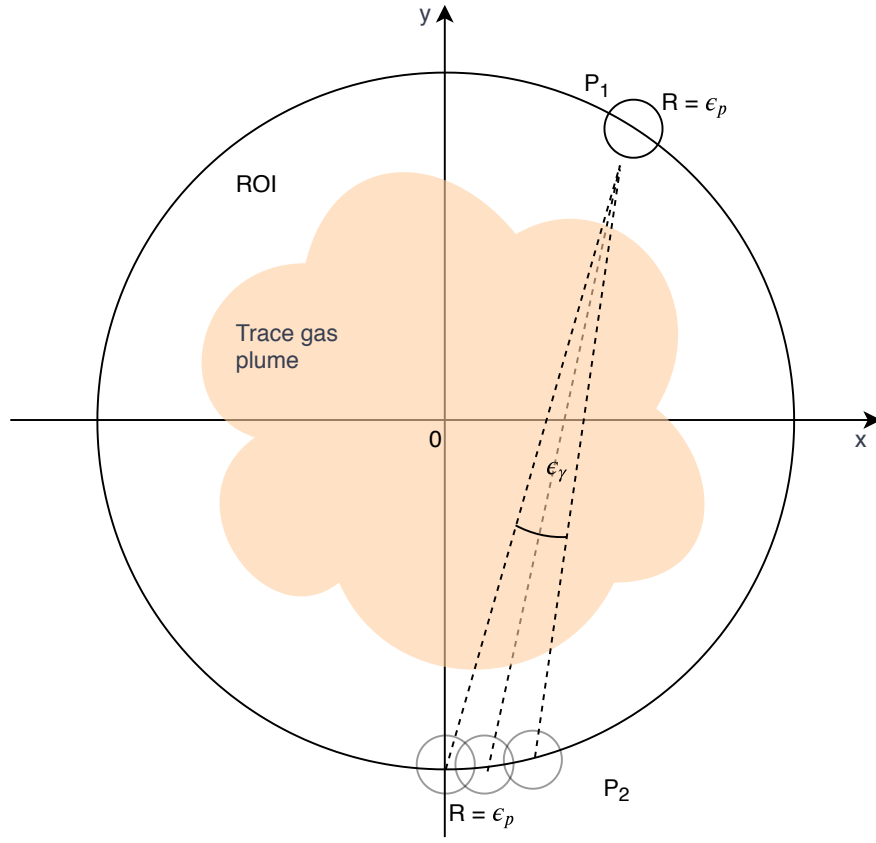


Figure 3.6: Error estimation graphical representation. Note errors are extremely exaggerated for visualisation purposes.

there are any types of shapes or areas in which the algorithm has more difficulties. The second way of using MSE to evaluate the reconstruction is to calculate a score through Equation 3.13. In this equation, and with respect to this simulator,  $f$  is the original image and  $g$  the one reconstructed from projections.

$$E = \sqrt{\frac{\sum |g(x, y) - f(x, y)|^2}{\sum |f(x, y)|^2}} \quad (3.13)$$

## 3.2 The Experiment

As stated in this chapter's introductory notes, this thesis main body of work revolves around two base assumptions, our hypothesis. The first one, about the information capturing by the idealised system, was addressed in lkjashdkjh . The second, more physical in nature, is the subject matter of this section. Our hypothesis states that the light absorption between points  $A$  and  $B$  (let's call it  $A_{AB}$ ) should be equal to the difference of the absorptions in  $A$  and  $B$ . We can write this, in a *Lambertian* manner

reference the correct subsection after merging with the mac branch

as in Equation 3.14.

$$I_B = I_A \cdot \exp \left[ -AB \cdot \sum_i \sigma_{ABi} \cdot c_{ABi} \right] \quad (3.14)$$

This is to say that the light intensity reaching point  $B$  is given by the intensity reaching  $A$ , exponentially decreased by the absorbers at interval  $AB$ . The intensities at  $A$  and  $B$  are written as in Equation 3.15.

$$\begin{aligned} I_B &= I_0 \cdot \exp \left[ -L_B \cdot \sum_i \sigma_{Bi} \cdot c_{Bi} \right] \\ I_A &= I_0 \cdot \exp \left[ -L_A \cdot \sum_i \sigma_{Ai} \cdot c_{Ai} \right] \end{aligned} \quad (3.15)$$

If we join all this information in the same expression, the equation is transformed into its final form, presented in Equation 3.16.

$$I_0 \cdot \exp \left[ -L_B \cdot \sum_i \sigma_{Bi} \cdot c_{Bi} \right] = I_0 \cdot \exp \left[ -L_A \cdot \sum_i \sigma_{Ai} \cdot c_{Ai} \right] \cdot \left[ -AB \cdot \sum_i \sigma_{ABi} \cdot c_{ABi} \right] \quad (3.16)$$

Equation 3.16 can be greatly simplified: we take the natural logarithm of both sides and we state that  $\sum_i \sigma_{Xi} \cdot c_{Xi} = S_i$ . These operations result in the simplified form of Equation 3.17.

$$L_B \cdot S_B = L_A \cdot S_A + L_{AB} \cdot S_{AB} \quad (3.17)$$

Now,  $L_X \cdot S_X$  can be thought of as the wavelength dependent light absorption in path  $X$ . In this case, the wavelength interval is always the same. We can therefore conclude that, theoretically, our hypothesis is valid: light absorption between points  $A$  and  $B$  can be expressed in terms of the absorption on both these points and corresponds to their difference.

Although mathematically this seems clear-cut, in the real world things can become more problematic, since we have to deal with the imperfections that characterise a real physical system. Noise, instrumental limitations, adverse environmental effects, etc.. The experiment we describe in the next few paragraphs aimed at determining target trace gas concentration in a set analysis field. This field is dimension-wise compatible with those that would be employed in the final working system. The experiment geographic information is presented in Figure 3.7.

### 3.3 Section Objectives

- Summarise, explain and recount how the question was answered;
- Discuss the previous point in details;

### **3.4. QUESTIONS THE READERS SHOULD BE ABLE TO ANSWER ONCE THEY'VE READ THE SECTION**

---

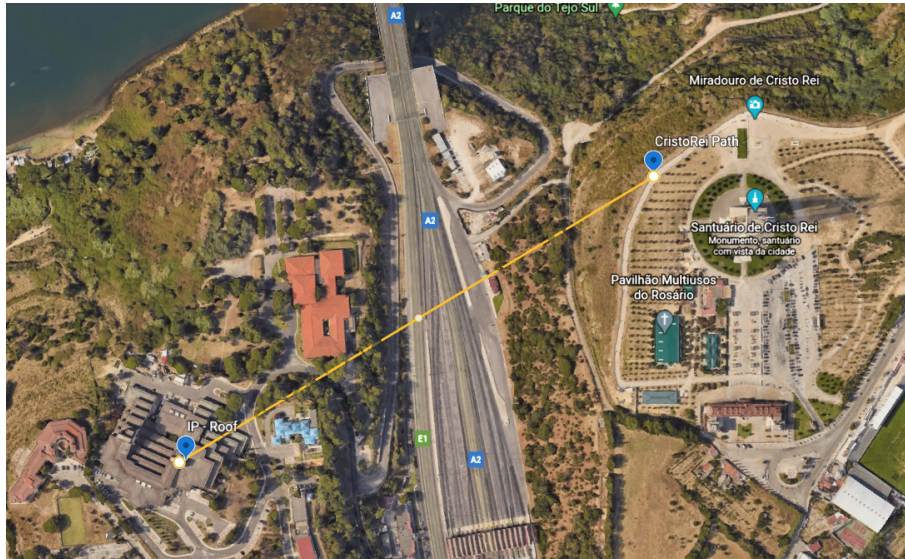


Figure 3.7: Location of observer points for the physical experiment.

- Why are techniques relevant;
- How were the techniques used;

## **3.4 Questions the readers should be able to answer once they've read the section**

- What are the results;
- How do the findings relate to previous studies;
- Was there anything surprising that did not go as planned;
- Why the presented conclusion have been reached;
- Explain results;

## **3.5 How was the question answered?**

### **Question**

How to design a miniaturised tomographic atmosphere monitoring system based on DOAS?

### **How was the question addressed?**

**Projection-based hypothesis:** first step was to design an information gathering approach. Ours was based on the definition of a particular trajectory for the measurement device. This had to be validated in computational and mathematical sense;

**Measurement based hypothesis:** although it is clearly implied by Lambertian theory, there is no literature that I know of that points to the fact that my measurements are correct. Therefore, the assumption that we can measure column densities between two points sequentially must be tested;

### 3.6 Detailed presentation of projection-based hypothesis

**Hypothesis:**

- A tomographic atmospheric measurement entails capturing projections in many different angles;

- The typical atmospheric tomographic DOAS application uses several tens of projections for reconstruction;
- A drone moving in a circular trajectory would be able to capture an array of fan-beam projections with a specially motorised spectroscopic assembly;
- In theory, this would be sufficient for reconstruction;
- For simplicity, in this application we use the re-sorting reconstruction algorithm, which applies the FBP algorithm to a synthetically created parallel beam sinogram;

**How is the trajectory defined:**

- circular;
- one stop at each  $\alpha$  degrees. At each one:
  - gymbal points to a number of directions (parameter) at regular intervals (parameter), taking one measurement at a time;
- on a second moment, the drone moves to the entry points of the rays that have been capturedd by the equipment, taking a measurement at each one, in the same direction;
- use the measurement hypothesis to determine the column densities between 1<sup>st</sup> measurement moment and the 2<sup>nd</sup>.

### 3.7 Calculation of Projections

1. Discretise the Region Of Interest

# CHAPTER 4

---

## Discussion

In this chapter, we discuss the results that we have obtained.



---

## Bibliography

- [1] P. Vieira, J. Matos, and M. Mendes. *Sistema para a detecção automática de incêndios florestais por espectroscopia óptica*. 2007.
- [2] P. Vieira and J. Matos. *System for Automatic Detection of Forest Fires Through Optical Spectroscopy*. 2008.
- [3] R. Valente de Almeida and P. Vieira. “Forest Fire Finder – DOAS application to long-range forest fire detection.” In: *Atmospheric Measurement Techniques* 10.6 (June 2017), pp. 2299–2311. issn: 1867-8548. doi: [10.5194/amt-10-2299-2017](https://doi.org/10.5194/amt-10-2299-2017). URL: <https://www.atmos-meas-tech.net/10/2299/2017/>.
- [4] C. Guerreiro, J. Soares, and A. G. Ortiz. *Air quality in Europe — 2019 report*. 5. Luxembourg: Publications Office of the European Union, 2019. isbn: 9789294800886. doi: [10.2800/822355](https://doi.org/10.2800/822355). URL: [papers2://publication/uuid/1D25F41B-C673-4FDA-AB71-CC5A2AD97FDD](https://doi.org/10.2800/822355).
- [5] CE Delft. *Health impacts and costs of diesel emissions in the EU*. Tech. rep. Delft: CE Delft, 2018, p. 72. URL: [www.cedelft.eu](http://www.cedelft.eu).
- [6] R. Gunderman. *Essential Radiology: Clinical Presentation, Pathophysiology, Imaging*, 2nd ed. 2nd ed. Thieme, 2006. isbn: 9781588900821.
- [7] A. Kak and M. Slaney. *Principles of Computerized Tomographic Imaging*. Society of Industrial and Applied Mathematics, 2001.
- [8] P. P. Bruylants. “Analytic and iterative reconstruction algorithms in SPECT.” In: *Journal of nuclear medicine : official publication, Society of Nuclear Medicine* 43.10 (2002), pp. 1343–58. issn: 0161-5505. URL: <http://jnm.snmjournals.org/cgi/content/abstract/43/10/1343> <http://jnm.snmjournals.org/cgi/content/full/43/10/1343> <http://www.ncbi.nlm.nih.gov/pubmed/12368373>.

## BIBLIOGRAPHY

---

- [9] G. T. Herman, A. Lent, and S. W. Rowland. “ART: Mathematics and applications. A report on the mathematical foundations and on the applicability to real data of the algebraic reconstruction techniques.” In: *Journal of Theoretical Biology* 42.1 (1973). issn: 10958541. doi: [10.1016/0022-5193\(73\)90145-8](https://doi.org/10.1016/0022-5193(73)90145-8).
- [10] G. T. Herman. “Image Reconstruction From Projections.” In: *Real-Time Imaging* 1.1 (1995), pp. 3–18. issn: 10772014. doi: [10.1006/rtim.1995.1002](https://doi.org/10.1006/rtim.1995.1002).
- [11] G. T. Herman. *Fundamentals of Computerized Tomography*. Advances in Pattern Recognition. London: Springer London, 2009. isbn: 978-1-85233-617-2. doi: [10.1007/978-1-84628-723-7](https://doi.org/10.1007/978-1-84628-723-7). url: <http://link.springer.com/10.1007/978-1-84628-723-7>.
- [12] M. Defrise, P. E. Kinahan, and C. J. Michel. *Positron Emission Tomography*. Ed. by D. L. Baley, D. W. Townsend, P. E. Valk, and M. N. Maisey. London: Springer London, 2005, pp. 63–91.
- [13] D. Perner, D. H. Ehhalt, H. W. Pätz, U. Platt, E. P. Röth, and A. Volz. “OH - Radicals in the lower troposphere.” In: *Geophysical Research Letters* 3.8 (Aug. 1976), pp. 466–468. issn: 00948276. doi: [10.1029/GL003i008p00466](https://doi.org/10.1029/GL003i008p00466). url: <http://doi.wiley.com/10.1029/GL003i008p00466>.
- [14] U. Platt and J. Stutz. *Differential Optical Absorption Spectroscopy - Principles and Applications*. Ed. by R. Guzzi, L. J. Lanzerotti, D. Imboden, and U. Platt. Heidelberg, Germany: Springer-Verlag Heidelberg Berlin, 2008. isbn: 9783540211938.
- [15] A. Merlaud. “Development and use of compact instruments for tropospheric investigations based on optical spectroscopy from mobile platforms.” PhD Thesis. Louvain: Faculté des Sciences - Université Catholique de Louvain, 2013. isbn: 978-2-87558-128-0. url: <http://books.google.com/books?hl=en%7B%5C%7Dlر=%7B%5C%7Did=inxVSYr82zwC%7B%5C%7Doi=fnd%7B%5C%7Dpg=PR3%7B%5C%7Ddq=Development+and+use+of+compact+instruments+for+tropospheric+investigations+based+on+optical+spectroscopy+from+mobile+platforms+sciences%7B%5C%7Dots=VdebeDBQMc%7B%5C%7Dsig=4G0eVEvthJXuqd8WI3IWjjVXuXc>.
- [16] I. Pundt, C. Hak, A. Hartl, K.-P. Heue, K. U. Mettendorf, U. Platt, D. Poehler, B. Rippel, B.-C. Song, A. Stelzer, T. Wagner, M. Bruns, J. Burrows, A. Richter, and P. Wang. “Mapping of tropospheric trace gas concentration distributions from ground and aircraft by DOAS-tomography (Tom-DOAS).” In: () .
- [17] T. Laepple, V. Knab, K.-U. Mettendorf, and I. Pundt. “Longpath DOAS tomography on a motorway exhaust gas plume: numerical studies and application to data from the BAB II campaign.” In: *Atmospheric Chemistry and Physics Discussions* 4.3 (May 2004), pp. 2435–2484. issn: 1680-7375. doi: [10.5194/acpd-4-2435-2004](https://doi.org/10.5194/acpd-4-2435-2004).

- 2435–2004. URL: [www.atmos-chem-phys.org/acp/4/1323/](http://www.atmos-chem-phys.org/acp/4/1323/) http://www.atmos-chem-phys-discuss.net/4/2435/2004/.
- [18] J. Stutz, S. C. Hurlock, S. F. Colosimo, C. Tsai, R. Cheung, J. Festa, O. Pikelnaya, S. Alvarez, J. H. Flynn, M. H. Erickson, and E. P. Olaguer. “A novel dual-LED based long-path DOAS instrument for the measurement of aromatic hydrocarbons.” In: *Atmospheric Environment* 147 (Dec. 2016), pp. 121–132. ISSN: 13522310. doi: 10.1016/j.atmosenv.2016.09.054. URL: <http://linkinghub.elsevier.com/retrieve/pii/S1352231016307713>.
- [19] E. Frins, N. Bobrowski, U. Platt, and T. Wagner. “Tomographic multiaxis-differential optical absorption spectroscopy observations of Sun-illuminated targets: a technique providing well-defined absorption paths in the boundary layer.” In: *Applied Optics* 45.24 (Aug. 2006), p. 6227. ISSN: 0003-6935. doi: 10.1364/AO.45.006227. URL: <https://www.osapublishing.org/abstract.cfm?URI=ao-45-24-6227>.
- [20] CABI. *Air Pollution: Sources, Impacts and Controls*. Ed. by P. Saxena and V. Naik. 1st. Vol. 53. 9. Oxfordshire, UK: CAB International, 2019, pp. 1689–1699. ISBN: 9781786393890.
- [21] N. Casaballe, M. Osorio, M. Di Martino, and E. Frins. “Comparison Between Regularized Optimization Algorithms for Tomographic Reconstruction of Plume Cross Sections in the Atmosphere.” In: *Earth and Space Science* 4.12 (Dec. 2017), pp. 723–736. ISSN: 23335084. doi: 10.1002/2017EA000341. URL: <http://doi.wiley.com/10.1002/2017EA000341>.
- [22] M. Johansson, B. Galle, C. Rivera, and Y. Zhang. “Tomographic reconstruction of gas plumes using scanning DOAS.” In: *Bulletin of Volcanology* 71.10 (Dec. 2009), pp. 1169–1178. ISSN: 0258-8900. doi: 10.1007/s00445-009-0292-8. URL: <http://link.springer.com/10.1007/s00445-009-0292-8>.
- [23] Python. *Python 3 Programming Language*. URL: <https://www.python.org/>.
- [24] T. E. Oliphant. “Python for Scientific Computing.” In: *Computing in Science & Engineering* 9.3 (2007), pp. 10–20. ISSN: 1521-9615. doi: 10.1109/MCSE.2007.58. URL: <http://ieeexplore.ieee.org/document/4160250/>.
- [25] D. Vallero. *Fundamentals of air pollution*. 5th ed. Oxford, UK: Academic Press - Elsevier, 2014. ISBN: 9780124017337.
- [26] M. L. Bell, D. L. Davis, and T. Fletcher. “A retrospective assessment of mortality from the london smog episode of 1952: The role of influenza and pollution.” In: *Urban Ecology: An International Perspective on the Interaction Between Humans and Nature* 6.1 (2008), pp. 263–268. doi: 10.1007/978-0-387-73412-5\_15.

## BIBLIOGRAPHY

---

- [27] M. Office. *The Great Smog of 1952*. 2019. URL: <https://www.metoffice.gov.uk/weather/learn-about/weather/case-studies/great-smog> (visited on 09/23/2019).
- [28] P. Frank and M. A. Ottoboni. *The Dose Makes The Poison: A Plain Language Guide to Toxicology*. 3rd Editio. Hoboken, New Jersey: John Wiley & Sons, Inc, 2011. ISBN: 9780470381120.
- [29] EEA. *Air quality in Europe*. Tech. rep. 28. 2016, p. 83. doi: 10.2800/80982.
- [30] EEA. *Air pollution in Europe 1990–2004*. Tech. rep. 2. 2007.
- [31] G. E. Nilsson. *Respiratory Physiology of Vertebrates Life with and without oxygen*. Ed. by G. E. Nilsson. Oslo, Norway: Cambridge University Press, 2010. ISBN: 9780521878548.
- [32] UNICEF. “Levels & Trends in Child Mortality: Report 2013-Estimates developed by the UN Inter-agency Group for Child Mortality Estimation.” In: *Unicef/Who/Wb/Un* (2013), pp. 1–32. ISSN: 19326203. doi: 10.1371/journal.pone.0144443.
- [33] F. C. Goldizen, P. D. Sly, and L. D. Knibbs. “Respiratory effects of air pollution on children.” In: *Pediatric pulmonology* 51.1 (2016), pp. 94–108. ISSN: 10990496. doi: 10.1002/ppul.23262.
- [34] R. D. Brook. “Cardiovascular effects of air pollution.” In: *Clinical Science* 115.5-6 (2008), pp. 175–187. ISSN: 01435221. doi: 10.1042/CS20070444.
- [35] T. Bourdrel, M.-A. Bind, Y. Béjot, O. Morel, and J.-F. Argacha. “Cardiovascular effects of air pollution.” In: *Archives of Cardiovascular Diseases* 110.11 (Nov. 2017), pp. 634–642. ISSN: 18752136. doi: 10.1016/j.acvd.2017.05.003. URL: <https://linkinghub.elsevier.com/retrieve/pii/S1875213617301304>.
- [36] S. Li, H. Wang, H. Hu, Z. Wu, K. Chen, and Z. Mao. “Effect of ambient air pollution on premature SGA in Changzhou city, 2013-2016: A retrospective study.” In: *BMC Public Health* 19.1 (2019), pp. 1–10. ISSN: 14712458. doi: 10.1186/s12889-019-7055-z.
- [37] D. Olsson, I. Mogren, and B. Forsberg. “Air pollution exposure in early pregnancy and adverse pregnancy outcomes: A register-based cohort study.” In: *BMJ Open* 3.2 (2013), pp. 1–8. ISSN: 20446055. doi: 10.1136/bmjopen-2012-001955.
- [38] S. Genc, Z. Zadeoglulari, S. H. Fuss, and K. Genc. “The adverse effects of air pollution on the nervous system.” In: *Journal of Toxicology* 2012 (2012). ISSN: 16878191. doi: 10.1155/2012/782462.

- [39] P. de Prado Bert, E. M. H. Mercader, J. Pujol, J. Sunyer, and M. Mortamais. “The Effects of Air Pollution on the Brain: a Review of Studies Interfacing Environmental Epidemiology and Neuroimaging.” In: *Current environmental health reports* 5.3 (2018), pp. 351–364. issn: 21965412. doi: [10.1007/s40572-018-0209-9](https://doi.org/10.1007/s40572-018-0209-9).
- [40] L. Calderón-Garcidueñas, R. Torres-Jardón, R. J. Kulesza, S. B. Park, and A. D’Angiulli. “Air pollution and detrimental effects on children’s brain. The need for a multidisciplinary approach to the issue complexity and challenges.” In: *Frontiers in Human Neuroscience* 8.AUG (2014), pp. 1–7. issn: 16625161. doi: [10.3389/fnhum.2014.00613](https://doi.org/10.3389/fnhum.2014.00613).
- [41] J.-M. Zhang and J. An. “Cytokines, Inflammation, and Pain.” In: *International Anesthesiology Clinics* 45.2 (2007), pp. 27–37. issn: 0020-5907. doi: [10.1097/AIA.0b013e318034194e](https://doi.org/10.1097/AIA.0b013e318034194e). URL: <http://journals.lww.com/00004311-200704520-00004>.
- [42] Oxford Press. *Lexico English Dictionary*. 2020. URL: <https://www.lexico.com/> (visited on 02/27/2020).
- [43] H. A. de Wit, J. P. Hettelingh, and H. Harmens. *ICP Waters Report 125/2015: trends in ecosystem and health responses to long-range transported atmospheric pollutants*. Tech. rep. 6946-2015. 2015.
- [44] G. M. Lovett, T. H. Tear, D. C. Evers, S. E. Findlay, B. J. Cosby, J. K. Dunscomb, C. T. Driscoll, and K. C. Weathers. “Effects of Air Pollution on Ecosystems and Biological Diversity in the Eastern United States.” In: *Annals of the New York Academy of Sciences* 1162.1 (Apr. 2009), pp. 99–135. issn: 00778923. doi: [10.1111/j.1749-6632.2009.04153.x](https://doi.org/10.1111/j.1749-6632.2009.04153.x). URL: <http://doi.wiley.com/10.1111/j.1749-6632.2009.04153.x>.
- [45] TSF and Lusa. *Erupção do Vulcão dos Capelinhos foi há 60 anos*. 2017. URL: <https://www.tsf.pt/sociedade/foi-ha-60-anos-a-erupcao-do-vulcao-dos-capelinhos-8798755.html> (visited on 04/11/2020).
- [46] U. S. D. of Agriculture. *Early History of the NCFS*. 2012. URL: <https://www.nrcs.usda.gov/wps/portal/nrcs/detail/national/about/history/?cid=stelprdb1049437> (visited on 04/11/2020).
- [47] R. Reis. *The Dust Bowl*. 1st ed. New York, New York, USA: Chelsea House, 2008. isbn: 978-0-7910-9737-3.
- [48] World Health Organization. *Radon and Health*. 2016. URL: <https://www.who.int/news-room/fact-sheets/detail/radon-and-health> (visited on 04/11/2020).
- [49] D. / ProTeste. *Radão: perigo que se esconde no granito*. 2003. URL: <https://www.deco.proteste.pt/institucionalemedia/imprensa/comunicados/2003/radao-perigo-que-se-esconde-no-granito> (visited on 04/11/2020).

## BIBLIOGRAPHY

---

- [50] 2 Degrees Institute. *CO<sub>2</sub> Levels*. 2020. URL: <https://www.co2levels.org/> (visited on 04/14/2020).
- [51] D. M. Etheridge, L. P. Steele, R. L. Langenfelds, and R. Francey. *Historical CO<sub>2</sub> record from the Law Dome DE08, DE08-2 and DSS ice cores*. Tech. rep. Aspendale, Victoria, Australia: Division of Atmospheric Research, CSIRO. URL: <http://cdiac.ornl.gov/ftp/trends/co2/lawdome.combined.dat>.
- [52] P. Tans, R. Keeling, S. J. Walker, S. C. Piper, and A. F. Bollenbacher. *Atmospheric CO<sub>2</sub> concentrations (ppm) derived from in situ air measurements at Mauna Loa Observatory, Hawaii*. Tech. rep. Mauna Loa, Hawaii, USA: NOAA/ESRL and Scripps Institution of Oceanography. URL: [ftp://aftp.cmdl.noaa.gov/products/trends/co2/co2%7B%5C\\_%7Dannmean%7B%5C\\_%7Dmlo.txt](ftp://aftp.cmdl.noaa.gov/products/trends/co2/co2%7B%5C_%7Dannmean%7B%5C_%7Dmlo.txt).
- [53] International Agency for Research on Cancer. *Outdoor Air Pollution. IARC Monograph 109*. Vol. 109. 2016, p. 454. ISBN: 9789283201755.
- [54] IEA. *Data & Statistics - International Energy Agency*. URL: [https://www.iea.org/data-and-statistics?country=WORLD%7B%5C&%7Dfuel=Energy%20supply%7B%5C&%7Dindicator=Total%20primary%20energy%20supply%20\(TPES\)%20by%20source](https://www.iea.org/data-and-statistics?country=WORLD%7B%5C&%7Dfuel=Energy%20supply%7B%5C&%7Dindicator=Total%20primary%20energy%20supply%20(TPES)%20by%20source) (visited on 04/17/2020).
- [55] World Bank. *World Bank Datasets*. URL: <data.worldbank.org> (visited on 04/17/2020).
- [56] EEA. *European Environmental Agency*. 2019. URL: <https://www.eea.europa.eu> (visited on 09/23/2019).
- [57] T. Danckaert, C. Fayt, M. Van Roozendael, I. de Smedt, V. Letocart, A. Merlaud, and G. Pinardi. *QDOAS*. 2015. URL: <http://uv-vis.aeronomie.be/software/QDOAS/>.
- [58] R. T. Brinkmann. “Rotational Raman scattering in planetary atmospheres.” In: *Astrophys J* 154 (1968), pp. 1087–1093. ISSN: 0004-637X. DOI: [10.1086/149827](https://doi.org/10.1086/149827).
- [59] J. F. GRAINGER and J. RING. “Anomalous Fraunhofer Line Profiles.” In: *Nature* 193.4817 (Feb. 1962), pp. 762–762. ISSN: 0028-0836. DOI: [10.1038/193762a0](https://doi.org/10.1038/193762a0). URL: <http://www.nature.com/doifinder/10.1038/193762a0>.
- [60] K. V. Chance and R. J. D. Spurr. “Ring effect studies: Rayleigh scattering, including molecular parameters for rotational Raman scattering, and the Fraunhofer spectrum.” In: *Applied Optics* 36.21 (July 1997), p. 5224. ISSN: 0003-6935. DOI: [10.1364/AO.36.005224](https://doi.org/10.1364/AO.36.005224). URL: <https://www.osapublishing.org/abstract.cfm?URI=ao-36-21-5224>.
- [61] W. H. Press, S. A. Teukolsky, W. T. Vetterling, and B. P. Flannery. *Numerical Recipes: The Art of Scientific Computing*. 3rd Editio. 2007. ISBN: 9788578110796. arXiv: [arXiv:1011.1669v3](https://arxiv.org/abs/1011.1669v3).

- [62] A. C. Kak and M. Slaney. *Principles of Computerized Tomographic Imaging*. 1. Society for Industrial and Applied Mathematics, Jan. 2001, pp. 49–112. ISBN: 978-0-89871-494-4. doi: 10.1137/1.9780898719277. URL: <http://pubs.siam.org/doi/book/10.1137/1.9780898719277>.
- [63] M. N. Asl and A. Sadremomtaz. “Analytical image reconstruction methods in emission tomography.” In: *Journal of Biomedical Science and Engineering* 06.01 (2013), pp. 100–107. ISSN: 1937-6871. doi: 10.4236/jbise.2013.61013. URL: <http://www.scirp.org/journal/doi.aspx?DOI=10.4236/jbise.2013.61013>.
- [64] B. Kitchenham and S. Charters. “Guidelines for performing Systematic Literature reviews in Software Engineering Version 2.3.” In: *Engineering* 45.4ve (2007), p. 1051. ISSN: 00010782. doi: 10.1145/1134285.1134500. arXiv: 1304.1186. URL: <http://scholar.google.com/scholar?hl=en%7B%5C%7DbtnG=Search%7B%5C%7Dq=intitle:Guidelines+for+performing+Systematic+Literature+Reviews+in+Software+Engineering%7B%5C%7D0%7B%5C%7D5Cnhttp://www.dur.ac.uk/ebse/resources/Systematic-reviews-5-8.pdf>.
- [65] R. L. Siddon. “Fast calculation of the exact radiological path for a three-dimensional CT array.” In: *Medical Physics* 12.2 (Mar. 1985), pp. 252–255. ISSN: 00942405. doi: 10.1118/1.595715. URL: <http://doi.wiley.com/10.1118/1.595715>.
- [66] L. A. Dewerd and M. Kissick. *The Phantoms of Medical and Health Physics*. Ed. by L. A. DeWerd and M. Kissick. Biological and Medical Physics, Biomedical Engineering. New York, NY: Springer New York, 2014, p. 286. ISBN: 978-1-4614-8303-8. doi: 10.1007/978-1-4614-8304-5. URL: <http://www.springer.com/series/3740%20http://link.springer.com/10.1007/978-1-4614-8304-5>.
- [67] C. Stachniss, C. Plagemann, and A. J. Lilienthal. “Learning gas distribution models using sparse Gaussian process mixtures.” In: *Autonomous Robots* 26.2-3 (Apr. 2009), pp. 187–202. ISSN: 0929-5593. doi: 10.1007/s10514-009-9111-5. URL: <http://link.springer.com/10.1007/s10514-009-9111-5>.
- [68] L. A. Shepp and B. F. Logan. “The Fourier reconstruction of a head section.” In: *IEEE Transactions on Nuclear Science* 21.3 (June 1974), pp. 21–43. ISSN: 0018-9499. doi: 10.1109/TNS.1974.6499235. URL: <http://ieeexplore.ieee.org/document/6499235/>.
- [69] D. Kazantsev, V. Pickalov, S. Nagella, E. Pasca, and P. J. Withers. “TomoPhantom, a software package to generate 2D–4D analytical phantoms for CT image reconstruction algorithm benchmarks.” In: *SoftwareX* 7 (Jan. 2018), pp. 150–155. ISSN: 2352-7110. doi: 10.1016/J.SOFTX.2018.05.003. URL: <https://www.sciencedirect.com/science/article/pii/S2352711018300335?via%7B%5C%7D3Dihub>.

## BIBLIOGRAPHY

---

- [70] J. Stutz and U. Platt. “Numerical analysis and estimation of the statistical error of differential optical absorption spectroscopy measurements with least-squares methods.” In: *Applied Optics* 35.30 (1996), p. 6041. issn: 0003-6935. doi: [10.1364/ao.35.006041](https://doi.org/10.1364/ao.35.006041).
- [71] G. Hönninger, C. von Friedeburg, and U. Platt. “Multi Axis Differential Optical Absorption Spectroscopy (MAX-DOAS).” In: *Atmospheric Chemistry and Physics Discussions* 4 (2004), pp. 231–254. url: [www.atmos-chem-phys.org/acp/4/231/](http://www.atmos-chem-phys.org/acp/4/231/).
- [72] R. W. Sanders, S. Solomon, J. P. Smith, L. Perliski, H. L. Miller, G. H. Mount, J. G. Keys, and A. L. Schmeltekopf. “Visible and near-ultraviolet spectroscopy at McMurdo Station, Antarctica: 9. Observations of OCIO from April to October 1991.” In: *Journal of Geophysical Research: Atmospheres* 98.D4 (Apr. 1993), pp. 7219–7228. issn: 01480227. doi: [10.1029/93JD00042](https://doi.org/10.1029/93JD00042). url: <http://doi.wiley.com/10.1029/93JD00042>.
- [73] N. Bobrowski, G. Hönninger, F. Lohberger, and U. Platt. “IDOAS: A new monitoring technique to study the 2D distribution of volcanic gas emissions.” In: *Journal of Volcanology and Geothermal Research* 150.4 (2006), pp. 329–338. issn: 03770273. doi: [10.1016/j.jvolgeores.2005.05.004](https://doi.org/10.1016/j.jvolgeores.2005.05.004).
- [74] T. G. Feeman. *The Mathematics of Medical Imaging*. Springer Undergraduate Texts in Mathematics and Technology. New York, NY: Springer New York, 2010. isbn: 978-0-387-92711-4. doi: [10.1007/978-0-387-92712-1](https://doi.org/10.1007/978-0-387-92712-1). url: <http://link.springer.com/10.1007/978-0-387-92712-1>.
- [75] R. Gordon. “A tutorial on art (algebraic reconstruction techniques).” In: *IEEE Transactions on Nuclear Science* 21.3 (1974), pp. 78–93. issn: 0018-9499. doi: [10.1109/TNS.1974.6499238](https://doi.org/10.1109/TNS.1974.6499238). url: <http://ieeexplore.ieee.org/document/6499238/>.
- [76] “Industrial Tomography - Systems and Applications.” In: *Industrial Tomography*. Ed. by M. Wang. Vol. 4. Elsevier, 2015. isbn: 9781782421184. doi: [10.1016/B978-1-78242-118-4.12001-5](https://doi.org/10.1016/B978-1-78242-118-4.12001-5). url: <http://linkinghub.elsevier.com/retrieve/pii/B9781782421184120015>.
- [77] C. Haisch. “Optical Tomography.” In: *Annual Review of Analytical Chemistry* 5.1 (2012), pp. 57–77. issn: 1936-1327. doi: [10.1146/annurev-anchem-062011-143138](https://doi.org/10.1146/annurev-anchem-062011-143138). url: <http://www.annualreviews.org/doi/10.1146/annurev-anchem-062011-143138>.
- [78] R. L. Byer and L. A. Shepp. “Two-dimensional remote air-pollution monitoring via tomography.” In: *Optics Letters* 4.3 (1979), pp. 75–77. issn: 0146-9592. doi: [10.1364/OL.4.000075](https://doi.org/10.1364/OL.4.000075). url: <http://eutils.ncbi.nlm.nih.gov/entrez/eutils/elink.fcgi?dbfrom=pubmed%7B%5C%7Did=19687805%7B%5C%7Dretmode=ref%7B%5C%7Dcmd=prlinks>.

- 
- [79] K. Petersen, R. Feldt, S. Mujtaba, and M. Mattsson. “Systematic Mapping Studies in Software engineering.” In: *Proceedings of the 12th International Conference on Evaluation and Assessment in Software Engineering (EASE '08)* (2008), pp. 1–10. doi: [citeulike-article-id:3955889](#).
  - [80] A. Harzing. *Publish or Perish*. URL: <http://www.harzing.com/pop.htm>.
  - [81] A. Hartl, B. C. Song, and I. Pundt. “Atmospheric Chemistry and Physics 2-D reconstruction of atmospheric concentration peaks from horizontal long path DOAS tomographic measurements: parametrisation and geometry within a discrete approach.” In: *Atmos. Chem. Phys* 6.3 (Mar. 2006), pp. 847–861. issn: 1680-7324. doi: 10.5194/acpd-5-11781-2005. URL: <http://www.atmos-chem-phys.net/6/847/2006/>.
  - [82] A. Hartl, K. U. Mettenorf, B. C. Song, U. Platt, and I. Pundt. “2d tomographic reconstruction of trace gas distributions from long-path DOAS measurements: General approach, validation and outlook on an experiment on an urban site.” In: *Proceedings, 31st International Symposium on Remote Sensing of Environment, ISRSE 2005: Global Monitoring for Sustainability and Security* 2 (2005).
  - [83] J. G. Murphy, S. O'Driscoll, and N. J. Smith. “Multipath DOAS for tomographic measurements.” In: *Opto-Ireland 2002: Optics and Photonics Technologies and Applications*. Ed. by T. J. Glynn. Vol. 4876. Mar. 2003, p. 875. doi: 10.1117/12.463960. URL: <http://proceedings.spiedigitallibrary.org/proceeding.aspx?doi=10.1117/12.463960>.
  - [84] S. O'Driscoll, J. G. Murphy, and N. J. Smith. “Computed tomography of air pollutants in street canyons.” In: *Spie* 4876 (2003), pp. 958–967. doi: 10.1117/12.463985.
  - [85] I. Pundt. “DOAS tomography for the localisation and quantification of anthropogenic air pollution.” In: *Analytical and Bioanalytical Chemistry* 385.1 (Apr. 2006), pp. 18–21. issn: 1618-2642. doi: 10.1007/s00216-005-0205-4. URL: <http://link.springer.com/10.1007/s00216-005-0205-4>.
  - [86] I. Pundt, K.-U. Mettendorf, T. Laepple, V. Knab, P. Xie, J. Lösch, C. Friedeburg, U. Platt, and T. Wagner. “Measurements of trace gas distributions using Long-path DOAS-Tomography during the motorway campaign BAB II: experimental setup and results for NO<sub>2</sub>.” In: *Atmospheric Environment* 39.5 (Feb. 2005), pp. 967–975. issn: 13522310. doi: 10.1016/j.atmosenv.2004.07.035. URL: <https://linkinghub.elsevier.com/retrieve/pii/S1352231004009628>.
  - [87] S. O'Driscoll, J. G. Murphy, and N. J. Smith. “Computed tomography of air pollutants in street canyons.” In: ed. by T. J. Glynn. Mar. 2003, p. 958. doi: 10.1117/12.463985. URL: <http://proceedings.spiedigitallibrary.org/proceeding.aspx?doi=10.1117/12.463985>.

## BIBLIOGRAPHY

---

- [88] K. U. Mettendorf, A. Hartl, and I. Pundt. “An indoor test campaign of the tomography long path differential optical absorption spectroscopy technique.” In: *J. Environ. Monit.* 8.2 (2006), pp. 279–287. issn: 1464-0325. doi: [10.1039/B511337G](https://doi.org/10.1039/B511337G). URL: <http://xlink.rsc.org/?DOI=B511337G>.
- [89] D. Poehler, B. Rippel, A. Stelzer, K. U. Mettendorf, A. Hartl, U. Platt, and I. Pundt. “Instrumental setup and measurement configuration for 2D tomographic DOAS measurements of trace gas distributions over an area of a few square km.” In: ().

---

# Systematic Review of DOAS Tomography

## A.1 Introduction

This article comes as a response to the necessary State of the Art search that was required for project ATMOS, which was a Portuguese EU funded project that aimed to develop a miniaturised spectroscopy system for atmospheric analysis and trace gas mapping using Differential Optical Absorption Spectroscopy (DOAS), with tomographic capabilities. FCT NOVA participated in this project as part of a consortium which also included Compta, one of the oldest IT groups in Portugal. The project aimed to develop a miniaturised and highly mobile spectroscopic system with tomographic capabilities, designed to map a small geographic region with respect to the concentration of a set of atmospheric trace gases, like  $\text{NO}_2$  or  $\text{O}_3$ , using a technique called Differential Optical Absorption Spectroscopy (DOAS).

DOAS is one of the most prominent methods for analysing and quantifying atmospheric chemistry, namely in what concerns trace gas concentrations. The technique, developed during the 70s by Perner and Platt [13], was popularised in the following decades by its use in detecting Ozone, Nitrogen Oxydes and studies of cloud radiative transport. DOAS is a type of absorption spectroscopy, which uses a clever mathematical and physical observation to overcome the difficulties of spectral measurement in the open atmosphere.

Through the setting of very careful geometric considerations, it is possible to combine DOAS with tomographic reconstruction methods in order to assemble a map of the gaseous concentrations in a given geographic region. Tomography is the process of reconstructing an image through projections obtained by subjecting a given target (in our case, the atmosphere) to being traversed by any kind of penetrating or reflecting wave, which in our case is visible light.

With this study, we have intended to capture the current literary landscape surrounding the usage of tomographic DOAS, assessing this technique's technological status. For this purpose, we have employed a review methodology originary from Evidence Based Medicine. This method, which has migrated to engineering through

Software Engineering, is called a Systematic Mapping Study (MS). It provides a framework that allows researchers to produce detailed and systematic search protocols, which are used to catalogue literature information and identify research gaps within a determined subject.

The search procedure that we have defined was carefully engineered to cover all tomographic DOAS research relevant to urban, rural or industrial environments, with the main goal of finding a new investigative path to follow. Through it, we were able to find several different applications, all pertaining to scientific research, which are similar regarding physical principle, but differ in objectives, equipment assembly, algorithms, software, and geometry. Most of the selected papers use an active DOAS principle for measuring atmospheric chemical concentrations, and all of them are either fixed or of low mobility.

The rest of this paper has the following structure: Section A.2 presents the context within which this study was written; Section A.3 describes how we have planned to perform the study and the methods we have used in doing it; Section A.4 describes the application of the said methods in the pursuit of our goals and presents the results we have obtained, as well as our evaluation of our processes; Section A.5 shows our conclusions and what we think might be retained from reading this paper.

## A.2 Background

### A.2.1 Differential Optical Absorption Spectroscopy

Absorption Spectroscopy is the term used to identify all techniques that use radiation absorption by matter to assess and quantify elements or molecules in a given spectroscopic sample. It had, and still has, a very important role in the study of the Earth's atmosphere [14].

It is, as many other spectroscopic techniques, based on Lambert-Beer's law, which states that 'in a medium of uniform transparency the light remaining in a collimated beam is an exponential function of the length of the path in the medium', as described originally by Pierre Bouguer in 1729, and can be written [14]:

$$I(\lambda) = I_0(\lambda) \cdot \exp[-L \cdot \sigma(\lambda) \cdot c] \quad (\text{A.1})$$

In Equation A.1,  $I$  is the light intensity as measured by the spectrometer,  $I_0$  the original light intensity at the source,  $L$  is the optical path in which the sample is exposed to the light,  $\sigma$  is the optical cross section of the sampled element or molecule and  $c$  is the sample's concentration.  $\lambda$  is the radiation's wavelength.

Lambert-Beer's equation, while valid in a laboratory setting, is generally not enough to determine gaseous concentrations in an open atmosphere experiment.  $I_0$  determination would require any absorbant from the medium, which is impossible. Besides, in this medium, there are many factors that influence measurements:

Rayleigh's scattering, Mie's scattering, thermal variations, turbulence and instrumental transmissivities. Differential Optical Absorption Spectroscopy (DOAS) overcomes these difficulties by capitalising on cross section's differences between interfering phenomena (normally broad spectral features) and certain trace gases (usually narrow spectral structure). The mathematical formulations behind the technique are well beyond the scope of this article, but suffice it to say that the broad structures are removed through subtraction of a fitted low order polynomial, and a fitting algorithm (such as Levenberg-Marquardt) is used to retrieve concentrations. Detailed presentations of these procedures are presented in [14] and [15].

In [14], the authors split the DOAS method into two fundamental families: passive and active. The passive family is characterised by being designed to capture and analyse natural light, whether from the Sun, the Moon or any other celestial body. This kind of measurement has the advantage of being simple to assemble, but natural light usage implies an additional technical effort for the retrieval of atmospheric concentrations. Active DOAS applications, on the other hand, use artificial light sources to make their measurements. This has been used extensively in the identification of several atmospheric components. Its concentration extraction procedure is simpler, at the expense of a more complex assembly.

DOAS has had a number of applications throughout the years. The technique was first applied in the 1970s. At that time, Perner used an active setup with a laser light source to identify the OH radical in the atmosphere [13]. More recently, researchers around the world have been employing broadband sources (such as Xenon lamps) to measure trace gases like Ozone, Nitrogen Dioxide or Sulphur Dioxide. Almost simultaneously, passive systems have been used to study stratospheric chemistry and radiative transport in clouds [14].

### A.2.2 Honourable Mentions

This paper, and its writing, intend to create an image of the relevant literature in the field of Tomographic DOAS. There are already established techniques that, although not providing exactly the same information, do have the ability to map atmospheric pollutants. These honourable mentions are Multi-Axis DOAS and Imaging DOAS.

Multi-Axis DOAS (MAX-DOAS) is one of the more recent applications of the DOAS technique. It represents a significant progress regarding zenith scattered sunlight measurements, a well established atmospheric analysis technique. It performs a series of passive DOAS measurements in several telescope elevations (typically 4 to 10) [71], either in sequence or simultaneously, according to the schematic representation in Figure A.1.

MAX-DOAS stems from another set of techniques called *off-axis*, which in this case means that the telescope is pointed at another angle than the zenith. Off-axis DOAS

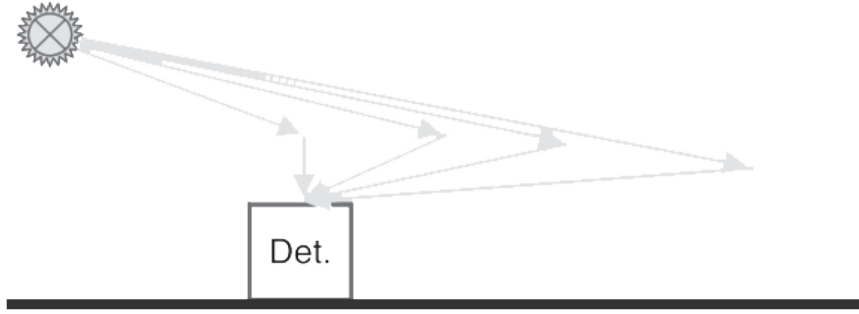


Figure A.1: MAX-DOAS schematic representation [14].

was first employed in 1993 when Sanders et al. [72] used it to assess OClO in Antarctica. During this experiment, the team concluded that the off-axis geometry greatly improves sensitivity for tropospheric species, but does not change the system's ability to quantify stratospheric absorbers. By evaluating several directions, the technique allows researchers to measure not only stratospheric contributors, as zenith sky assemblies, but also to detect absorbers at ground level, as an active DOAS instrument would.

Imaging DOAS combines spectral and spatial information by combining an imaging spectrometer with a scanning system. The resulting data clearly resembles that of a hyperspectrum. The method, developed by Bobrowsky et al. [73], employs a 2D CCD detector. One dimension measures spectral information, while the other contains spatial information for one direction. The other spatial direction is obtained by scanning the field of view with the pushbroom method.

DOAS is used to yield slant column density values for the absorbers for each pixel. The values are colour coded and produce an image describing the gas distribution. This technique is included in this paper because it exists in order to produce a two-dimensional image from spectral information. This image, however, does not come from a tomographic reconstruction procedure, nor is spatial information recovered from projections, but instead comes directly from the acquisition method. Hence, we did not include articles on this method in this study.

### A.2.3 Tomography

Tomography refers to the set of techniques that aim to produce a cross sectioning image from data collected by exposing a given target body to some kind of penetrating or reflecting wave from many different directions [11, 62].

The initial theories that gave rise to tomography were laid out by Johannes Radon in 1917, with a mathematical operation that would later be known as the Radon transform. This process maps a function  $f$ , defined in the plane, to the function  $Rf$ , comprised of the values of the line integrals of  $f$ , taken in  $\theta$  directions. In practice, this

formulation allows the reconstruction of an image by its projections, which are in fact line integrals [74].

Tomographic image reconstruction can be achieved by running one of several algorithms through a computer program. The presentation of these algorithms is completely beyond the scope of this article, but a good starting point for learning about these operations is *The Mathematics of Medical Imaging*, by Timothy Freeman [74]. It is in the scope of this article, however, to make a small introduction to a particular set of reconstruction methods. The reason for this being the prevalence of these methods in the field of DOAS tomography, which is the main subject of this study. These techniques are thus:

**Algebraic Reconstruction Techniques (ART)** Proposed in 1970 by Gordon and Herman [9], these techniques are based on successive approximations between the actual projection data and the sum of the reconstruction elements which represent it [75]. The process is conducted line by line, until a satisfactory convergence condition is met.

**Simultaneous ART** Simultaneous ART is very similar to the ART algorithm. The difference being that the iterative changes occur for all lines at the same time, instead of in only one.

**Simultaneous Iterative Reconstruction Techniques (SIRT)** The main difference between SIRT and SART is that in the former, cell changes are not reflected immediately after one calculation. Updates occur at the end of each iteration. At this point, the change for each cell is the average correction calculated for it taking all equations into account [7].

During the second half of the twentieth century, tomographic processes have had a revolutionary influence in many fields of study, but especially in medicine. Computational tomography scanners allow doctors to see their patients interior in a highly detailed and extremely safe fashion. At first, tomographic imaging was performed only with X-Rays. Their attenuation throughout the patient's body being used as a projection. Nowadays, there are much more methods of image retrieval, such as radioisotopes, ultrasound or particle annihilation [11, 62, 74].

Although it was the field of medicine was more influenced by tomographic procedures than any other, the applications of these methods are not restricted to it. One can find numerous industrial and research applications [76, 77, 78]. One of which is the application to atmospheric research, namely in conjunction with DOAS. In recent years, scientists have been working on tomographic methods for measuring atmospheric trace gas concentration values. The field is interesting because it allows for 2D or even 3D mapping of a given region, with respect to those trace gases. This article aims to make an assessment of the status of this tomographic application, by analysing current literature on the subject.

#### A.2.4 Mapping Study

A Systematic Mapping Study (MS) is a type of secondary study designed to determine the general features of the research landscape in the subject they are addressing [64, 79].

An MS is driven by broad (and often multiple) research questions and applies an also broad data extraction protocol. This is in line with the fact that this kind of study aims to summarise its findings, answering the research questions, and in-depth analysis is not required. It is common for an MS to be a precursor to a Systematic Literature Review (SLR), which is a much deeper kind of systematic study. Guidelines for performing studies of both kinds can be found in a report made by Kitchenham and Charters in 2007 [64]. In this document, the authors establish the 3 stages which all MS and SLR generally have:

**Planning** This stage includes all preliminary considerations regarding the MS or SLR in the making. All protocols, from search to evaluation, through data extraction, are devised;

**Conduction** During this staged, researchers apply what they have planned in the previous phase. Protocols are *actually* run, and data is synthesised;

**Reporting** In this phase, the team has to define their dissemination strategy, and implement it. It is in this stage that a final report is written and evaluated.

Although it is logical (and fundamentally correct) to assume that these steps are sequential, this may not be, and usually is not, accurate. Many of these stages and their intermediate steps require iteration. For instance, some inclusion or exclusion criteria may only be found necessary once the search protocol is implemented.

### A.3 Methods

An MS, as this article intends to be, always aims to answer its research questions in a broad but definite way. It is a way of understanding a given field of research, and being able to systematise how this understanding is achieved. In this case, the overarching goal of this study was to provide a solid landscape for the current state of the art in the field of atmospheric tomography using DOAS as the projection collection method.

#### A.3.1 Research Questions

Before delving into any kind of literary search, we have used the PICOC(Population, Intervention, Context, Outcome and Comparison) method for structuring our goals and defining our research questions. This is summarised in Table A.1, and led us to our research goal: *assess research status for the DOAS tomography technique, and*

*identify new investigative approaches.* This paper's research question aims to provide the foundation for our research goal: **what is the current status of the technology used in tomographic DOAS?**

Table A.1: PICOC analysis.

<b>Population</b>	DOAS research in general.
<b>Intervention</b>	The papers must address tomographic DOAS.
<b>Outcome</b>	Status <b>assessment</b> for DOAS tomography.
<b>Context</b>	Research papers.

The mentioned research question is too vague to pursue in a systematic fashion, so we had to slice it into smaller and more objective chunks. This sectioning is presented in Table A.2.

Table A.2: Research question slicing

<b>Original</b>	What is the current status of the technology used in tomographic DOAS?
<b>RQ1</b>	Is there a typical hardware setup used in tomographic DOAS studies?
<b>RQ2</b>	Is there a standard software used to perform these analysis?
<b>RQ3</b>	What are the algorithms more commonly used?

The research question is one of the most important steps in planning a Systematic Literature Review, but it cannot be entered into a library's search box. Therefore, we have to define our search terms before we can make any effort of answering our questions.

### A.3.2 Search Query Definition, Library Selection and Filter Definition

Preliminary searches, ran as tests for this study, indicated that there were a very low number of studies in DOAS tomography, in comparison to other subjects to which this methodology is commonly applied. As consequence, the search terms were purposefully chosen as to maintain a broad scope and retrieve the largest possible amount of articles. The selected terms were: **DOAS atmosphere\* tomography**<sup>1</sup>. The same strategy was applied to the selection of electronic libraries, as these preliminary searches revealed that there was a poor availability of relevant information in the most commonly used libraries. This in itself motivated a two stage approach to the search effort, in which we use several libraries to complement an initial Google Scholar search. Libraries used are summarised in Table A.3.

In addition to the search libraries, the study's results will be heavily influenced by the inclusion and exclusion filters that we apply to the search results. There are 3 Inclusion Criteria (IC) and one Exclusion Criteria (EC). The IC determined that selected documents should be journal papers written in English and be fundamentally

<sup>1</sup>The asterisk acts as a wildcard.

Table A.3: Electronic libraries used in this study.

Library	URL
Google Scholar (GS)	<a href="https://scholar.google.com/">https://scholar.google.com/</a>
Web of Knowledge (WoK)	<a href="https://webofknowledge.com">https://webofknowledge.com</a>
Scopus (SD)	<a href="https://www.scopus.com">https://www.scopus.com</a>

about DOAS tomography. The Exclusion Criteria determined that selected papers do not include studies about satellite data. These criteria are reflected in Table A.4.

Table A.4: Selection filters in use for this study's search.

	Criterium	Definition
<b>Exc. Criteria</b>	EC1	Satellite data papers are not accepted
	IC1	Results must be journal papers
<b>Inc. Criteria</b>	IC2	Results must be about Tomographic DOAS
	IC3	Results must be written in English

### A.3.3 Data Extraction Strategy

The data extraction process is a key part of any systematic review. That being the case, it is also true that there is no "one size fits all" solution, and that this is probably the part of the study where scope adaptation is more important. With this in mind, we started defining our data extraction strategy during the preliminary searches. As already stated, these searches demonstrated that we would not have many papers to work with. Moreover, only one element of the team had DOAS expertise. This led to a data extraction strategy that was comprised of two stages: in the first stage, the DOAS expert would run the search and analyse the results. The second stage would see the other team members reading the analysed articles, ensuring all the inclusion and exclusion criteria were being correctly applied. Analysis control was conducted using a shared spreadsheet created in Microsoft Excel.

### A.3.4 Quality Assessment

Assessing an article's quality is not a trivial matter. Normally, there is almost an immediate association between the term quality and which paper is "better or worse". This implicit thinking has a subjective flavour to it that is not welcome in the kind of analysis one needs in a Systematic Mapping Study. To eliminate this problem, researchers usually choose some kind of metric of objective nature and rate the various papers in accordance to this metric. In our case, we have chosen to evaluate the citation number for each one of the selected articles, their age and the general quality of the publishing method that was used. The formula used in this calculation takes the form

of Equation A.2. In this equation,  $Q_i$  is the journal's quartile, and  $C_i$  is the number of citations of each particular article. The  $Age_i$  factor in the formula is used for relaxing the citation criteria, according to the age of the article, which will act as a normalising factor in the number of citations, with the logical reasoning that older articles will naturally have more citations.

$$S = Q_i \cdot \frac{C_i}{Age_i} \quad (\text{A.2})$$

## A.4 Conduction

### A.4.1 Search Results

The search phrase, as was determined in Section A.3 was run through the selected libraries using a specialised software called *Publish or Perish* [80]. This software allows exporting search results into a comma-separated-values (csv) file, that is easily imported into a spreadsheet program such as Microsoft Excel and making the process a lot more expedient. Since one of the electronic search engines that were used was Google Scholar, which is much more powerful and broad than the other libraries, it demanded some special attention due to the many repeated entries that we were sure to find using this method. The flowchart depicted in Figure A.2 illustrates the search stages. In the end, our search resulted in a total of 61 articles in all libraries. Almost half of them (29 in 61) were excluded due to the application of some exclusion criteria. The high number of excluded papers is mostly a result of Google Scholar's search broadness (25 excluded results vs 3 in Scopus and 1 in WoS). 19 of the entries retrieved using Scopus and WoS were already in GS, which combined with the numerous exclusions, resulted in a final number of 13 papers. A summary of these results can be found in Table A.5, and the list of selected papers can be seen in Table A.6.

Table A.5: Search results summary.

<b>Library</b>	<b>Results</b>	<b>Excluded</b>	<b>In GS</b>	<b>Final</b>	<b>Weight in study</b>
<b>GS</b>	37	25	0	12	92,31%
<b>Scopus</b>	15	3	12	0	0%
<b>WoS</b>	9	1	7	1	7,69%
<b>Total</b>	<b>61</b>	<b>29</b>	<b>19</b>	<b>13</b>	<b>100,00%</b>

### A.4.2 Discussion

The final goal of this study was to identify a possible means of approaching DOAS tomography in an innovative way. For this, we have used the information contained

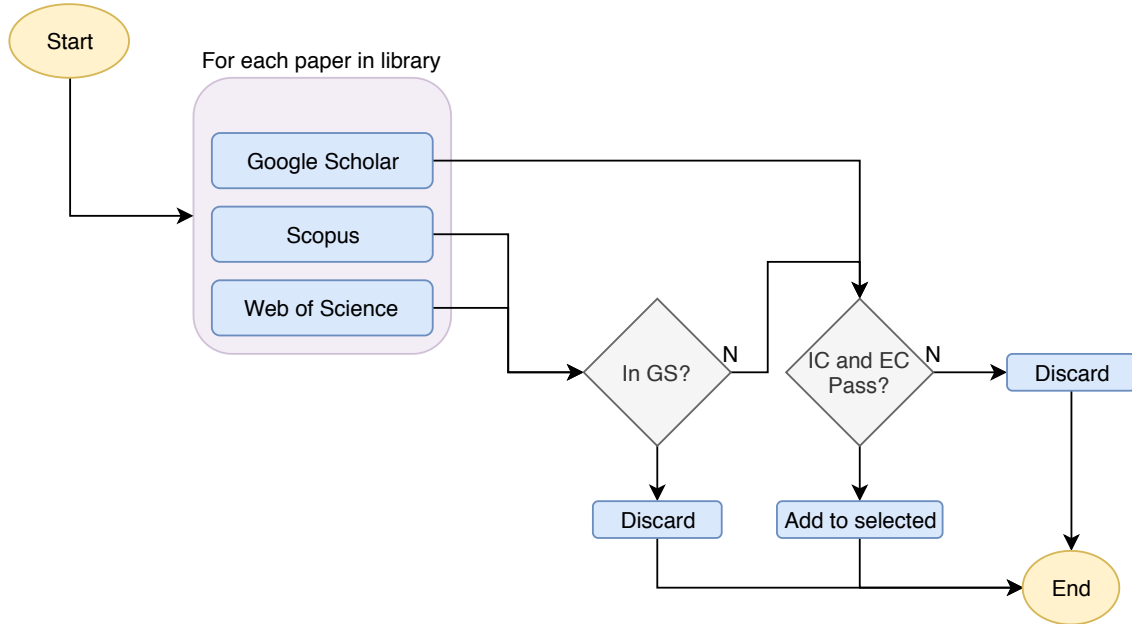


Figure A.2: Conduction stage flowchart. Libraries are searched independently through *Publish or Perish*, but results must be checked to ensure they are not counted twice, due to the imbalance of power between GS's search engine and the others.

in the 13 selected articles, trying to find some commonalities and patterns that can be useful to us.

One of the first patterns that can be observed is that most of the literature in this subject was written on the application of active DOAS systems, i.e., systems that use some kind of artificial light source to perform their spectroscopic analysis. Active systems are instrumentally much more complex than passive systems. However, they allow a more thorough analysis of the studied trace gases. In addition, passive systems also imply dealing with much more complicated physical phenomena, such as radiative transfer equations. Another almost immediate observation that can be raised is that many studies (6/13) originate from the BABII campaign, which was an initiative of the Institute for Meteorology and Climate Research in Karlsruhe, Germany. The campaign intended to experimentally monitor the traffic emissions in the A656 motorway [17]. Judging by the number of papers this initiative created, this was the largest tomographic DOAS campaign ever made.

All of the active DOAS solutions that were selected in our study are Long Path DOAS applications. Also all of the systems were custom built for their particular study or campaign. The group associated with the BABII campaign had two telescopes with diameters in the order of 200 mm and a focal length of around 1 m to simultaneously emit the light from a Xenon lamp towards a constellation of 8 retro-reflectors, which were assembled on two towers, on both sides of the motorway that connects Heidelberg with Mannheim [16]. The same assembly and instruments were used by the other papers of the group, namely [17, 81, 89]. The paper identified in [88] is also from

Table A.6: References and relevant data for the selected papers, including their score, which was calculated according to Equation A.2.

Number	Reference	Quartile	Citations	Year	Score
1	[81]	1	35	2006	2,69
2	[82]	1	2	2005	0,14
3	[17]	1	30	2004	2,00
4	[16]	2	1	2005	0,05
5	[83]	3	6	2003	0,19
6	[19]	1	8	2006	0,62
7	[22]	2	26	2009	1,95
8	[84]	4	0	2003	0,00
9	[85]	1	12	2006	0,92
10	[86]	1	42	2005	3,00
11	[87]	4	1	2003	0,02
12	[88]	1	4	2006	0,31
13	[21]	1	2	2017	1,00

the same group, but the article had a very different approach and purpose. Instead of aiming to map a given region (which in this case would be a motorway vicinity), the authors wanted to validate the two-dimensional reconstruction technique that would be used in the other studies, by conducting an indoor experiment using three multibeam instruments consisting in a telescope (1.5 m focal length and 300 mm diameter) that acted as both emitter and receiver, together with three fixed "towers" that held the retro-reflectors and a Xenon lamp as light source.

The work done by the group that wrote [18] took a different but similar approach to a completely different application. They used an LED light source with a narrow wavelength interval light in the UV region (around 290 nm) and a custom built instrument assembly that was used as a fence line monitor for a refinery in Los Angeles and then to monitor the two-dimensional concentration fields for Benzene, Toluene and Xylenes in Houston, Texas. Both experiments have found the system's findings to be satisfactory, and the device was able to map the concentration for the target chemical species with success. In addition to this study's inherent research interest, it is also good to note that Stutz' paper describes a system that could easily be converted to a commercial product.

The research group at the Cork Institute of Technology, in Ireland, has approached the problem in a different way. In the three papers from this group [83, 84, 87] that were selected for this study, the authors present and discuss three new tomographic approaches. The first is a new optical design, based on a multipath assembly that allows for a significant increase in the number of optical paths produced by a single

light source; the second was an attempt at reconstructing the tomographic image through the use of evolutionary algorithms; and the third was the application of the tomographic DOAS technique to a simulated urban canyon. These three articles were deemed relevant for this study because they do have technological novelty. However, it should be noted that on a more literary level, the three papers were among the weakest in the selected group, and were only published as conference proceedings.

Regarding passive DOAS applications, the two papers we have found come with two completely different paradigms. The first article [22] was written in 2009 and details the application of a tomographic inversion algorithm to a scanning DOAS application, designed to work with trace gas plumes like the ones above volcanoes or power stations. The team present a system composed of two DOAS devices, with sufficient distance with themselves as to allow tomographic reconstruction, but sufficiently small to allow the light path to be considered a straight line from the point of last scattering to the detector. The authors applied an adapted version of the Lower Third Derivative (LTD) algorithm to the projections obtained by pointing the set of fixed DOAS apparatus towards the plume in different angles. Besides simulations for their proposed method, the authors have also conducted practical experiments, both over a power plant in Spain and a volcano in Italy. Results from these experiments display a good agreement between reality and simulation results, proving the technique's validity.

The second Passive DOAS application is a paper published by Frins et al. [19]. In this study, the researchers detail a particular application in which they measure light coming from bright and nonreflecting sun-illuminated objects in their field of view. They use this light to retrieve column density values for a number of trace gases. The proposed method also includes a way with which to remove the stratospheric contribution that appears in the measured light besides the target column. The authors discuss how radiative transfer can influence measurements, but they also present a number of approaches to mitigate this problem, ensuring the validity of their approach. Besides presenting the method, the authors also describe an experiment they conducted by assembling and manoeuvring a DOAS system on top of a building in Heidelberg, Germany.

#### A.4.3 Validity Threats

When writing an MS or an SLR, authors always have to analyse their findings and methods in order to mitigate potential sources of error or lack of validity. This is called a validity threat analysis.

There are two main families of validity threats. They can be internal, i.e., they come from the methods employed used in conducting the study; or external, which means that the threat comes from the applicability (or lack thereof) of the effects observed in the study, outside of its scope.

On the level of internal validity of our study, two main observations come to mind:

**Relevant papers left out** The very low number of found studies could be an indication that our inclusion and exclusion filters were set in a too restrictive manner. It could also happen that some relevant papers were not found due to being written in such a way that the libraries' search engines did not find them with our search phrase. This same problem would also occur if for some reason, an important library was left out of the study, and therefore not searched. We mitigate all these risks by selecting a purposefully broad search phrase, by using powerful general search engines (eg. Google Scholar) and by running several undocumented test-runs with other search phrases. A common strategy used for tackling this kind of threat is to extend the study through snowballing, which in our case would not make a great difference, due to the fact that many of the identified papers reference one-another.

**Quality of selected papers** Papers were selected according to the inclusion criteria defined in Section A.3. In the same section, we have discussed how the articles were assessed regarding their quality, and stated that the method with which the articles are ranked in this regard exclusively depends on the number of citations. This number, in a field with so few papers in the literature, will always be small and can be deceiving if one tries to read the paper's relevance with this score.

On the external threat plane, we contend with the applicability of our findings outside our study. The study itself had the clear purpose of identifying a *vector of approach* for an innovative product in DOAS tomography. As long as we accomplish this objective, we can regard it as externally valid, even if it is of little use outside the field of study.

## A.5 Conclusions

The initial goal of this study was the assessment of the technological status of the tomographic DOAS method for atmospheric pollutant mapping, with the overarching objective of finding an innovative approach to the subject.

We have begun by identifying a set of representative electronic libraries through a preliminary search. Then, we have constructed a purposefully broad search phrase, which we applied to the selected libraries. This search has rendered a total of 61 articles, of which only 13 (around 22%) were considered relevant and therefore further studied. The application of the search strategy detailed in Section A.3 shows that with the great finding power of Google's literature-oriented search engine comes an also great need for scrutiny, since the inherent broadness of the tool results in a large number of unwanted detections (24 exclusions vs 1 in WoS and 3 in Scopus).

Our search has found that active tomographic DOAS is far more common than the passive counterpart (11 out of 13 articles discussed this method). This preference can be explained by the fact that the results produced by this kind of system are

generally superior to those obtained by passive methods. However, passive applications are normally much less demanding on a technical level, and are simpler to run and assemble. Much as a result of this, we have also identified that the systems used in the literature were not mobile or had a very low mobility level which in turn caused that all the systems were working with low projection numbers (as was identified in several of the selected papers). This should be taken into account in future research on the topic.

As a final note, we would also like to point out that there seem to be no commercially available systems for this kind of application, although some of the articles, like the one by Stutz in 2016 [18] detail systems which could easily be adapted to that end.